Imperial College London
Department of Electrical and Electronic Engineering

Towards a Cost-Effective Operation of Low-Inertia Power Systems

Luis Badesa Bernardo

A thesis submitted to Imperial College London
for the degree of Doctor of Philosophy

June 2020

To Esther, Javier, Miguel and Rocío.

Declaration of Originality

The material contained within this thesis is my own work, except where other work is appropriately referenced. Any use of the first-person plural is for reasons of clarity.

Copyright Declaration

The copyright of this thesis rests with the author. Unless otherwise indicated, its contents are licensed under a Creative Commons Attribution-Non Commercial-No Derivatives 4.0 International Licence (CC BY-NC-ND 4.0).

Under this licence, you may copy and redistribute the material in any medium or format on the condition that: you credit the author, do not use it for commercial purposes and do not distribute modified versions of the work.

When reusing or sharing this work, ensure you make the licence terms clear to others by naming the licence and linking to the licence text.

Please seek permission from the copyright holder for uses of this work that are not included in this licence or permitted under UK Copyright Law.

Abstract

Modern power systems throughout the world, particularly in islands such as Great Britain, face a major problem: the significantly reduced level of system inertia due to integration of Renewable Energy Sources (RES). Inertia, which refers to the physical inertia of the rotating masses in thermal generators, acts as a buffer of kinetic energy, which helps prevent blackouts in the event of an unexpected generator outage. Given that most RES such as wind and solar are decoupled from the power grid through power electronics converters, they do not naturally contribute to system inertia, therefore reducing this valuable energy buffer. In order to avoid blackouts in low-carbon systems, a higher amount of alternative ancillary services such as Frequency Response becomes necessary.

This thesis focuses on studying mathematical methods to schedule ancillary services for frequency security in a cost-effective manner. To do so, we have obtained novel conditions for post-fault frequency security that can be implemented as constraints into optimisation problems such as the Unit Commitment, in order to co-optimise the provision of energy and frequency ancillary services. The key challenge lies in incorporating the differential-equation-driven frequency dynamics into an algebraic-equation-constrained optimisation problem. Furthermore, the constraints for frequency security must be computationally efficient, since they may be used in computationally intense problems like Stochastic Unit Commitment: while Mixed-Integer Linear Programming has been extensively used in power system scheduling and markets, this thesis exploits the recent development of convex optimisation algorithms to also propose Mixed-Integer Second-Order Cone constraints for a safe post-fault frequency evolution.

The developed frequency-secured optimisation framework has been applied to several relevant case studies, which allow to inform sensible designs for ancillary-services markets and planning decisions that would lead to an optimal operation of a low-carbon power system, achieving significant economic savings and reduction in carbon emissions. An optimal procurement of these services is of uttermost practical relevance in modern power grids, as highlighted by recent events such as the Great Britain blackout of August 9$^{\text{th}}$, 2019.

Contents

Acknowledgements

First, I would like to thank Prof. Goran Strbac and Dr. Fei Teng for their supervision during this doctorate. Prof. Strbac gave me the task of finding ways to optimise the operation of a low-inertia system, a task that I have found both challenging and enriching. On his side, Dr. Teng has been an important support during my time at Imperial. His guidance has been instrumental to the successful completion of this thesis, for which I am certainly grateful to him.

My family has been a great support throughout my studies. My parents, Javier and Esther, and my brother Miguel have given me unconditional love, always listened to my concerns and given me thoughtful advice. It is because of them that I found the strength to keep working when I was lacking motivation.

I would also like to thank my friends and colleagues in the Control & Power research group at Imperial for the community that they created and made me part of. Lively lunch breaks, games of squash, football and ping-pong, and evening beers at h-bar are some of many memories that I will cherish. Furthermore, I would like to show my appreciation to Johan Löfberg for creating the very useful optimisation tool YALMIP, which I have used frequently during the development of this thesis.

Most of all, I thank Rocío, without whom the time spent working on this thesis would have been much less enjoyable. She is the reason why I am excited about the chapter that begins now.

Last, I would like to thank any reader of this thesis for their interest in this work. Completing a PhD takes a significant effort and it is very gratifying that one's research is of actual interest to others. I hope you find this thesis useful for developing your own ideas, and may those ideas help us reach a carbon-free future.

List of Publications

Journals

[1] L. Badesa, F. Teng, and G. Strbac, "Simultaneous scheduling of multiple frequency services in stochastic unit commitment," *IEEE Transactions on Power Systems*, vol. 34, no. 5, pp. 3858-3868, 2019. [Online]. Available: https://arxiv.org/abs/1809.10391

[2] L. Badesa, F. Teng, and G. Strbac, "Optimal portfolio of distinct frequency-response services in low-inertia systems," *IEEE Transactions on Power Systems*, accepted for publication. [Online]. Available: https://arxiv.org/abs/1908.07856

[3] L. Badesa, F. Teng, and G. Strbac, "Pricing inertia and frequency response with diverse dynamics in a Mixed-Integer Second-Order Cone Programming formulation," *Applied Energy*, vol. 260, p. 114334, 2020. [Online]. Available: https://arxiv.org/abs/1909.06671

[4] J. Guo, L. Badesa, F. Teng, B. Chaudhuri, S. Y. R. Hui, and G. Strbac, "Value of point-of-load voltage control for enhanced frequency response in future Great Britain power system," *IEEE Transactions on Smart Grid*, accepted for publication. [Online]. Available: http://arxiv.org/abs/2006.03559

[5] S. Camal, F. Teng, A. Michiorri, G. Kariniotakis, and L. Badesa, "Scenario generation of aggregated wind, photovoltaics and small hydro production for power systems applications," *Applied Energy*, vol. 242, pp. 1396-1406, 2019. [Online]. Available: https://hal-mines-paristech.archives-ouvertes.fr/hal-02081282

[6] L. Badesa, F. Teng, and G. Strbac, "Conditions for regional frequency stability in power systems—Part I: Theory," *IEEE Transactions on Power Systems*, in preparation.

[7] L. Badesa, F. Teng, and G. Strbac, "Conditions for regional frequency stability in power systems—Part II: Applications," *IEEE Transactions on Power Systems*, in preparation.

Conference (peer-reviewed)

[8] L. Badesa, F. Teng, and G. Strbac, "Economic value of inertia in low-carbon power systems," in *2017 IEEE PES Innovative Smart Grid Technologies Conference Europe (ISGT-Europe)*, Torino (Italy), Conference Proceedings. [Online]. Available: https://arxiv.org/abs/2001.03763

[9] L. Badesa, F. Teng, and G. Strbac, "Optimal scheduling of frequency services considering a variable largest-power-infeed-loss," in *2018 IEEE Power & Energy Society General Meeting (PESGM)*, Portland, Oregon (USA), Conference Proceedings. [Online]. Available: https://arxiv.org/abs/2001.03751

List of Figures

List of Tables

Nomenclature

Abbreviations and Acronyms

BESS	Battery Energy Storage Systems.
CCGT	Combined Cycle Gas Turbine.
COI	Centre Of Inertia.
ED	Economic Dispatch.
EFR	Enhanced Frequency Response.
FR	Frequency Response.
GB	Great Britain.
KKT	Karush-Kuhn-Tucker.
LSB	Least Significant Bit.
MILP	Mixed-Integer Linear Program.
MISOCP	Mixed-Integer Second-Order Cone Program.
MSG	Minimum Stable Generation.
OCGT	Open Cycle Gas Turbine.
OPF	Optimal Power Flow.
PFR	Primary Frequency Response.
q-s-s	Quasi-steady-state.
RES	Renewable Energy Sources.
RoCoF	Rate of Change of Frequency.
SI	Synthetic Inertia.
SOC	Second-Order Cone.
SoC	State of Charge.
SUC	Stochastic Unit Commitment.
UC	Unit Commitment.
UFLS	Under Frequency Load Shedding.

Indices and Sets

$g,\ \mathcal{G}$	Index, Set of generators.
$i,\ j,\ n$	All-purpose indices.
$\mathcal{J}_i$	Set of neighbouring regions to region i.
$k,\ \mathcal{K}$	Index, Set of FR services fully delivered by nadir.
$l,\ \mathcal{L}$	Index, Set of bits in binary expansion of $R_{\mathcal{G}}$, used in Chapter 2.
$l,\ \mathcal{L}$	Index, Set of FR services ramping up by the nadir, used in Chapter 3.
$n,\ \mathcal{N}$	Index, Set of nodes in the scenario tree in the SUC, used in Chapter 1.
$p,\ \mathcal{P}$	Index, Set of overestimating planes.
$s,\ \mathcal{S}$	Index, Set of storage units, used in Chapter 2.
$s,\ \mathcal{S}$	Index, Set of FR services, used in Chapter 3.
$\lvert\mathcal{S}\rvert$	Cardinality of set $\mathcal{S}$, used in Chapter 3.

Constants and Parameters (taking a constant value in every optimisation problem)

$\Delta\tau(n)$	Time-step corresponding to node n in the SUC (h).
$\Delta f_{\max}$	Maximum admissible frequency deviation at the nadir (Hz).
$\Delta f_{\max}^{\mathrm{ss}}$	Maximum admissible frequency deviation at quasi-steady-state (Hz).
α	Probability of meeting the nadir constraint.
δ_i^{ss}	Pre-fault, steady-state phase angle of voltage in bus i (rad).
η	Probability of meeting the RoCoF constraint.
$\pi(n)$	Probability of reaching node n in the SUC.
ϕ_i	Phase shift of the inter-area oscillations for region i (rad).
σ	Standard deviation of inertia from demand (MW·s).
τ_1	Time-constant of FR provider 1 (s).
τ_2	Time-constant of FR provider 2 (s).
τ_{b}	Time-constant of the BESS dynamics (s).
τ_{g}	Time-constant of the generator dynamics (s).
ω_i	Angular frequency of the inter-area oscillations for region i (rad/s).
a_i	Attenuation factor of the inter-area oscillations for region i (s^{-1}).
A_i	Amplitude of the inter-area oscillations for region i (Hz).
a_p, b_p, c_p	Parameters of overestimating plane p.
c^{LS}	Value of lost load (£/MWh).
$\mathrm{c}_g^{\mathrm{m}}$	Marginal cost of generating units g (£/MWh).

$\mathrm{c}_g^{\mathrm{nl}}$	No-load cost of generating units g (£/h).
$\mathrm{c}_g^{\mathrm{st}}$	Start-up cost of generating units g (£).
D	Load damping factor (%/Hz).
D'	Multiplication of $\mathrm{D} \cdot \mathrm{P_D}$ (MW/Hz).
f_0	Nominal frequency of the power grid (Hz).
H_g	Inertia constant of generating units g (s).
$\mathrm{H_L}$	Inertia constant of the generator producing power P_L (s).
H_μ	Forecast for inertia from demand (MW·s).
$\mathrm{H_W}$	Inertia constant of wind turbines (s).
K_1	Droop gain for FR provider 1 (Hz/MW).
K_2	Droop gain for FR provider 2 (Hz/MW).
$\mathrm{K_b}$	Droop gain for the BESS dynamics (Hz/MW).
$\mathrm{K_g}$	Droop gain for the generator dynamics (Hz/MW).
$\mathrm{N}_\mathcal{M}$	Number of must-run generators.
$\mathrm{P_D}$	Total demand (MW).
$\mathrm{P_g^{max}}$	Maximum power output of units g (MW).
$\mathrm{P_g^{msg}}$	Minimum stable generation of generator g (MW).
$\mathrm{P_L^{max}}$	Upper bound for the largest power infeed P_L (MW).
$\mathrm{P_i^L}$	Segment i in the discretisation of P_L in the nadir constraint (MW).
$\mathrm{P_R}$	Power produced from RES (MW).
$\mathrm{R_g^{max}}$	FR capacity of generator g (MW).
$\mathrm{RoCoF_{max}}$	Maximum admissible RoCoF (Hz/s).
$R_{\mathcal{S},\mathrm{max}}$	Upper bound for linear expression $R_\mathcal{S}$ (MW).
$\mathrm{T}_{\mathrm{del},i}$	Delay in provision of FR service i (s).
$\mathrm{T}_{\mathrm{del},s}$	Delay in provision of FR service s (s).
$\mathrm{T_g}$	Delivery time of PFR (s).
T_i	Delivery time of FR service i (s).
$\mathrm{T}_{i,j}$	Electrical stiffness of the transmission line connecting buses i and j (MW).
$\mathrm{T_s}$	Delivery time of EFR (s), used in Chapter 2.
T_s	Delivery time of FR service s (s), used in Chapter 3.
V_i	Voltage magnitude in bus i (kV).
$\mathrm{X}_{i,j}$	Reactance of the transmission line connecting buses i and j (Ω).

Decision Variables (continuous unless otherwise indicated)

$\lambda_1, \lambda_2, \mu$	Dual variables for the SOC nadir constraint.
λ_R	Dual variable for the RoCoF constraint.
λ_qss	Dual variable for the q-s-s constraint.
k_l	Auxiliary variables for linearisation of the products $R_\mathcal{S} \cdot z_l$ (MW).
m_l	Auxiliary variables for linearisation of the products $H \cdot z_l$ (MW·s^2).
m_i^L	Binary variables for discretisation of P_L in the nadir constraint.
$N_g^\mathrm{sg}(n)$	Number of units g that start generating in node n in the SUC.
N_g^up	Number of online generating units of type g in the SUC.
P_g	Power produced by generating units g (MW).
P_L	Largest power infeed (MW).
$P_\mathrm{nadir}^\mathrm{L}$	Auxiliary variable for the discretisation of P_L in the nadir constraint (MW).
P^LS	Load shed (MW).
$P_\mathcal{M}$	Power produced by must-run units (MW).
$P_\mathrm{R}^\mathrm{curt}$	RES power curtailed (MW).
P_W	Online power from wind (MW).
R_g	PFR provision from generating units g (MW).
R_i	FR provision from service i (MW).
R_s	EFR provision from storage units s (MW), used in Chapter 2.
R_s	FR provision from service s (MW), used in Chapter 3.
y_g	Binary variable, commitment decision for generator g.
z_l	Binary variables for binary expansion of linear expression $R_\mathcal{G}$.

Functions and Operators

$\overline{\cdot}$	Conjugate of a complex number.
$\lVert \cdot \rVert$	ℓ^2-norm.
$\Delta f(t)$	Time-evolution of post-fault frequency deviation from nominal state (Hz).
$\Delta F_i(s)$	Laplace transform of $\Delta f_i(t)$ (Hz).
$\Delta \mathrm{P}_i^\mathrm{import}(t)$	Deviation from steady-state power import to region i, after an outage (MW).
$\delta_i(t)$	Post-fault phase angle of voltage in bus i (rad).
$\Phi(\,\cdot\,)$	Standard normal cumulative distribution function.
$\mathscr{L}\{\,\cdot\,\}$	Laplace transform operator.
$\mathscr{L}^{-1}\{\,\cdot\,\}$	Inverse Laplace transform operator.

$\mathcal{N}(\cdot,\cdot)$	Normal distribution.
$\mathrm{FR}(t)$	Time-evolution of aggregated system FR (MW).
$\mathbf{P}(\cdot)$	Probability operator.
$\sup\{\cdot\}$	Supremum of a set.
t^*	Time when the frequency nadir occurs (s), used in Chapter 2.
t_{nadir}	Time when the frequency nadir occurs (s).

Linear Expressions (linear combinations of decision variables)

$C_g(n)$	Operating cost of units g at node n in the SUC (£).
H	System inertia (MW·s).
$R_{\mathcal{G}}$	Total PFR from all generators (MW).
$R_{\mathcal{S}}$	Total EFR from all storage units (MW).

Random Variables

H_{D}	System inertia from the demand side (MW·s).

Chapter 1

Introduction

This chapter gives the introduction to the thesis, by explaining the motivation for undertaking this task, describing the approach used to tackle the research questions and stating the original contributions of the work presented here.

1.1 Motivation and background

In the last decade, there has been increasing interest in Renewable Energy Sources (RES) due to public awareness of the negative effects on the environment of conventional electricity generation resources like coal and oil. The EU set the target of an 80% to 95% reduction of greenhouse gas emissions by 2050, compared to 1990 levels [10], while the United Kingdom has already committed to net-zero emissions by 2050 [11]. In order to achieve this goal, it is expected that the European and British electricity sectors will be largely decarbonised in the coming years, with significantly increased levels of RES.

The integration of RES in a power system involves significant challenges. A traditional power system is dominated by relatively flexible and controllable generation plants, that follow a fluctuating but low-uncertain demand. However, the future low-carbon Great Britain electricity system will be characterised by a generation mix including significant amounts of difficult to predict, intermittent RES, mainly wind and solar, in combination with a highly inflexible nuclear fleet [12]. Therefore, a fundamental review of the current methodologies for the system's control, operation and planning is needed. This thesis addresses the operational aspects of low-carbon grids from the economic and engineering perspectives.

One of the major problems in the operation of a power system with high RES-penetration is a significant deterioration in electric frequency performance. This presents a threat to security of supply, which has been a crucial issue since the use of electricity became widespread: our society is absolutely dependent on electricity, and therefore electric utilities incur enormous economic penalties in the event of a blackout. In order to guarantee electricity supply, frequency security must be assured, which means that the system's electric frequency must be contained within a narrow band around the nominal value of 50Hz. Outside this secure range generating units could be damaged, so they would be disconnected from the grid by the action of protection devices [13]. This could in turn cause a cascading failure and the system could then potentially reach a blackout state.

Frequency deviations from steady state are due to a generation-demand imbalance. The electric frequency in the grid is determined by the rotating speed of thermal generators, which spontaneously slow down when demand is higher than generation, as they release the kinetic energy in their rotating masses in order to restore the power equilibrium (the opposite is true when generation is higher than demand) [14]. Therefore, in the event of an unplanned generation outage in the system, frequency would drop rapidly and significantly. The rate at which the frequency drops is inversely proportional to the level of inertia in the power grid. The aforementioned deterioration of frequency performance in low-carbon grids is due to a greatly reduced level of inertia in the system, as most RES such as wind and solar are decoupled from the grid through power electronics converters and therefore do not naturally contribute to system inertia.

In order to assure a secure operation of the system from a frequency-performance point of view, system operators must make sure that three requirements are met: first, the Rate-of-Change-of-Frequency (RoCoF) must never exceed a certain limit in order to avoid the tripping of RoCoF-sensitive relays; second, the frequency nadir (minimum value of frequency) must always be above a certain value to prevent the activation of Under-Frequency Load Shedding; and third, the frequency deviation in quasi-steady-state (defined as the stable value that frequency must reach 60 seconds after a power outage) must be below a predefined threshold [15]. To maintain the system's frequency within these secure ranges at all times, system operators schedule certain frequency services that would only come into play in the event of a frequency drop.

Frequency services are any type of ancillary service that helps comply with frequency regulation, that is, that helps restore a power equilibrium after a generation/demand outage. Frequency services are: inertia (either traditional inertia from synchronous generators or synthetic inertia from non-synchronous devices such as most RES), Frequency Response (provided by any device such as generators, storage or demand response, each of which have different dynamics in FR provision), damping (typically provided by frequency-responsive loads that reduce their consumption after a frequency drop) and the size of the largest possible loss of generation or demand (since the $N-1$ reliability criterion applies to frequency-services scheduling, operators plan for the worst possible case). For the rest of this document, the cause of a generation-demand imbalance will be limited to a generation outage, leaving out the possibility of a demand outage that would cause a frequency rise. The reason for this choice is that the case studies will be focused in the Great Britain (GB) system, where the biggest concern is a large generation outage, while in other countries like Iceland the opposite is true [16]. However, note that the mathematical formulations presented in this thesis would apply also to a loss-of-demand scenario.

Since the main providers of frequency services are generators, loads and storage devices, these services are inherently related to energy provision. While system inertia and FR were services widely available in grids dominated by thermal generation as by-products of energy production, the increasing scarcity of these services in low-carbon system increments the costs associated to their provision [17]. The cost of operating a traditional power system, was mainly driven by the cost of burning fuel for energy production, but modern RES-dominated power systems show a different behaviour: the overall cost of operating the grid is reduced, since there is no fuel-cost associated with RES, but the fraction of total cost due to providing frequency services has greatly increased, and could reach more than 10% of overall cost in some cases [18]. The cost increase from this higher need for frequency services, driven by the low system inertia levels caused by the non-synchronous RES, could be a barrier to further increasing the share of renewables if efficient methods for scheduling frequency services are not available.

In this context, several works have studied optimal strategies to provide inertia and FR [19–30]. Traditionally, the generation-scheduling algorithms for power grids only enforced the total amount of FR to be above a predefined threshold [19]. Due to the abundant system inertia from conventional thermal plants, this threshold was mainly driven by the requirement for frequency to return to its nominal value following a power outage, i.e. the frequency steady-state limit. However, given that system inertia may be highly scarce at times when high RES production coincides with low demand, the limit for frequency nadir during the transient period starts to drive the FR requirement [25], which requires explicit consideration of post-fault frequency dynamics in order to maintain system security.

Diverse ways of obtaining the frequency-security constraints, namely maximum admissible RoCoF, minimum admissible frequency at nadir and minimum admissible frequency at quasi-steady-state, have been proposed in the literature. Certain assumptions were made in these studies to overcome the mathematical difficulties and obtain relatively simple algebraic constraints suitable for implementation in a Mixed-Integer Linear Program (MILP). Authors in [20] studied the design of an ancillary-service market for FR, based on solving a constrained optimisation problem that guarantees frequency security. The frequency-security constraints were obtained heuristically from dynamic simulations of the system. A similar approach was used in [21, 22], while the other works focus on deducing the frequency-security region by analytically solving the differential equation describing post-fault frequency dynamics. Reference [23] considered the system inertia to be a fixed, known value. Linearisation techniques are proposed in [25,26,28,29] to transform their deduced non-linear constraints. Except [25,26,28], all previous work neglected the effect of load damping on frequency evolution, leading to an overestimation of the frequency challenge and preventing incentivising the potential damping providers.

Since frequency-constrained optimisation is a relatively new area of research, several questions are still open, notably how to obtain security conditions while considering FR services with diverse dynamics, how to optimally schedule the size of the largest loss and how to model regional variations in post-fault frequency within a power system. All these questions are addressed in the present thesis.

1.2 Problem statement and research approach

The main goal of this PhD thesis is to facilitate the integration of RES in a cost-effective manner by developing efficient ways to schedule power generation and frequency services. This scheduling methodology should allow to comply with frequency regulation while minimising the operational costs of a power grid. In order to achieve cost effectiveness, the scheduling method must take into account the high uncertainty in renewable generation. The starting point of the present thesis was to generalise the frequency-security conditions deduced in [17] and integrating the developed constraints in optimisation problems such as the Stochastic Unit Commitment (SUC).

As discussed in Section 1.1, the simultaneous optimisation of energy and frequency services can be achieved by appropriately constraining a scheduling algorithm to guarantee frequency security. The key challenge for obtaining frequency constraints lies on the mathematical complexity of incorporating the differential-equation-driven frequency evolution into the algebraic-equation-constrained optimisation problem. The challenge on mapping the differential equations that describe frequency dynamics into algebraic constraints applicable to a scheduling algorithm comes from the distinct time-scales of both problems: while the scheduling is typically performed every hour, and certainly not more frequently than every few minutes by any system operator, the period of interest for frequency dynamics ranges from sub-seconds to tens of seconds.

With the emergence of new technologies in power grids, new possibilities arise for the delivery of FR. Some devices such as Battery Energy Storage Systems (BESS) have much faster dynamics than thermal generators, and therefore can deliver FR in a significantly shorter time. Therefore, the first research question tackled in this thesis was *how to optimise the FR dynamics from fast devices such as BESS*. These fast dynamics had already been identified by some system operators as a valuable resource to cope with the low-inertia problem, like National Grid, who introduced in 2017 the Enhanced Frequency Response (EFR) service [31]. In the past, Primary Frequency Response (PFR) was the only service considered to contain a frequency decline, for which response must be delivered within ten seconds after a generation-demand imbalance, while EFR must be delivered in just one second. However, no tool was available to co-optimise the provision of these two services.

A graphical description of the FR services defined in Great Britain (GB) at the time of writing this thesis is provided in Figure 1.1, along with an illustration of post-fault frequency regulation [32].

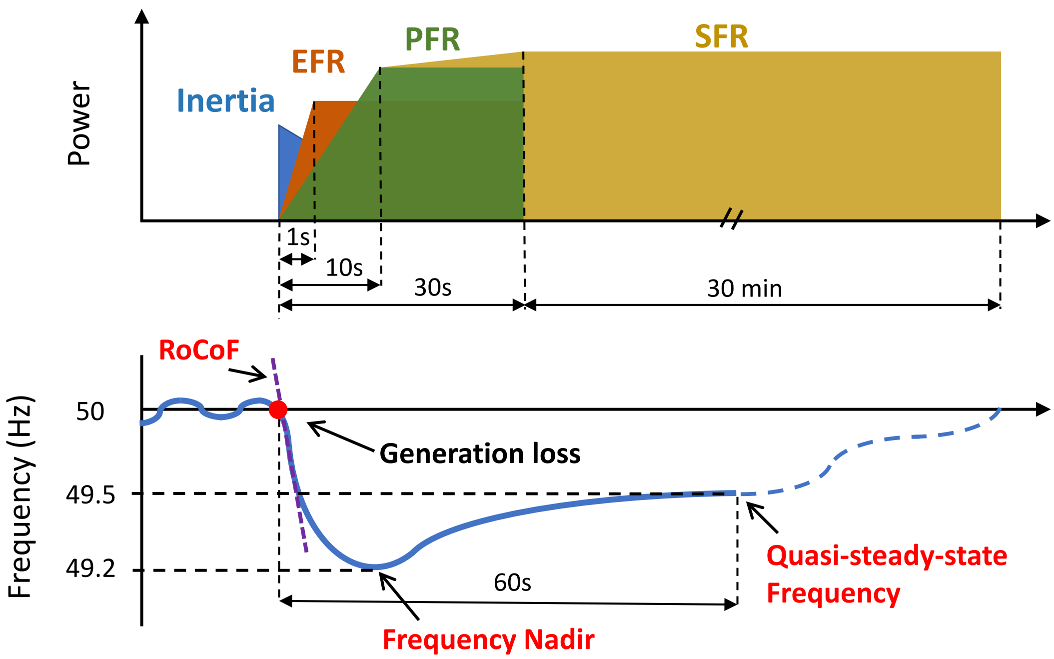

Figure 1.1: Post-fault frequency evolution and the limits that must be respected in GB as per National Grid regulation, along with the power contribution from the different frequency services defined: inertia, Enhanced Frequency Response (EFR), Primary Frequency Response (PFR) and Secondary Frequency Response (SFR).

The second research question addressed in this work was *how to optimise the provision of FR dynamics from any generic provider*, in order to extract the full value of flexibility available in a power system: instead of forcing devices to participate in either the EFR or the PFR services defined by National Grid, such a tool would allow a system operator to co-optimise the FR provision from devices that might not be able to comply with the one-second dynamics established by EFR but are faster than the ten-second definition for PFR.

Finally, the last research question addressed was *how to take into account different regional variations in electric frequency within the power system.* Although frequency has been traditionally assumed to be roughly equal in all of the system's buses, non-uniform distributions of inertia in some systems, driven by the typically remote location of some non-synchronous

RES such as wind, make this assumption less accurate. A detailed discussion of this problem is included in Chapter 4.

The methodology chosen to tackle all these research questions was to obtain analytical, closed-form solutions for the frequency-security region, following the steps of works like [25]. The starting point for this approach is the swing equation, which describes post-fault frequency dynamics in a power system and is discussed in detail in following chapters of this thesis. The choice for deducing security conditions by using analytical methods was driven by the rigorous mathematical descriptions of the frequency-security region that these methods provide, as opposed to the heuristics needed for some methods proposed in the literature which are based on solving comprehensive dynamic simulations of the system. However, in many cases the analytical conditions take the form of very convoluted expressions, or are even impossible to obtain from an exact dynamic model, so some approximations must be used, as discussed in following chapters of this document.

Once the frequency-security constraints are deduced, they can be implemented in optimisation problems to understand the implications of frequency regulation in the operating cost of a power system. Since the Stochastic Unit Commitment (SUC) is used throughout this thesis to analyse such cost, a description of the SUC is provided in the next section.

1.2.1 Stochastic Unit Commitment

The tool used for scheduling power system's generation is called Unit Commitment (UC). The UC is a problem of particular interest when studying the provision of frequency services, since the scheduling of thermal generation determines the level of system inertia, the key driver of post-fault frequency evolution.

UC involves solving an optimisation problem in which the decision variables are the commitment status (on/off) of each generator and the power output of online generators. The objective is to minimise the system's operational cost, subject to several system constraints, such as generation-demand balance, and numerous inter-temporal constraints such as start-up times or maximum ramp rates of thermal units. The UC problem considers a period in the future, typically one day, for which it schedules the system's generation over several planning periods, typically every hour [33].

The traditional type of Unit Commitment is deterministic. This type of UC schedules the generation in the system by assuming that the demand and intermittent generation from RES will mostly follow the forecasts, while some minimum reserve levels are enforced to maintain security of supply in the case of deviations from the forecast. It has been widely used in the past, and it provided an acceptable solution for the operation of traditional power systems, in which penetration of RES was low. However, the use of deterministic UC in low-carbon power systems might lead to either high operation cost or high risk of load shedding, both of which could limit the integration of RES. Therefore, new methods have been developed in recent years to optimally schedule generation in the low carbon power system, notably the Stochastic Unit Commitment (SUC).

SUC considers a wide range of possible realisations of the stochastic variables in the system, particularly RES generation, and it seeks to minimise the expected operating costs of the system. The infinite set of possible realisations is typically discretised into a representative scenario tree, in which each scenario is related to a certain probability of occurrence. SUC has significant advantages over deterministic UC, as demonstrated by several studies such as [25, 34, 35], with the drawback of a much higher computational burden.

The frequency-security constraints deduced in this thesis are implemented in the SUC developed in [36]. Therefore, the frequency-constrained SUC allows to appropriately model the two main operational challenges of systems with high penetration of non-synchronous RES: uncertainty and low inertia. A brief description of the SUC is provided in this section, and the interested reader can refer to [34, 36] for a comprehensive explanation of the model.

This SUC optimally schedules energy production and reserve, minimising the expected operational cost of the system while taking into account the uncertainty in wind generation (other RES could be modelled in a similar fashion). Uncertainty is explicitly modelled by means of a scenario tree, a schematic of which is provided in Figure 1.2. The tree is built by using the quantile-based, scenario-generation method described in [34], where each scenario corresponds to a user-defined quantile of the distribution of net demand (demand minus wind power). From these quantiles, the probability of reaching a particular node in the tree can be derived. For simplicity, scenario trees are constructed in this SUC with branching only at the current-time node, as this approach has been demonstrated to provide similar results to more intricate structures while greatly reducing computational time [34].

A rolling-planning approach is used in the SUC: first, a full SUC optimisation is computed with a 24-hour horizon in an hourly time-step ($\Delta\tau(n) = 1$h). Only the here-and-now decisions in the current-time node are applied, while all future decisions are discarded. In the next time-step, the realisation of the stochastic variable becomes available, as well as updated forecasts. A new scenario tree is then built, covering another 24-hour time horizon, and the SUC optimisation is run again respecting all previous decisions and inter-temporal constraints. This methodology, consisting on building new scenario trees for each time-step, is repeated for the whole duration of the simulation, hence the term rolling-planning.

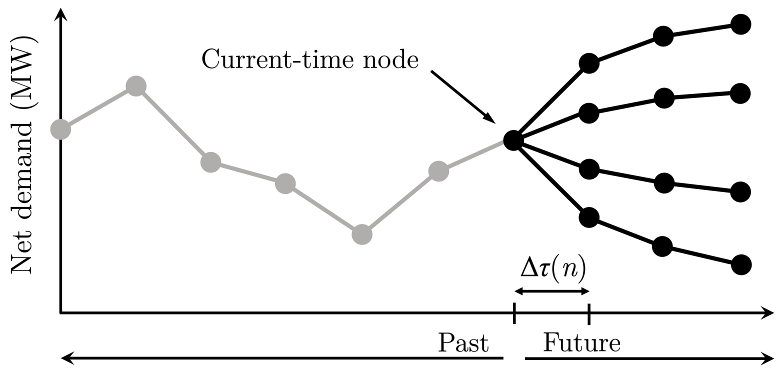

Figure 1.2: Example of a scenario tree used in the Stochastic Unit Commitment. The source of stochasticity is variability of wind generation, which is characterised using wind speed statistics.

The SUC is formulated as an MILP, since Stochastic Programming is a computationally demanding problem so a non-convex formulation would likely be intractable. The objective function of the SUC is the expected operation cost over all nodes in the scenario tree:

$$\min \quad \sum_{n\in\mathcal{N}} \pi(n) \left(\sum_{g\in\mathcal{G}} C_g(n) + \mathrm{c}^{\mathrm{LS}} \cdot \Delta\tau(n) \cdot P^{\mathrm{LS}}(n) \right) \tag{1.1}$$

The sum of the operating cost C_g of all thermal units at each node n, plus the penalties paid for load shedding, is weighted by the probability of reaching that node, $\pi(n)$. The calculation of the probability $\pi(n)$ associated to node n is derived from the user-defined quantiles, using the procedure defined in [34]. The operating cost of generating units g is given by:

$$C_g(n) = \mathrm{c}_g^{\mathrm{st}} \cdot N_g^{\mathrm{sg}}(n) + \Delta\tau(n) \left[\mathrm{c}_g^{\mathrm{nl}} \cdot N_g^{\mathrm{up}}(n) + \mathrm{c}_g^{\mathrm{m}} \cdot P_g(n)\right] \tag{1.2}$$

Note that generating units with the same characteristics are clustered in the SUC to reduce the computational burden [36].

The objective function (1.1) is subject to several constraints, in order to correctly model the behaviour of a power system and assure system security, which are omitted here as they can be found in [34]. Index (n) is dropped from decision variables in following equations in this thesis to make the expressions clearer.

The advantage of SUC over deterministic UC is a lower operational cost in systems with significant penetration of intermittent RES. In particular, the SUC methodology discussed in [35] could reduce operating costs by around 4% when compared to a deterministic UC approach in a system with a 50% wind penetration. The reason behind these savings is the optimal balance between spinning and standing reserve for compensating errors in the RES forecast: while spinning reserve (typically provided by CCGTs in GB) has lower operational cost, it is less flexible due to longer start-up times; standing reserve (provided mainly by OCGTs in GB) has a higher operational cost and therefore its scheduling should be minimised, but it provides higher flexibility with close to zero start-up times.

It is key to be aware of the computational burden of an SUC, which was analysed in [34]. In broad terms, a single UC is solved in each of the quantiles in the scenario tree, while the final solution has to minimise the expected cost over all these UCs. Furthermore, this thesis uses the aforementioned rolling-planning approach in simulations that span up to one year of the operation of a power system, in order to understand the value of different technologies over a long period. Therefore, it becomes necessary to obtain a computationally-efficient formulation for the optimisation problem, including for the frequency constraints which are deduced in the present thesis.

This SUC entails a risk-neutral optimisation, which therefore guarantees minimum expected cost, but might lead to more frequent load shedding than society is used to nowadays. Risk-limiting constraints could be added, such as enforcing a maximum amount of load shedding allowed, so that the impact on public opinion or political consequences are reduced, at the expense of a higher operational cost. These matters are out of the scope of the present work.

A simplified version of the SUC developed in [36], solving a single scenario tree, is freely available in this link for the interested reader:
https://github.com/badber/StochasticUnitCommitment.

By implementing frequency constraints into the SUC, the model assures frequency security by optimally scheduling inertia and FR. Note that there is no explicit cost for these frequency services in the SUC: the cost of frequency services is implicitly considered by the lower efficiency of part-loaded generators.

To illustrate this point, a graphical description of the cost of operating a thermal generator is provided in Figure 1.3, assuming linear pricing for the generator. The cost per MWh of operating a thermal unit always decreases with increasing loading level of the generator, being rated power $\mathrm{P}_g^{\max}$ the most economically-efficient operating point. This implies that part-loading thermal units in order to provide FR always increases the operational cost of the system, even if no explicit cost for FR is considered (note that the FR provision from a generator is given by its headroom). The same reasoning applies for inertia: bringing online a higher number of part-loaded thermal units in order to increase system inertia, increases the per MWh cost of providing energy when compared to the same amount of energy provided by a lower number of fully-loaded generators. Note that the inertia contribution of a generator depends only on its commitment state, not on its power output, as discussed in more detail in Chapter 2.

To summarise, the extra cost per MWh induced by using a higher number of part-loaded generators when compared to generating the same amount of energy using fewer, fully-loaded generators, represents the cost of frequency-services provision in the SUC.

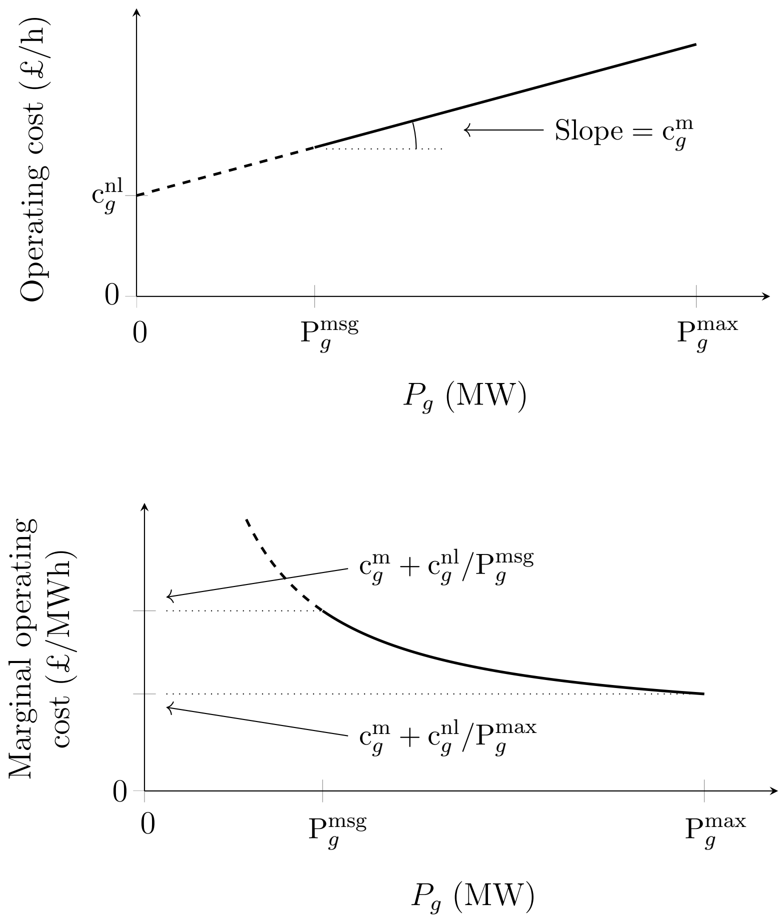

Figure 1.3: Graphical explanation of the operating cost and marginal operating cost of a thermal generator.

1.2.2 Great Britain 2030 power system

The power system considered to conduct simulations in this thesis is the Great Britain 2030 system, which considers a partially-decarbonised generation mix as the United Kingdom implements its green agenda on the road to net-zero emissions by 2050 [11].

This system is characterised by:

1. An inflexible nuclear fleet providing base load and driving the $N-1$ reliability requirement for frequency services, due to the large power rating of some of these nuclear units (such as the operational Sizewell B power station and Hinkley Point C, still under construction).

2. A fleet of gas-fired power plants of two types: Combined-Cycle Gas Turbines (CCGTs) and Open-Cycle Gas Turbines (OCGTs). CCGTs are slow-start generators with high thermal

efficiency (i.e. a high amount of the energy contained in natural gas can be converted into useful electric energy) while OCGTs sacrifice efficiency (and therefore incur in higher fuel costs) for achieving a fast start.

3. Increasing levels of wind penetration. Note that the installed capacity of wind power is a key sensitivity in the case studies in this thesis, as it is still uncertain how much wind power will be available in Great Britain in coming decades. The installed wind capacity will largely drive net demand in GB (demand minus RES power, which must be covered by dispatchable synchronous generators), therefore making wind a key driver of the reduction of inertia in the future GB power system.

4. Varying levels of Battery Energy Storage Systems (BESS) are also considered in the different case studies in Chapters 2 and 3, as this is a recent technology in GB but is expected to keep increasing its penetration due to its advantageous characteristics to operate in conjunction with RES.

5. Power demand ranging from 20GW to a peak of 60GW, higher than current demand levels in GB. This increase reflects the expected growth in demand by 2030 due to partial electrification of heat and transport. The demand profile considered accounts for daily and seasonal variabilities.

The parameters defining the thermal fleet are included in Table 1.1. Some variations of the parameters included in this table are considered in this thesis to run various sensitivity analyses. When such changes to these parameters are considered for a certain case study, these changes are explicitly described in the relevant section.

A copper-plate model is considered in this thesis, i.e. no network constraints are included. This is a typical assumption in scheduling problems such as the Unit Commitment, as an Optimal Power Flow (OPF) could be later solved using the commitment decision from the UC, so that network constraints are respected. Decoupling the UC from the OPF makes each of the two optimisation problems tractable for real systems. The focus on this thesis is put on the UC, since it determines the on/off state of generators and therefore the inertia level of the grid, which is the major driver for post-fault frequency stability.

Table 1.1: Characteristics of thermal plants in GB's 2030 system

	Nuclear	CCGT	OCGT
Number of Units	4	100	30
Rated Power (MW)	1800	500	100
Min Stable Generation (MW)	1400	250	50
No-Load Cost c_g^{nl} (£/h)	0	4500	3000
Marginal Cost c_g^{m} (£/MWh)	10	47	200
Start-up Cost c_g^{st} (£)	N/A	10000	0
Start-up Time (h)	N/A	4	0
Min Up Time (h)	N/A	4	0
Min Down Time (h)	N/A	1	0
Inertia Constant H_g (s)	5	4	4
Max R_g deliverable (MW)	0	50	20
Emissions (tonCO_2/MWh)	0	0.394	0.557

In addition, thermal units are clustered by technology type as presented in Table 1.1, e.g. all CCGTs are modelled as a reference CCGT unit with average characteristics. This helps reduce the computational burden of the SUC, while still providing sufficient insight on the operational cost of the power system: while for a real-time scheduling of a power grid every generator would have to be modelled in detail, clustering by technology type does not distort the average annual operational cost of the system and therefore it is applicable to offline studies for understanding the different drivers of system costs.

Finally, a note on the applicability of results obtained through simulation of the GB 2030 system to other power systems in the world: the qualitative findings of this thesis apply to any system with increasing penetration of non-synchronous generation (wind and solar), although quantitative results would certainly differ. The low inertia induced by higher RES capacity is expected to manifest in isolated or weakly interconnected grids such as GB in the next five years [37], which is why this system has been chosen for showcasing results in this thesis. Nevertheless, although the low-inertia effect will likely appear later in continental grids which are connected through ac transmission lines to neighbouring countries, it is credible that low inertia will also become a concern in the European system as it becomes decarbonised by 2050.

1.3 Thesis structure

This thesis is organised into three technical chapters, with most of the relevant literature review contained within each chapter.

Chapter 2 presents a novel frequency-secured formulation that allows to simultaneously schedule every frequency service currently available in Great Britain: inertia, EFR, PFR and a reduced largest-loss. The chapter starts with a discussion on the economic value of inertia, which is quantified through simulations using the SUC presented in the previous section. Then, a modelling framework is proposed which allows to also co-optimise the size of the largest loss. Lastly, the model is generalised to also consider the provision of EFR. Case studies using the SUC are presented, which show that significant economic savings and carbon-emission reductions can be achieved by applying these operational strategies, while highlighting the synergies and conflicts among alternative frequency services.

Chapter 3 proposes new frequency-security constraints that allow to co-optimise any finite number of FR services with distinguished characteristics, such as different delivery times and activation delays. The problem defined by these frequency-security constraints can be formulated as a Mixed-Integer Second-Order Cone Program (MISOCP), which can be efficiently handled by off-the-shelf conic optimisation solvers. A marginal-pricing scheme for frequency services is deduced from the MISOCP, allowing for the first time to appropriately value multi-speed FR. Furthermore, the model can also take into account the uncertainty in inertia contribution from the demand side by formulating the frequency-security conditions as chance constraints, for which an exact convex reformulation is provided.

Chapter 4 studies the phenomenon of distinct regional frequencies in some low-carbon power systems. Conditions for guaranteeing frequency security in all regions of such systems are proposed, using a mixed analytical-numerical approach that combines theoretical mathematical techniques with regression methods on simulation samples. The deduced constraints are linear and allow the co-optimisation of all frequency services available.

Finally, Chapter 5 summarises the achievements of this thesis and considers some further work that could lead to a more efficient operation of low-inertia systems.

1.4 Original contributions

The main contributions of this thesis are four-fold:

- To develop novel mathematical models that allow to optimise new frequency services that have been proposed by some electricity system operators such as National Grid (Enhanced Frequency Response, reduced largest loss) or have been envisioned for the future (frequency response with diverse dynamics, market for inertia).
- To ensure the computational efficiency of the deduced frequency constraints, which are implemented in the burdensome Stochastic Unit Commitment (SUC) problem. By running SUC case studies we not only demonstrate the effectiveness of the proposed model, but also analyse the value of new technologies to provide frequency services, such as EFR from battery storage or synthetic inertia from wind turbines (which implies extracting the kinetic energy stored in the wind turbine through an appropriate control of the power electronics).
- To develop a marginal-pricing scheme for frequency services that would put in place the right incentives for providers to improve their characteristics, allowing for the first time to appropriately value multi-speed frequency response. Several Economic Dispatch (ED) and Unit Commitment (UC) case studies demonstrate the applicability of this pricing scheme.
- To deduce, for the first time, conditions for regional frequency security in a power grid. As the uniform frequency model is becoming less accurate due to non-uniform distributions of inertia, there is a need to go beyond this model for modelling post-fault frequency evolution. This thesis does so and obtains constraints that guarantee security in a multi-region system.

Chapter 2

Simultaneous Scheduling of Multiple Frequency Services in Stochastic Unit Commitment

This chapter discusses the co-optimisation of energy and frequency-services provision. The chapter starts with a study of the economic value of inertia, using the frequency-secured model developed in [17]. Then, this model is generalised to consider the possibility of optimising the largest loss, therefore dynamically changing the size of the $N-1$ reliability requirement.

Finally, a novel frequency-secured model is developed, which allows to co-optimise every frequency service currently defined in any power system in the world: inertia, Enhanced Frequency Response (EFR), Primary Frequency Response (PFR) and the dynamically-reduced largest loss.

This chapter is based on conference papers [8] and [9], and journal paper [1]. The model presented here has also been used in journal paper [4].

2.1 Understanding the value of inertia

This section discusses the economic value of physical inertia in low-carbon power grids. This value has been quantified by using the SUC framework presented in Section 1.2.1, while including frequency-security constraints that are introduced in this section. The results demonstrate that enhanced provision of inertia would lead to significant economic savings, although these savings vary under different system conditions. The contents of this section correspond to paper [8].

As discussed in Chapter 1, one of the main factors that cause frequency deterioration in low-carbon grids is a highly reduced level of inertia, which is expected to be present in some systems such as Great Britain (GB) in coming years [37]. Therefore, provision of extra inertia from auxiliary sources could support frequency deterioration. The extra inertia could be provided by thermal generators, rotating loads, or even wind generators. Thermal generators and rotating loads could be manufactured with a higher inertia constant, while wind generators could potentially provide "synthetic inertia" through a supplementary control loop in the wind turbine controller, as shown by several studies such as [38–40]. An increased system inertia would induce a decrease in operational costs, as it would not be necessary to schedule as many thermal plants to comply with dynamic frequency regulation.

However, the current market mechanisms do not reward the provision of inertia and therefore there is a lack of incentive for investors to develop as alternative providers of inertia. Reference [20] pointed out the potential benefits of implementing a market for inertia. This section hence focuses on understanding the value of inertia provision and informs the design of market mechanisms for inertia. This study is of interest to both energy market operators and market participants. Its aim is to inform market operators of the necessity for an ancillary-services market for inertia, by quantifying how much they should incentivise inertia provision depending on the system's characteristics and operating conditions. As well, manufacturers of generating plants will be able to assess the revenue that making generators with higher inertia would bring, given that the appropriate market framework is put in place.

In fact, very few studies have analysed the economic value of inertia. The only paper that has attempted to address this issue is [41], in which a security-constrained UC framework is used to quantify the value of inertia in a system with wind generation. However, some assumptions made by this work might lead to imprecise conclusions. A load damping factor of zero is considered, which could lead to over-estimating the value of inertia. A deterministic UC model is used to quantify the value of inertia, which may give inaccurate results when considering wind generation due to the stochastic nature of wind. Furthermore, although the paper uses a security-constrained UC model, only the maximum frequency deviation (frequency nadir) is assured to be maintained under acceptable limits. The maximum RoCoF and quasi-steady-state requirements are not considered. The RoCoF requirement is particularly important when assessing the value of inertia because RoCoF is limited only by scheduling inertia. Ignoring the RoCoF requirement may lead to an underestimation of the value of inertia. Therefore, there is a clear need to accurately assess the value of inertia in power systems.

The following sections present the economic value of inertia, computed from SUC simulations of the GB system with and without extra freely-available inertia. The value of inertia was calculated as the reduction in operational cost for the cases with freely-available extra inertia.

2.1.1 Frequency-security constraints

Certain dynamic-frequency requirements must be complied with to maintain power system security. In GB, the frequency requirements following a power outage are [15]:

- RoCoF must be below 0.125Hz/s at all times to avoid the tripping of RoCoF-sensitive protection relays.

- The frequency nadir must never be below 49.2Hz to prevent the activation of Low Frequency Demand Disconnection (also called Under Frequency Load Shedding).

- Frequency must recover to be above 49.5Hz within 60s after the outage, referred to as the frequency quasi-steady-state requirement.

Due to increasing penetration of non-synchronous RES which would significantly increase the cost of frequency services needed to comply with this regulation, the RoCoF limit is proposed to be relaxed in the near future to 0.5Hz/s through the Loss of Mains Change Programme [42, 43].

The SUC must be constrained so that a sufficient amount of inertia and frequency response are scheduled to guarantee that the RoCoF, nadir and q-s-s limits are respected in the event of a power outage. These frequency-security constraints were deduced in [25] and are as follows.

As explained in [25], the frequency-security constraints can be deduced from the swing equation, which describes the time evolution of frequency deviation after a generation outage [14]:

$$2H \cdot \frac{\mathrm{d}\Delta f(t)}{\mathrm{d}t} + \mathrm{D} \cdot \mathrm{P_D} \cdot \Delta f(t) = \sum_{g \in \mathcal{G}} \mathrm{PFR}_g(t) - \mathrm{P_L^{max}} \tag{2.1}$$

PFR provision by thermal unit g is modelled as:

$$\mathrm{PFR}_g(t) = \begin{cases} \dfrac{R_g}{\mathrm{T_g}} \cdot t & \text{if } t \leq \mathrm{T_g} \qquad (2.2a) \\ R_g & \text{if } t > \mathrm{T_g} \qquad (2.2b) \end{cases}$$

By solving the swing equation (2.1), the RoCoF, nadir and q-s-s constraints can be obtained (refer to [25] for a detailed description of the mathematical process), which are respectively:

$$H \geq \frac{\mathrm{P_L^{max}}}{2 \cdot \mathrm{RoCoF_{max}}} \tag{2.3}$$

$$\frac{2H \cdot R_{\mathcal{G}}}{\mathrm{T_g}} \cdot \log\left(\frac{2H \cdot R_{\mathcal{G}}}{\mathrm{T_g} \cdot \mathrm{P_L^{max}} \cdot \mathrm{D} \cdot \mathrm{P_D} + 2H \cdot R_{\mathcal{G}}}\right) \geq (\mathrm{D} \cdot \mathrm{P_D})^2 \cdot \Delta f_{\mathrm{max}} - \mathrm{P_L^{max}} \cdot \mathrm{D} \cdot \mathrm{P_D} \tag{2.4}$$

$$R_{\mathcal{G}} \geq \mathrm{P_L^{max}} - \mathrm{D} \cdot \mathrm{P_D} \cdot \Delta f_{\mathrm{max}}^{\mathrm{ss}} \tag{2.5}$$

The system level of inertia after the largest possible outage, H, is given by:

$$H = \frac{\sum_{g \in \mathcal{G}} \mathrm{H}_g \cdot \mathrm{P}_g^{\mathrm{max}} \cdot y_g - \mathrm{P_L^{max}} \cdot \mathrm{H_L}}{f_0} \tag{2.6}$$

And the aggregated system PFR is simply the total PFR provided by all thermal generators, i.e. $R_{\mathcal{G}} = \sum_{g \in \mathcal{G}} R_g$.

While the RoCoF and q-s-s constraints, (2.3) and (2.5), are linear, the nadir constraint (2.4) is non-convex in decision variables H and $R_{\mathcal{G}}$. To overcome this problem, reference [25] proposes to reformulate (2.4) as:

$$H \cdot R_{\mathcal{G}} \geq k^* \tag{2.7}$$

Where k^* is the numerical solution of the following equation:

$$\frac{2k^*}{\mathrm{T_g}} \cdot \log\left(\frac{2k^*}{\mathrm{T_g} \cdot \mathrm{P_L^{max}} \cdot \mathrm{D} \cdot \mathrm{P_D} + 2k^*}\right) = (\mathrm{D} \cdot \mathrm{P_D})^2 \cdot \Delta f_{\mathrm{max}} - \mathrm{P_L^{max}} \cdot \mathrm{D} \cdot \mathrm{P_D} \tag{2.8}$$

Note that (2.8) can be solved before solving an optimisation problem such as the UC, since it depends on parameters Δf_{max}, D, $\mathrm{T_g}$ and $\mathrm{P_L^{max}}$, which are fixed for a given power system, and parameter $\mathrm{P_D}$, which varies within time-steps of the UC but is also fixed for each time-step. It is important to point out that k^* is a decreasing function of $\mathrm{P_D}$, as load damping supports frequency recovery in the post-fault state.

Constraint (2.7) contains the bilinear term $H \cdot R_{\mathcal{G}}$, and therefore it is still a non-convex constraint. However, making use of the fact that H is an integer decision variable, since it depends on the binary commitment decision of thermal generators, y_g, reference [25] proposes a big-M linearisation method. Big-M linearisation allows to linearise a bilinear constraint (i.e. containing the product of two linear variables) where at least one of the variables is integer. This is achieved through introducing an auxiliary binary variable and four additional constraints, the interested reader is referred to the several available texts on the topic for further details [44, 45]. This big-M linearisation allows to implement the frequency-security constraints (2.3), (2.5) and (2.7) in a Mixed-Integer Linear Program (MILP) such as the SUC presented in Section 1.2.1.

To conclude the discussion on frequency-security constraints, note that an increased system inertia would induce a decrease in operational costs, as the SUC algorithm would not need to schedule as much inertia to comply with (2.3) and (2.7). Further discussion on this reasoning is included in the following section, making use of examples to better illustrate our point.

2.1.2 Annual value of inertia

This section presents the results and analysis of the case studies run to understand the value of inertia in low-carbon systems. The characteristics of the generation mix used for this work are included in Table 2.1. The load damping factor, D, was set to 0.5%/Hz. For the SUC, a scenario tree branching only in the current-time node was used, as the one shown in Figure 1.2, with net-demand quantiles of 0.005, 0.1, 0.3, 0.5, 0.7, 0.9 and 0.995. (refer to [34] for further explanation on scenario trees in SUC). A penalty for emissions of £150/ton$\mathrm{CO_2}$ was also considered.

First, the annual savings due to one extra unit of inertia (one $\mathrm{MW{\cdot}s^2}$) are analysed under two different RoCoF requirements: a $\mathrm{RoCoF_{max}}$ of 0.5Hz/s and a $\mathrm{RoCoF_{max}}$ of 0.25Hz/s. Although current National Grid regulation establishes that RoCoF must be below 0.125Hz/s [15], relaxing this requirement was proposed by [42], and [25] demonstrated that a relaxed $\mathrm{RoCoF_{max}}$ would

Table 2.1: Characteristics of thermal plants

	Nuclear	CCGT	OCGT
Number of Units	6	110	30
Rated Power (MW)	1800	500	200
Min Stable Generation (MW)	1800	200	50
No-Load Cost c_g^{nl} (£/h)	0	7809	8000
Marginal Cost c_g^{m} (£/MWh)	10	51	110
Start-up Cost c_g^{st} (£)	N/A	9000	0
Start-up Time (h)	N/A	4	0
Min Up Time (h)	N/A	4	0
Min Down Time (h)	N/A	1	0
Inertia Constant H_g (s)	5	5	5
Max R_g deliverable (MW)	0	50	20
Emissions (kgCO_2/MWh)	0	368	833

significantly reduce the system's operational cost. Therefore, we consider here two different values for this relaxed RoCoF limit. The results are presented in Figure 2.1 for several levels of wind capacity, since wind capacity is a variable of interest because the level of wind penetration in the future GB system remains uncertain: while there are roughly 20GW of wind installed in GB as of 2020, up to 60GW are considered in this thesis. The level of 60GW could be reached sometime within the 2030 to 2050 period, according to National Grid's projections [46].

As can be seen in Figure 2.1, the value of inertia monotonically increases with installed capacity of wind generation. In the case of low installed capacity of wind, the value of inertia is relatively low. This is the case in the present British system, which is still dominated by conventional plants, hence there is no need to establish a market for inertia. However, in the case of 60GW of wind capacity, one extra unit of inertia would reduce the annual system operation cost by more than £1m, for a $\text{RoCoF}_{\text{max}}$ of 0.5Hz/s. Figure 2.1 also shows that relaxing the RoCoF requirement to 0.5Hz/s would reduce the value of inertia. Nevertheless, inertia would still have a significant value in this scenario.

In order to analyse the relative savings due to addition of inertia, let's consider a particular example. For the case of 30GW of wind capacity and a $\text{RoCoF}_{\text{max}}$ of 0.5Hz/s, the annual operational cost of the system is of £12.22bn. The value of inertia for that same case is of

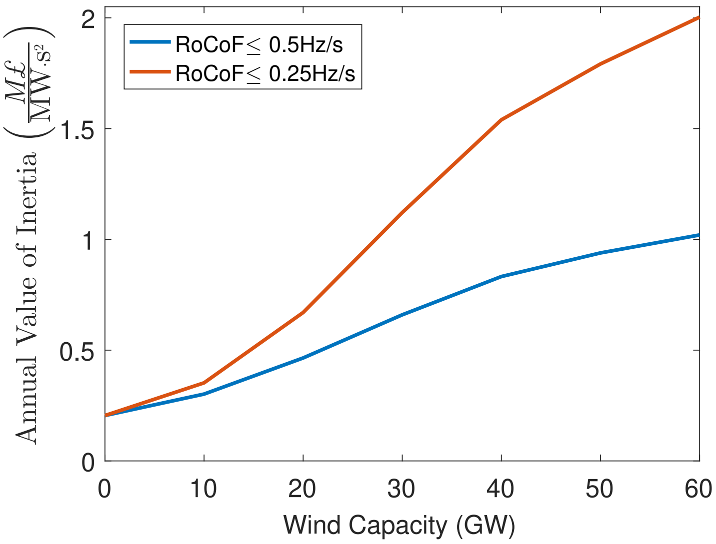

Figure 2.1: Annual value of inertia for different levels of wind capacity.

£659.5k, as can be observed in Figure 2.1. This might seem as an insignificant reduction in cost. However, this is the value of just one extra unit of inertia (one MW$\cdot$s^2), so the savings would be much higher if the extra inertia in the system was further increased.

It has been demonstrated that provision of extra inertia leads to a reduction in operational costs. This should be recognised and rewarded, so that the investors would be incentivised to invest in alternative sources for the provision of inertia. Under a market that properly rewards the provision of inertia, the results in Figure 2.1 can be used to inform the investment.

2.1.3 Instantaneous value of inertia

In addition to annual benefits from extra inertia provision, it is also important to recognise that the value of inertia may vary significantly from hour to hour, depending on the system's conditions. Therefore, we further analyse the hourly economic savings that an additional unit of inertia (one MW$\cdot$s^2) in the system would deliver, for a particular demand-wind condition. The results are presented in Figure 2.2 for a RoCoF$_{\text{max}}$ of 0.5Hz/s and 0.25Hz/s.

As shown in Figure 2.2a, the value of inertia is directly linked with the level of net demand (difference between demand and wind generation). Two distinctive areas can be observed: an area with a low value for inertia, but with an increasing trend, located in the high-demand, low-wind region of the graph; and a relatively flat area with a high value for inertia, located in

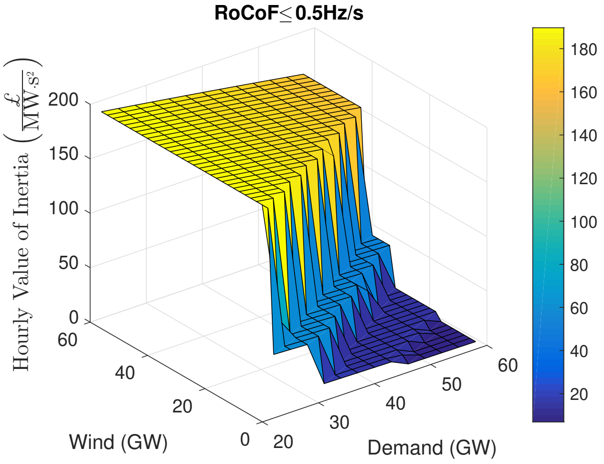

(a) RoCoF requirement of 0.5Hz/s

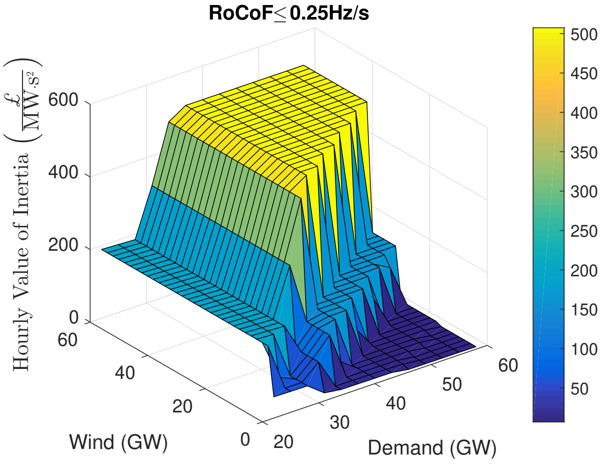

(b) RoCoF requirement of 0.25Hz/s

Figure 2.2: Instantaneous value of inertia under different demand-wind conditions.

the high-wind region. The difference between these two areas can be explained if we consider the effect of wind curtailment. When net demand is low, the frequency-response requirement is high due to the low level of system inertia (note that nadir is the binding constraint, as explained further on). Then, wind generation must be curtailed in order to maintain enough conventional plants online, as they need to provide sufficient inertia and frequency response to assure frequency security. In those cases, adding extra inertia allows for less wind to be curtailed, therefore highly reducing the operational costs as wind generation has zero marginal cost and zero carbon emissions. This situation corresponds to the high-wind region of the graph. One can also notice that the value of inertia in this high-wind region slowly decreases for increasing demand. This result can be explained by the fact that nadir is the binding constraint, as the increased contribution of load damping lowers the requirement for H and $R_{\mathcal{G}}$ for higher levels of demand (refer to constraint (2.7) to understand the contribution of load damping on supporting the nadir).

The other distinctive area in Figure 2.2a is related to cases with high net demand, in which no wind generation would be curtailed. In those cases, corresponding to the high-demand, low-wind region, the extra inertia still has some value, but one order of magnitude lower than in the wind-curtailment cases. For these high-net-demand cases, extra inertia reduces the requirement for provision of frequency response $R_{\mathcal{G}}$, allowing a smaller number of thermal units to run in the partially-loaded mode. This effect slightly reduces the operational cost of the system.

This same study was repeated for a $\text{RoCoF}_{\text{max}}$ of 0.25Hz/s and the results are presented in Figure 2.2b. The two distinctive areas in Figure 2.2a can also be seen in Figure 2.2b: a flat area with a high value for inertia, located in the high-demand, high-wind region; and an area with a low value for inertia, located in the high-demand, low-wind region of the graph. The value of inertia is much higher in both these areas, when compared to those same regions in Figure 2.2a. This higher value is due to RoCoF being the binding constraint for a level of demand higher than 30GW in Figure 2.2b. As load damping helps lower the nadir requirement for high levels of demand and the RoCoF requirement is tighter in this case (remember that $\text{RoCoF}_{\text{max}} = 0.25$Hz/s), RoCoF becomes the binding constraint for demand levels higher than 30GW. This is graphically demonstrated in Figure 2.2b: the value of inertia in the yellow area does not decrease for increasing demand, meaning that nadir is not the binding constraint (no load damping effect is present).

Note that the value of inertia in Figure 2.2b is highest in the yellow area of the graph. As RoCoF is the binding constraint there and net demand is very low, a high number of conventional plants are scheduled only to provide inertia. Extra inertia provision for those wind-demand conditions would directly reduce the number of online plants and therefore significantly reduce the curtailment of wind, which explains the very high value of inertia in that region. Notice however that for levels of demand lower than 30GW, inertia has the same value as in the $\text{RoCoF}_{\text{max}} = 0.5$Hz/s case (shown in Figure 2.2a). That is because nadir is the binding constraint in that region, as the effect of load damping is not very significant due to the low level of demand. In summary, inertia is more valuable when RoCoF is the binding constraint, as RoCoF directly depends on the system's level of inertia H (see constraint (2.3)), while nadir depends on the product $H \cdot R_{\mathcal{G}}$ (see constraint (2.7)).

The main conclusion that can be made from these results is that the instantaneous value of the system must be carefully studied for each power system before designing an adequate inertia market, as there are many nuances. However, a key result that holds true for any system, regardless of which constraint is binding, is that inertia is most valuable when it allows for wind curtailment to be reduced. Notice also that inertia is more valuable if the RoCoF requirement is tighter, but it still has a significant value in a relaxed-RoCoF scenario.

The study presented in this section serves as a starting point for informing the design of an hourly inertia market, as it clearly demonstrates the time-varying value of inertia provision, depending on the different system's conditions.

2.1.4 Marginal value of inertia

The previous two studies have demonstrated the value of adding an extra unit of inertia in the system. This section will focus on analysing how much extra inertia the system would need. Figure 2.3a shows the results for a one-year-long simulation, considering two levels of wind penetration: 15GW, roughly the current wind capacity of the Great Britain network [47]; and 50GW, a possible future scenario with high wind penetration. A $\text{RoCoF}_{\text{max}}$ of 0.5Hz/s has been considered for that study. The results of the same study, but considering a $\text{RoCoF}_{\text{max}}$ of 0.25Hz/s, are shown in Figure 2.3b.

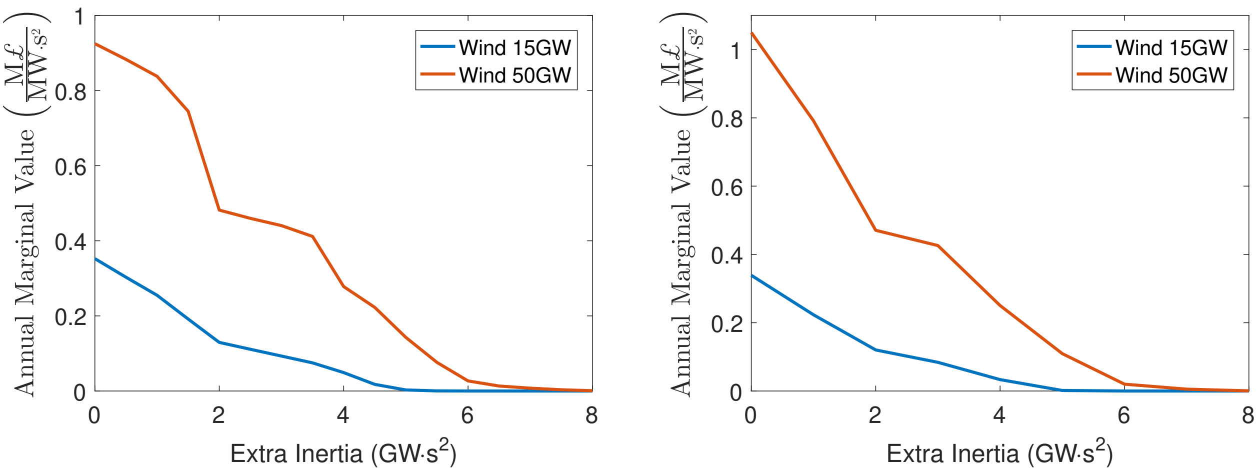

(a) RoCoF requirement of 0.5Hz/s

(b) RoCoF requirement of 0.25Hz/s

Figure 2.3: Annual marginal value of inertia.

The marginal value presented in these figures has been calculated as the difference between economic savings from adding a certain amount of extra inertia to the system, and savings from adding the immediately lower amount of extra inertia. As can be seen in both Figures 2.3a and 2.3b, the marginal value declines along with increased provision of inertia, and saturates when more than 5GWs^2 are added to the 15GW-wind-capacity case, or 7GWs^2 to the 50GW-wind-capacity case.

The results presented in this section need to be taken into consideration when developing market mechanisms for inertia, because the value of inertia would start decreasing as investors decide to provide higher amounts of extra inertia.

2.2 Optimising the size of the largest-possible outage

One potential solution for the low-inertia challenge consists on reducing the largest possible outage in the system, as proposed by National Grid in a recent report [31]. In Great Britain's (GB) system, this would be achieved by part-loading nuclear plants under certain system's conditions, as these are the largest sources of power in the grid. However, the effectiveness of this option has not yet been analysed, due to the lack of a tool allowing to carry out this study. The present section focuses on developing such a tool and using it to analyse the operational benefits that this "nuclear part-loading" approach would bring, both in terms of reduction in cost and in carbon emissions. Note that the optimisation of the size of the largest loss is done for minimising overall system costs, that is, the combined cost of energy and frequency services.

The size of the largest contingency was modelled in a frequency-secured UC formulation in [48], which considered a variable largest outage in a competitive market-dispatch framework. Simulations were used to deduce the frequency-security constraints, an approach which only allows to cover some of the operational conditions. Instead, here we deduce analytical constraints from a mathematical model of the time-evolution of frequency.

The present section builds on the work in [25], which introduced inertia-dependent Frequency Response (FR) requirements in an SUC. The SUC formulation in [25] is expanded here in order to explicitly model a variable largest-possible power loss in the system. The largest loss is now considered as a decision variable in the UC, which then optimises the system's operation by dynamically balancing the cost of deloading and the savings from a reduced need for inertia and FR. Decreasing the largest loss might be optimal depending on the demand and RES generation in the system.

In addition, here we propose an approximation for the effect of load damping on frequency nadir. Most of the previous work on frequency-secured UC such as [21, 23, 24] has neglected the effect of load damping, as it would yield complicated mathematical expressions for the nadir requirement. Authors typically argue that the impact of load damping on the need for inertia and FR would be small in any case, and therefore it is acceptable to ignore it. However, [25] demonstrated that a damping factor of 1%/Hz would reduce operational costs by 5%, for the GB power system. The approximation proposed here allows to model the non-negligible effect of load damping, while still giving a simple linear expression for the nadir constraint.

2.2.1 Modelling the largest-possible outage as a decision variable

This section presents frequency-security conditions which constitute an expanded version of the framework described in [25]. As compared to [25], where the largest possible loss took a fixed value ($P_\mathrm{L} = \mathrm{P}_\mathrm{L}^\mathrm{max}$), the largest loss is modelled here as a decision variable defined as:

$$P_\mathrm{L} \geq P_g \qquad \forall g \in \mathcal{G} \tag{2.9}$$

Note that (2.9) is easily generalisable to consider any source of power production, such as an interconnector importing power from another grid.

The frequency-security constraints presented in Section 2.1 are now modified to account for this variable P_L. Constraints (2.3) and (2.5) are still linear even when $\mathrm{P}_\mathrm{L}^\mathrm{max}$ is substituted by P_L, and therefore can be directly implemented in an MILP. However, as P_L is modelled as a decision variable in the present work, the nadir constraint (2.4) becomes non-convex. It is not possible to linearise this constraint for its inclusion in an MILP, given the logarithmic function and the several bilinear terms $H \cdot R_\mathcal{G}$, some of which appear within the argument of this logarithmic function. Therefore, here we deduce a new nadir constraint, which is obtained again by solving the swing equation (2.1), but this time neglecting its load-damping term. The nadir constraint then becomes:

$$H \cdot R_\mathcal{G} \geq \frac{(P_\mathrm{L})^2 \cdot \mathrm{T_g}}{4 \cdot \Delta f_\mathrm{max}} \tag{2.10}$$

Neglecting the effect of load damping yields a more conservative nadir constraint, as load

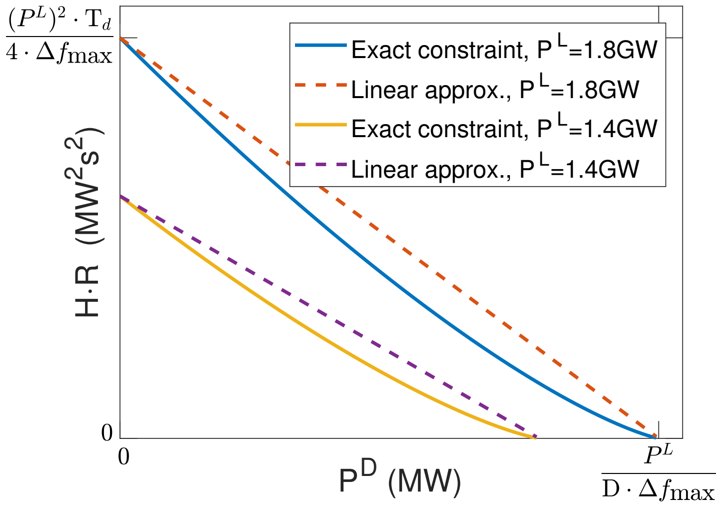

Figure 2.4: Feasible regions defined by constraint (2.4), for two different values of P_{L}. The feasible region for each value of P_{L} is the epigraph of each curve.

damping helps complying with the nadir requirement. However, in the following section we propose a linear approximation to the effect of load damping on supporting the frequency nadir. In addition, we linearise the nadir constraint for its inclusion in an MILP.

In order to model the effect of load damping on the nadir constraint, we propose the following linear term:

$$H \cdot R_{\mathcal{G}} \geq \frac{(P_{\mathrm{L}})^2 \cdot \mathrm{T_g}}{4 \cdot \Delta f_{\mathrm{max}}} - \frac{\mathrm{D} \cdot \mathrm{P_D} \cdot \mathrm{T_g}}{4} \cdot P_{\mathrm{L}} \tag{2.11}$$

This linear term can be deduced by careful examination of (2.4). The graphical solution for the exact nadir constraint (2.4) is given in Figure 2.4, for two different fixed values of P_{L}. As $H \cdot R_{\mathcal{G}} = f(\mathrm{P_D})$ is a convex and monotonically decreasing function, it can be inner-approximated by a line. The y-intercept of that line is given by the right-hand side of (2.10), while the slope of the line can be obtained by considering the largest possible value that $\mathrm{P_D}$ can take. Therefore, the linearised effect of load damping on nadir, represented by the dashed lines in Figure 2.4, is given by (2.11).

Note that the inner approximation of the nadir constraint by a line implies an underestimation of the actual effect of load damping, as can be clearly observed in Figure 2.4. However, this underestimation is still less conservative than simply neglecting the effect of damping.

Constraint (2.11) must be linearised before being implemented in an MILP, as it contains two non-linear terms: "$H \cdot R_{\mathcal{G}}$" and "$(P_{\mathrm{L}})^2$". In an SUC problem, it is critical to use an MILP formulation: a Mixed-Integer Non-Linear Program would considerably increase the computational time needed to solve the problem, so the SUC would likely become intractable. In order to linearise the squared term in constraint (2.11), decision variable P_{L} can be discretised in s segments as follows:

$$\begin{cases} H \cdot R_{\mathcal{G}} + \beta \cdot \mathrm{P}^{\mathrm{L}}_{1} \geq \left(1 - m^{\mathrm{L}}_{1} \; \cdots - m^{\mathrm{L}}_{\mathrm{s}}\right) \cdot \dfrac{(\mathrm{P}^{\mathrm{L}}_{1})^2 \cdot \mathrm{T_g}}{4 \cdot \Delta f_{\mathrm{max}}} & (2.12.1) \\ H \cdot R_{\mathcal{G}} + \beta \cdot \mathrm{P}^{\mathrm{L}}_{2} \geq \left(1 - m^{\mathrm{L}}_{2} \; \cdots - m^{\mathrm{L}}_{\mathrm{s}}\right) \cdot \dfrac{(\mathrm{P}^{\mathrm{L}}_{2})^2 \cdot \mathrm{T_g}}{4 \cdot \Delta f_{\mathrm{max}}} & (2.12.2) \\ \qquad\vdots & \\ H \cdot R_{\mathcal{G}} + \beta \cdot \mathrm{P}^{\mathrm{L}}_{\text{s-1}} \geq \left(1 - m^{\mathrm{L}}_{\mathrm{s}}\right) \cdot \dfrac{(\mathrm{P}^{\mathrm{L}}_{\text{s-1}})^2 \cdot \mathrm{T_g}}{4 \cdot \Delta f_{\mathrm{max}}} & (2.12.(\text{s-1})) \\ H \cdot R_{\mathcal{G}} + \beta \cdot \mathrm{P}^{\mathrm{L}}_{\mathrm{s}} \geq \dfrac{(\mathrm{P}^{\mathrm{L}}_{\mathrm{s}})^2 \cdot \mathrm{T_g}}{4 \cdot \Delta f_{\mathrm{max}}} & (2.12.\mathrm{s}) \\ m^{\mathrm{L}}_{1} + m^{\mathrm{L}}_{2} + \cdots + m^{\mathrm{L}}_{\mathrm{s}} \leq 1 & (2.12.(\text{s+1})) \end{cases}$$

Where β is defined as:

$$\beta = \frac{\mathrm{D} \cdot \mathrm{P_D} \cdot \mathrm{T_g}}{4} \tag{2.13}$$

The binary variables m^{L}_{i} enforce that only one of the constraints in (2.12) is activated. For this discretisation of P_{L} to hold, a new decision variable must be defined:

$$P^{\mathrm{L}}_{\mathrm{nadir}} = m^{\mathrm{L}}_{1} \cdot \mathrm{P}^{\mathrm{L}}_{1} + m^{\mathrm{L}}_{2} \cdot \mathrm{P}^{\mathrm{L}}_{2} \cdots + m^{\mathrm{L}}_{\mathrm{s}} \cdot \mathrm{P}^{\mathrm{L}}_{\mathrm{s}} \tag{2.14}$$

The following constraint applies to $P^{\mathrm{L}}_{\mathrm{nadir}}$:

$$P^{\mathrm{L}}_{\mathrm{nadir}} \geq P_{\mathrm{L}} \tag{2.15}$$

By enforcing constraints (2.12) and (2.15), the squared term $(P_{\mathrm{L}})^2$ in (2.11) is linearised. Then, the bilinear term $H \cdot R_{\mathcal{G}}$ appearing in each of the constraints in (2.12) must also be linearised, for which we use a big-M method [44, 45]. With these two linearisations, the nadir constraint can be implemented in an MILP.

2.2.2 Cost of providing frequency services

In order to demonstrate the benefits from dynamically limiting the largest power infeed loss, the SUC model described in Section 1.2.1 was used to run several case studies. Each case study simulated one full year of operation of the GB power grid, considering the system characteristics described in Section 2.1.2. Different wind-penetration levels were analysed, as the amount of renewable generation that will be present in the GB system in the future is still uncertain. The results of these simulations are analysed here, in terms of the operational cost of the system, load factor of large nuclear units and carbon emissions.

As mentioned before, reducing the largest possible power loss could be achieved in GB's system by deloading large nuclear plants. It is important to remark that the reason behind deloading nuclear units might not always be to reduce the cost of frequency services, i.e. the cost of providing inertia and PFR. In high-wind-generation conditions, deloading nuclear allows to accommodate more wind, which is zero-cost energy, therefore reducing the total cost of energy provision. However, the present study focuses on deloading nuclear plants just to reduce the need for inertia and FR.

In this section we analyse the cost of providing frequency services, namely inertia and FR. The amount of inertia and FR needed to comply with the frequency-security constraints is provided by running part-loaded thermal generators. Running a high number of part-loaded generators is more expensive than producing the same amount of energy from a lower number of fully-loaded generators, and it potentially causes RES curtailment. The difference in operational cost between these two cases is what we refer to as "cost of frequency services".

For these simulations, we compare three different scenarios: the current largest loss in GB's system, of 1.32GW; the projected largest loss in 2030, which will be of 1.8GW; and a variation of the latter scenario in which several nuclear plants, not just one, are rated at 1.8GW.

First of all, we analyse the benefits from deloading based on the current single largest plant in GB. In Figure 2.5 the annual cost of frequency services for the 1.32GW-largest-loss case is presented. Two different operational strategies are considered: in "Fixed Largest Loss", the largest nuclear plant is forced to operate at maximum output at all times; in "Optimised Largest Loss", this plant is allowed to reduce its power output by 33% of its rating. Although the

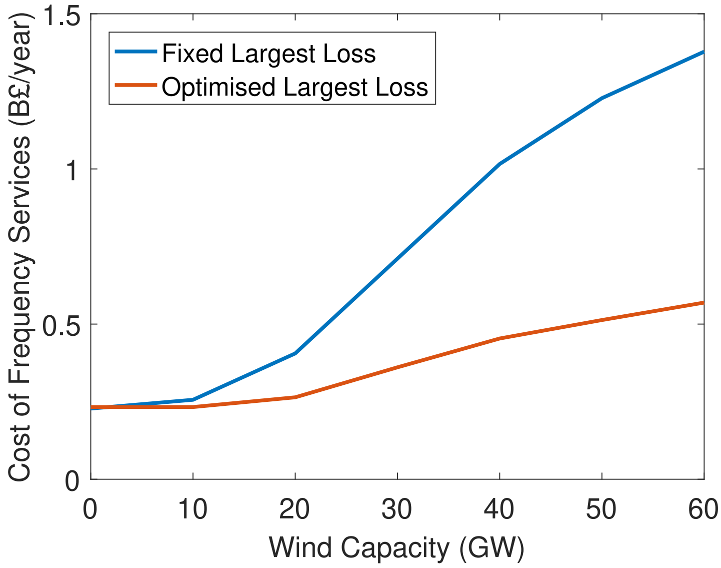

Figure 2.5: Annual cost of frequency services under different wind-penetration scenarios, for a largest possible loss of 1.32GW.

quantitative results presented in Figure 2.5 might vary depending on the characteristics of the power system studied, this figure shows a clear trend that would hold in any system: reducing the largest loss has a significant positive impact in the cost of frequency services, particularly for high-wind-penetration cases.

Here we also study the impact of a higher largest-possible-loss in the future GB system. In Figure 2.6 we present the cost of frequency services for the projected largest loss of 1.8GW, as well as a variation of this scenario in which 6 nuclear plants have a 1.8GW rating. Large nuclear plants are again allowed to deload by 33% of their rating. Note that the cost of frequency services for the "Fixed Largest Loss" case is the same for both the scenario with one large plant rated at 1.8GW, and for the one with 6 large plants. By comparing this "Fixed Largest Loss" case in Figure 2.6 with the one in Figure 2.5, one can notice that the cost of frequency services roughly doubles in Figure 2.6 for every wind-penetration scenario. This issue should be brought to the attention of system planners, since a larger nuclear plant may be a sensible option from an energy-cost point of view, but its implications in increased ancillary-services cost for the system must also be considered. Figure 2.6 also demonstrates that deloading large nuclear units brings even further savings, in absolute terms, for a 1.8GW-largest-loss when compared to the 1.32GW case. Regarding the scenario with 6 plants rated at 1.8GW, as all 6 plants must be

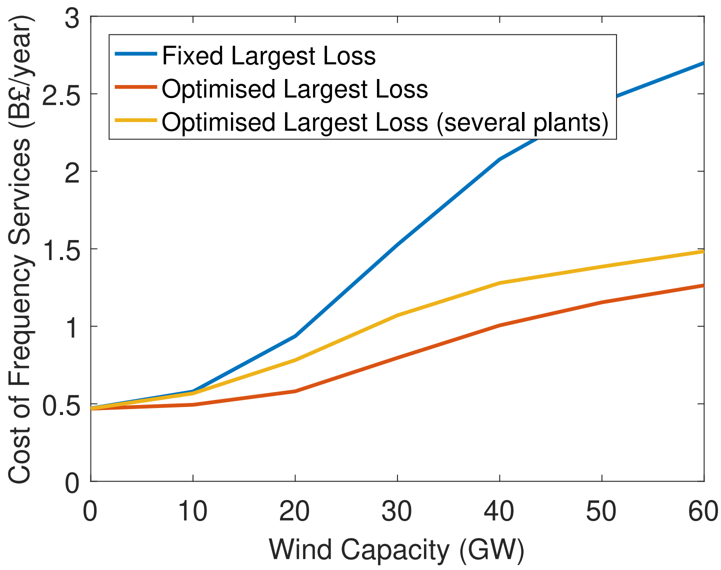

Figure 2.6: Annual cost of frequency services under different wind-penetration scenarios, for a largest possible loss of 1.8GW.

deloaded in order to effectively reduce the largest possible loss, the deloading strategy is less effective, although it still leads to significant savings.

Finally, one can notice that for all scenarios in both Figures 2.5 and 2.6, the cost of frequency services increases with increasing wind penetration, as would be expected: when non-synchronous wind generation, which does not contribute to inertia or FR, replaces conventional generators, the system's levels of inertia and FR are reduced; then, part-loaded conventional generators must be brought online just to provide frequency services, therefore increasing the operational cost of the system.

2.2.3 Analysis of the load factor of nuclear units

In Section 2.2.2 the savings in operational cost due to reducing the largest possible loss have been demonstrated. However, the impact of deloading nuclear units on the investment return of these generation plants should also be considered.

Nuclear plants have very high investment costs, and they are expected to provide inexpensive, carbon-free, base-load energy. However, if these plants do not operate in a base-load mode but are instead deloaded at times in order to reduce the largest possible loss, the investment might be less attractive. While the present work focuses on the operational aspects of the power grid,

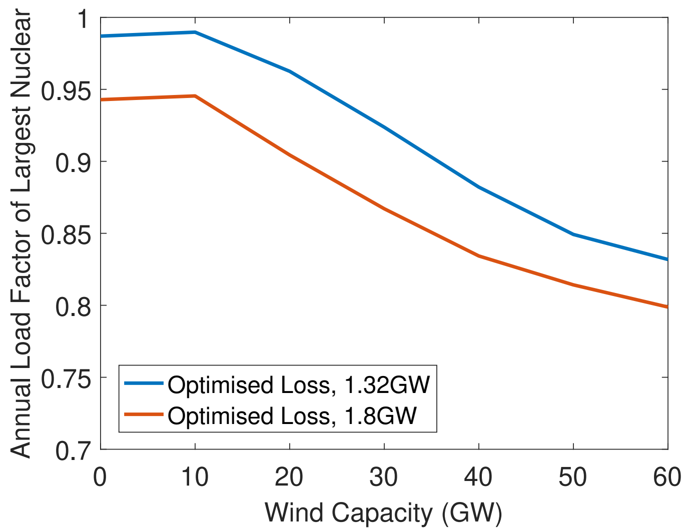

Figure 2.7: Annual load factor of the largest nuclear unit as a function of wind capacity. Two different ratings of the largest nuclear unit are considered.

and therefore investment costs are not taken into account, we analyse the load factor of the largest nuclear unit to inform system planners of this issue.

Figure 2.7 presents the results of our study. One can notice that an increased rating of the largest nuclear plant decreases the load factor, as the 1.8GW plant is more frequently deloaded than the 1.32GW plant. If deloading nuclear units were a strategy to be implemented by system operators, system planners should be aware that this strategy might lead to a significantly reduced load factor for these units.

2.2.4 Impact on carbon emissions

As mentioned in Section 2.2.2, in certain occasions a number of part-loaded thermal generators must be online in order to provide inertia and FR. In high-wind-generation conditions, wind power might be curtailed in order to keep these part-loaded thermal plants online. By reducing the largest possible loss, less inertia and FR is needed, and therefore less part-loaded plants are required to be online. Then, by reducing the largest loss, carbon emissions are also reduced, since more wind power can be accommodated.

Figure 2.8 shows the amount of carbon emissions that would be cut annually by allowing the largest nuclear plant to deload. A very significant reduction in carbon emissions is achieved, particularly for cases of high wind capacity and a 1.8GW largest loss. Nevertheless, even for a

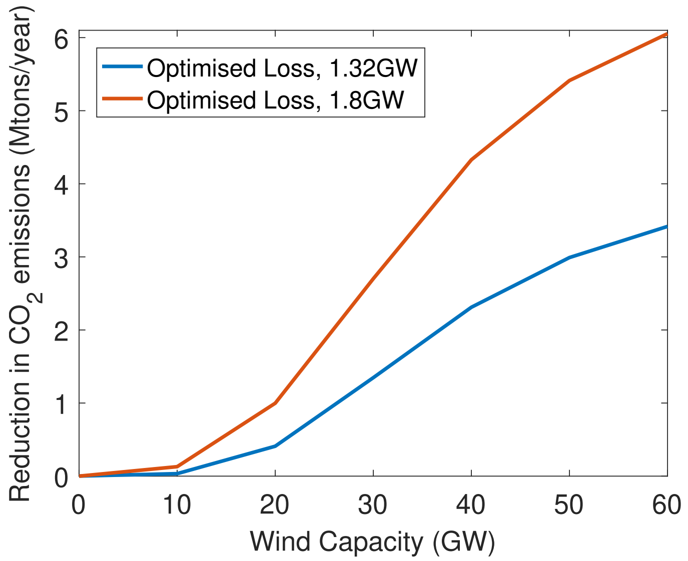

Figure 2.8: Reduction in carbon emissions due to allowing the largest nuclear unit to deload, as a function of wind power capacity.

1.32GW-largest-loss case the reduction in emissions is considerable. Given the strict emission targets recently set in countries all over the world, reducing the largest possible loss has proved to be an effective strategy to comply with this legislation.

2.3 Co-optimisation of multiple frequency services

Due to the need for alternative frequency services, particularly in weakly-interconnected system that are expected to suffer from low inertia such as Great Britain (GB), National Grid has recently proposed two new services: Enhanced Frequency Response (EFR), which was introduced as a product in 2017 [49], and a reduced largest loss, which was proposed as a more efficient alternative to creating a market for inertia in a report in 2017 [31]. However, the tools to optimise the provision of these two services were not available at the time of writing this report. It is critical to develop such a tool in order to fully understand the economic value of each service. Regarding EFR, optimising its provision would allow to quantify the amount of EFR the system needs, so that the appropriate market structure for it can be created. Furthermore, only by optimising a dynamically-reduced largest power infeed in the scheduling of the GB system one could carry out an accurate analysis of the claim made in [31] that a reduced largest loss would be more efficient than creating a market for inertia.

EFR was defined as a service for which response must be delivered in less than one second, as opposed to ten seconds for PFR. This service allows to recognise the faster dynamics in power injection of some novel technologies such as Battery Energy Storage Systems (BESS). A pre-defined amount of 200MW EFR was procured throughout the year in 2017, while the optimal portfolio of frequency services actually varies along with changes in system conditions. The only work that has studied the impact of EFR in the UC problem is [29], which proposed a UC framework to optimise EFR provision from BESS. However, this work relied on the assumption that EFR is delivered instantaneously after a power outage, an assumption that greatly reduces the mathematical complexity of the resulting constraints but fails to reflect the actual characteristics of EFR.

Regarding the largest power infeed, the security standard states that enough FR must be scheduled to cover the loss of this largest infeed ($N-1$ reliability requirement). Recently, National Grid has proposed to reduce the largest infeed [31], as a measure to tackle the frequency stability challenge under certain system conditions. Our previous work [9] introduced a model allowing to optimise the size of the largest infeed, while that model is generalised here to allow the co-optimisation of alternative frequency services such as EFR.

Moreover, synthetic inertia (SI) provision from wind turbines has been considered as an alternative to resolve the frequency-decline challenge. Although some studies have analysed the potential value of SI such as [50], it is not clear yet how SI would affect the value of alternative frequency services.

Given this background, this section proposes analytical constraints for a secure post-fault frequency evolution in an SUC model. The key contributions of this work are three-fold:

1. We propose novel frequency stability constraints that, for the first time, allow to simultaneously co-optimise the provision of synchronised and synthetic inertia, PFR, EFR and a dynamically-reduced largest power infeed. The contribution of load damping to support the frequency nadir is also modelled through a linear inner approximation.

2. The resulting non-convex frequency-nadir constraint is linearised for implementation in a

computationally-demanding SUC framework. The accuracy of the linearisation method can be tuned by the user, while frequency security is guaranteed in all cases.

3. The proposed model is applied to the GB 2030 system to demonstrate the benefits of simultaneously co-optimising a portfolio of diverse frequency services, as well as the impact of competition among these services.

The model presented here generalises the model in Section 2.2, since the present model adds the option to optimise EFR provision. However, the deduction of frequency-security constraints presented here is not equivalent to the one in Section 2.2, since the generalisation to include EFR cannot be done using the same mathematical steps.

2.3.1 Conditions for complying with post-fault frequency requirements

The mathematical deduction of the constraints that guarantee compliance with post-fault requency requirements is presented here, as well as the proposed linearisations to include them in an MILP. These frequency-security constraints can be obtained by solving the swing equation, which describes the time-evolution of frequency deviation after a generation outage [14]:

$$\frac{2H}{f_0} \cdot \frac{\mathrm{d}\Delta f(t)}{\mathrm{d}t} + \mathrm{D} \cdot \mathrm{P_D} \cdot \Delta f(t) = \sum_{s \in \mathcal{S}} \mathrm{EFR}_s(t) + \sum_{g \in \mathcal{G}} \mathrm{PFR}_g(t) - P_\mathrm{L} \tag{2.16}$$

Where EFR and PFR are modelled as:

$$\mathrm{EFR}_s(t) = \begin{cases} \dfrac{R_s}{\mathrm{T_s}} \cdot t & \text{if } t \leq \mathrm{T_s} \quad (2.17\text{a}) \\ R_s & \text{if } t > \mathrm{T_s} \quad (2.17\text{b}) \end{cases}$$

$$\mathrm{PFR}_g(t) = \begin{cases} \dfrac{R_g}{\mathrm{T_g}} \cdot t & \text{if } t \leq \mathrm{T_g} \quad (2.18\text{a}) \\ R_g & \text{if } t > \mathrm{T_g} \quad (2.18\text{b}) \end{cases}$$

The need for inertia and FR increases along with a higher largest power infeed in the system. The present work considers the option to dynamically reduce the largest power infeed, as a measure to lower the need for inertia and FR when it is optimal to do so. Then, the largest power infeed is modelled as a decision variable in the scheduling problem, defined by the following constraint:

$$P_{\mathrm{L}} \geq P_g \qquad \forall\, g \in \mathcal{G} \tag{2.19}$$

Note that (2.19) is easily generalizable to consider any source of power production, such as an interconnector importing power from another grid. As the SUC used for this work uses clustering of equivalent generators, the right-hand side of (2.19) must be divided by N_g^{up}. The resulting constraint can be linearised using a big-M method, given that N_g^{up} is an integer decision variable. For the particular case of the GB system, the largest sources of power are nuclear units, which are modelled as must-run generators. Therefore, the right-hand side of (2.19) becomes $P_{\mathcal{M}}/\mathrm{N}_{\mathcal{M}}$, yielding a linear constraint.

By solving (2.16), the conditions for respecting post-fault frequency requirements can be derived. The constraint that guarantees RoCoF security is directly obtained from (2.16) by realising that the highest value for RoCoF is achieved at the very instant of the outage ($t = 0$), when frequency deviation is effectively zero:

$$|\mathrm{RoCoF}| = \frac{P_{\mathrm{L}} \cdot f_0}{2H} \leq \mathrm{RoCoF}_{\mathrm{max}} \tag{2.20}$$

The level of system inertia after the largest loss is given by:

$$H = \sum_{g \in \mathcal{G}} \mathrm{H}_g \cdot \mathrm{P}_g^{\mathrm{max}} \cdot N_g^{\mathrm{up}} + \mathrm{H}_{\mathrm{W}} \cdot P_{\mathrm{W}} - \mathrm{P}_{\mathrm{L}}^{\mathrm{max}} \cdot \mathrm{H}_{\mathrm{L}} \tag{2.21}$$

The constraint for assuring quasi-steady-state (q-s-s) security can be obtained from (2.16) by assuming that RoCoF is effectively zero in quasi-steady-state:

$$|\Delta f^{\mathrm{ss}}| = \frac{(P_{\mathrm{L}} - R_{\mathcal{S}} - R_{\mathcal{G}})}{\mathrm{D} \cdot \mathrm{P_D}} \leq \Delta f^{\mathrm{ss}}_{\mathrm{max}} \tag{2.22}$$

Therefore, the required levels of EFR and PFR to comply with q-s-s regulation are:

$$R_{\mathcal{G}} + R_{\mathcal{S}} \geq P_{\mathrm{L}} - \mathrm{D} \cdot \mathrm{P_D} \cdot \Delta f^{\mathrm{ss}}_{\mathrm{max}} \tag{2.23}$$

Note that the total amount of EFR is defined as $R_{\mathcal{S}} = \sum_{s\in\mathcal{S}} R_s$ and the total amount of PFR as $R_{\mathcal{G}} = \sum_{g\in\mathcal{G}} R_g$, that is, the aggregated EFR and PFR ($R_{\mathcal{S}}$ and $R_{\mathcal{G}}$) are the sums of the EFR and PFR available from each device (R_s and R_g), respectively.

The nadir requirement is respected if the following inequality holds true:

$$|\Delta f_{\mathrm{nadir}}| = |\Delta f(t = t^*)| \leq \Delta f_{\mathrm{max}} \tag{2.24}$$

Where t^* is the time when the nadir is reached. The expression for $\Delta f_{\mathrm{nadir}}$ can be obtained by solving (2.16). However, if damping is considered in (2.16), it is not possible to obtain an analytical expression for $\Delta f_{\mathrm{nadir}}$ as this would imply solving an equation involving sums of exponential functions, which is only solvable by numerical methods. Therefore, here we first obtain the constraint for nadir without considering the effect of load damping, which yields a more conservative condition. Nevertheless, a term approximating the contribution of damping to support the frequency nadir is proposed in Section 2.3.1.

In order to obtain $\Delta f_{\mathrm{nadir}}$, eq. (2.16) must be solved for time interval $t \in [\mathrm{T_s}, \mathrm{T_g})$: the nadir must certainly occur before $\mathrm{T_g}$, as otherwise frequency would drop indefinitely; furthermore, the nadir will take place after T_s if $R_{\mathcal{S}}$ is lower than the largest power infeed, which is certainly the case for any operating condition in GB's power grid. Then, by neglecting the damping term in (2.16) and solving:

$$\Delta f(t^*) = \frac{f_0}{2H}\left[\frac{R_{\mathcal{G}}}{2\mathrm{T}_g}\cdot (t^*)^2 + R_{\mathcal{S}}\left(t^* - \frac{\mathrm{T}_s}{2}\right) - P_{\mathrm{L}}\cdot t^*\right] \tag{2.25}$$

The time at which nadir is reached can be calculated from (2.16), by setting the derivative of frequency deviation to zero:

$$t^* = \frac{(P_{\mathrm{L}} - R_{\mathcal{S}})\cdot \mathrm{T_g}}{R_{\mathcal{G}}} \tag{2.26}$$

By substituting (2.26) into (2.25), and then substituting the resulting expression into (2.24), the constraint that guarantees compliance with the nadir requirement can be obtained:

$$\left(\frac{H}{f_0} - \frac{R_{\mathcal{S}} \cdot \mathrm{T_s}}{4 \cdot \Delta f_{\max}}\right) \cdot R_{\mathcal{G}} \geq \frac{(P_{\mathrm{L}} - R_{\mathcal{S}})^2 \cdot \mathrm{T_g}}{4 \cdot \Delta f_{\max}} \tag{2.27}$$

Both FR services are assumed in (2.17) and (2.18) to start providing response right after the generation outage: the frequency deadband of turbine governors and BESS' control systems is neglected in this study in order to make following mathematical expressions less intricate. However, if a deadband were to be considered, the procedure presented in [25] could be followed for obtaining the nadir constraint, resulting in an equivalent formulation to (2.27).

The RoCoF constraint (2.20), q-s-s constraint (2.23) and nadir constraint (2.27) assure post-fault frequency security in a power grid. By including these constraints in any optimisation routine, such as a UC formulation, a secure post-fault frequency evolution is guaranteed without the need to refine the time-interval for solving the optimisation: the UC can still be solved in the typical hourly or half-hourly basis. The frequency-security constraints enforce that a sufficient amount of resources such as inertia and FR are scheduled so that, if a power outage were to occur during this time interval, the sub-second dynamics of frequency are guaranteed to be within limits.

Contribution of load damping to supporting the nadir

Most of the previous work on frequency-secured optimisation has neglected the contribution of load damping on supporting the frequency nadir, as authors typically argue that this contribution would be small in any case. Here we propose a linear term to be included in (2.27) in order to account for the non-negligible contribution of load damping.

First, $\Delta f(t^*)$ is obtained while considering damping in (2.16):

$$\begin{aligned}\Delta f(t^*) \cdot \frac{\mathrm{D}'}{f_0} = \left(\mathrm{e}^{-\frac{\mathrm{D}'}{2H}t^*} - 1\right)\left(P_{\mathrm{L}} + \frac{2H \cdot R_{\mathcal{G}}}{\mathrm{D}' \cdot \mathrm{T_g}}\right) + \frac{R_{\mathcal{G}}}{\mathrm{T_g}}t^* \\ + R_{\mathcal{S}}\left[1 + \frac{2H}{\mathrm{D}' \cdot \mathrm{T_s}}\left(\mathrm{e}^{-\frac{\mathrm{D}'}{2H}t^*} - \mathrm{e}^{-\frac{\mathrm{D}'}{2H}(t^* - \mathrm{T_s})}\right)\right]\end{aligned} \tag{2.28}$$

Where $\mathrm{D}' = \mathrm{D} \cdot \mathrm{P_D} \cdot f_0$ and t^* can be obtained from setting RoCoF to zero in (2.16):

$$t^* = \frac{(P_\mathrm{L} - R_\mathcal{S} - \mathrm{D} \cdot \mathrm{P_D} \cdot |\Delta f_\mathrm{nadir}|) \cdot \mathrm{T_g}}{R_\mathcal{G}} \tag{2.29}$$

Since (2.28) implicitly describes a monotonically increasing function $\Delta f(R_\mathcal{G})$, the necessary $R_\mathcal{G}$ for a particular system condition can be obtained by numerically solving the following equation:

$$\begin{aligned} -\Delta f_\mathrm{max} \cdot \frac{\mathrm{D}'}{f_0} = \left(\mathrm{e}^{-\gamma} - 1\right)\left(P_\mathrm{L} + \frac{2H \cdot R_\mathcal{G}}{\mathrm{D}' \cdot \mathrm{T_g}}\right) + P_\mathrm{L} - R_\mathcal{S} \\ - \frac{\mathrm{D}'}{f_0} \cdot \Delta f_\mathrm{max} + R_\mathcal{S}\left[1 + \frac{2H}{\mathrm{D}' \cdot \mathrm{T_s}}\left(\mathrm{e}^{-\gamma} - \mathrm{e}^{-\gamma + \frac{\mathrm{D}'}{2H}\mathrm{T_s}}\right)\right] \end{aligned} \tag{2.30}$$

Where γ is defined as:

$$\gamma = \frac{\mathrm{D} \cdot \mathrm{P_D} \cdot f_0 \cdot \mathrm{T_g} \cdot (P_\mathrm{L} - R_\mathcal{S} - \mathrm{D} \cdot \mathrm{P_D} \cdot \Delta f_\mathrm{max})}{2H \cdot R_\mathcal{G}} \tag{2.31}$$

Eq. (2.30) implicitly describes a convex function $R_\mathcal{G}(\mathrm{P_D})$, as shown by the solid curve in Figure 2.9, which represents the numerical solution of (2.30) for several values of $\mathrm{P_D}$. As $R_\mathcal{G}$ and $\mathrm{P_D}$ are both positive physical magnitudes, the range of $\mathrm{P_D}$ for which (2.30) has a solution is:

$$\mathrm{P_D} \in \left(0,\ \frac{(P_\mathrm{L} - R_\mathcal{S})}{\mathrm{D} \cdot \Delta f_\mathrm{max}}\right) \tag{2.32}$$

As the function $R_\mathcal{G}(\mathrm{P_D})$ described by (2.30) is convex and monotonically decreasing, it can be inner-approximated by a line. A graphical representation of this linear approximation is also provided in Figure 2.9. Therefore, the linearised effect of load damping on nadir can be included in the previously obtained nadir constraint (2.27) as follows:

$$\left(\frac{H}{f_0} - \frac{R_\mathcal{S} \cdot \mathrm{T_s}}{4 \cdot \Delta f_\mathrm{max}}\right) \cdot R_\mathcal{G} \geq \alpha - \beta \cdot \mathrm{P_D} \tag{2.33}$$

Where:

$$\alpha = \frac{(P_\mathrm{L} - R_\mathcal{S})^2 \cdot \mathrm{T_g}}{4 \cdot \Delta f_\mathrm{max}}, \quad \beta = \frac{(P_\mathrm{L} - R_\mathcal{S}) \cdot \mathrm{T_g} \cdot \mathrm{D}}{4} \tag{2.34}$$

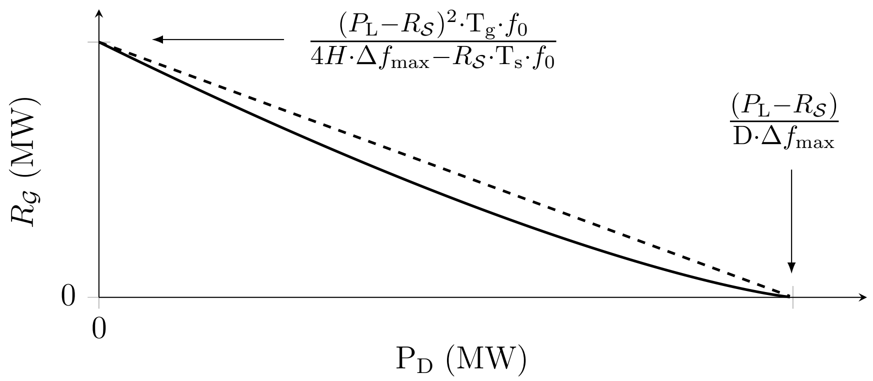

Figure 2.9: Exact feasible region for respecting the nadir requirement, given by the epigraph of the solid curve; and feasible region defined by the proposed linear approximation, given by the epigraph of the dashed line.

The inner approximation leads to an underestimation of the actual contribution from load damping, as can be clearly observed in Figure 2.9: the feasible region defined by the linear approximation, which is the epigraph of the dashed line, is tighter than the actual feasible region, epigraph of the solid curve. Nevertheless, this underestimation is significantly less conservative than simply neglecting the effect of damping. The quantitative assessment of this proposed linear approximation is presented in Section 2.3.3.

Linearisation of the frequency-nadir constraint

The RoCoF and q-s-s constraints, (2.20) and (2.23) respectively, are linear. However, the nadir constraint with the proposed damping term (2.33) is non-convex. An efficient linearisation method is proposed so that this constraint can be implemented in an MILP model while guaranteeing frequency security in all cases.

Constraint (2.33) contains three non-linear terms: two products of continuous variables on its left-hand side, namely $H \cdot R_\mathcal{G}$ and $R_\mathcal{S} \cdot R_\mathcal{G}$, and the quadratic term $(P_\mathrm{L} - R_\mathcal{S})^2$ on its right-hand side. Although it is not possible to exactly linearise these terms, we propose a method to approximate them by linear expressions to any desired level of accuracy. This method consists of the following steps:

1. For the right-hand side of the constraint, use an inner approximation by overestimating planes as in [51], applicable as the quadratic term is a convex function.

2. For the left-hand side, the technique proposed in [52] can be applied. This technique consists on representing one of the continuous variables by its binary expansion, so that the product of two continuous variables is converted into products of a continuous and several binary variables, which can then be exactly linearised. In this thesis, the decision variable chosen to be represented by its binary expansion is $R_{\mathcal{G}}$, since it appears in both products on the left-hand side of constraint (2.33).

Using the inner approximation with overestimating planes for the right-hand side of (2.33), (2.35) is obtained:

$$\left(\frac{H}{f_0} - \frac{R_{\mathcal{S}} \cdot \mathrm{T_s}}{4 \cdot \Delta f_{\max}}\right) \cdot R_{\mathcal{G}} \\ \geq \ \mathrm{a}_p \cdot P_\mathrm{L} + \mathrm{b}_p \cdot R_{\mathcal{S}} + \mathrm{c}_p - \frac{(P_\mathrm{L} - R_{\mathcal{S}}) \cdot \mathrm{T_g} \cdot \mathrm{D}}{4} \cdot \mathrm{P_D} \qquad \forall p \in \mathcal{P} \qquad (2.35)$$

A graphical example of the inner approximation using two planes is presented in Figure 2.10, where each of the planes covers one-half of the domain of the squared function α defined in (2.34). Only one of the two planes has been graphed for clarity. The code used to calculate the parameters for these planes to be implemented in the optimisation can be found in this link: https://github.com/badber/overestimating_planes.

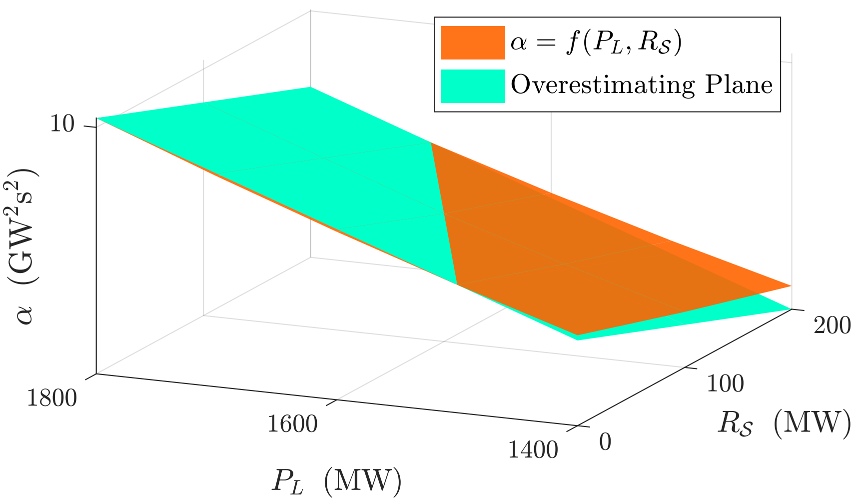

Figure 2.10: Representation of the surface defined by α in (2.34) and a plane which overestimates the surface in one-half of its domain.

Regarding the linearisation of the left-hand side of (2.33), the binary expansion of $R_{\mathcal{G}}$ is defined as:

$$R_{\mathcal{G}} = \sum_{l \in \mathcal{L}} z_l \cdot 2^l \tag{2.36}$$

After using this binary expansion, the product of continuous variables H and $R_{\mathcal{S}}$ by each of the binary variables z_l can be linearised using the standard big-M technique described in [44, 45], which yields the fully linearised nadir constraint:

$$\begin{aligned} &\frac{1}{f_0} \sum_{l \in \mathcal{L}} m_l \cdot 2^l - \frac{\mathrm{T_s}}{4 \cdot \Delta f_{\max}} \cdot \sum_{l \in \mathcal{L}} k_l \cdot 2^l \\ &\qquad \geq \; \mathrm{a}_p \cdot P_{\mathrm{L}} + \mathrm{b}_p \cdot R_{\mathcal{S}} + \mathrm{c}_p - \frac{(P_{\mathrm{L}} - R_{\mathcal{S}}) \cdot \mathrm{T_g} \cdot \mathrm{D}}{4} \cdot \mathrm{P_D} \qquad \forall p \in \mathcal{P} \end{aligned} \tag{2.37}$$

In (2.37), $m_l = H \cdot z_l$ and $k_l = R_{\mathcal{S}} \cdot z_l$. The following constraints must also be included, as part of the big-M linearisation method:

$$\begin{cases} m_l \leq \mathrm{M}_1 \cdot z_l & \forall\, l \in \mathcal{L} \quad (2.38\text{a}) \\ m_l \leq H & \forall\, l \in \mathcal{L} \quad (2.38\text{b}) \\ m_l \geq H - (1 - z_l) \cdot \mathrm{M}_1 & \forall\, l \in \mathcal{L} \quad (2.38\text{c}) \\ m_l \geq 0 & \forall\, l \in \mathcal{L} \quad (2.38\text{d}) \end{cases}$$

$$\begin{cases} k_l \leq \mathrm{M}_2 \cdot z_l & \forall\, l \in \mathcal{L} \quad (2.39\text{a}) \\ k_l \leq R_{\mathcal{S}} & \forall\, l \in \mathcal{L} \quad (2.39\text{b}) \\ k_l \geq R_{\mathcal{S}} - (1 - z_l) \cdot \mathrm{M}_2 & \forall\, l \in \mathcal{L} \quad (2.39\text{c}) \\ k_l \geq 0 & \forall\, l \in \mathcal{L} \quad (2.39\text{d}) \end{cases}$$

M_1 and M_2 are big-M constants, whose value must be close to the upper bounds of H and $R_{\mathcal{S}}$, respectively. Note that choosing a value for the big-M constants which is significantly larger that the upper bounds of H and $R_{\mathcal{S}}$ would likely introduce numerical issues when solving the optimisation, refer to [44] for more details.

Both of the approximations proposed in this section can be scaled up to achieve any level of accuracy desired, with the trade-off of a higher computational burden when solving the scheduling problem. The inner approximation by overestimating planes becomes more precise with increasing number of planes, while it adds a higher number of constraints to the optimisation. The binary expansion of $R_{\mathcal{G}}$ provides a better approximation of the continuous variable when a higher number of binary decision variables is used. A quantification of the trade-off between accuracy and computational burden is presented in Section 2.3.3.

2.3.2 Validation of the frequency-security constraints

In order to validate the frequency-security constraints obtained in Section 2.3.1, dynamic simulations of post-fault frequency evolution were run using MATLAB/Simulink. The system presented in Figure 2.11 was considered. The model used for generator dynamics is equivalent to that considered in [27, 48], consisting of a droop control and a first-order model for governor dynamics, followed by a saturation block. The model used for BESS dynamics is based on the one considered in [53], again using a first-order dynamics block.

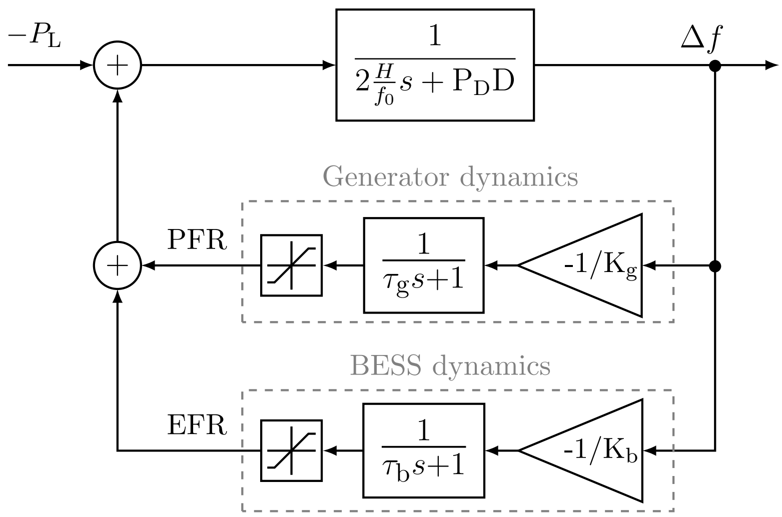

Figure 2.11: Block diagram for the simulation of the system frequency dynamics.

An example solution from the proposed SUC model with binding nadir constraint is fed into the dynamic model in Simulink. This SUC solution scheduled values of $H = 132$GWs, $R_{\mathcal{S}} = 0.22$GW, $R_{\mathcal{G}} = 2.24$GW, $P_{\mathrm{L}} = 1.66$GW, and the demand level was $\mathrm{P_D} = 38.3$GW. Time-constants of $\tau_{\mathrm{g}} = 5$s and $\tau_{\mathrm{b}} = 0.1$s were considered for the simulation. As shown in Figure 2.12, the nadir obtained from the dynamic simulation is 0.72Hz, while the limit for

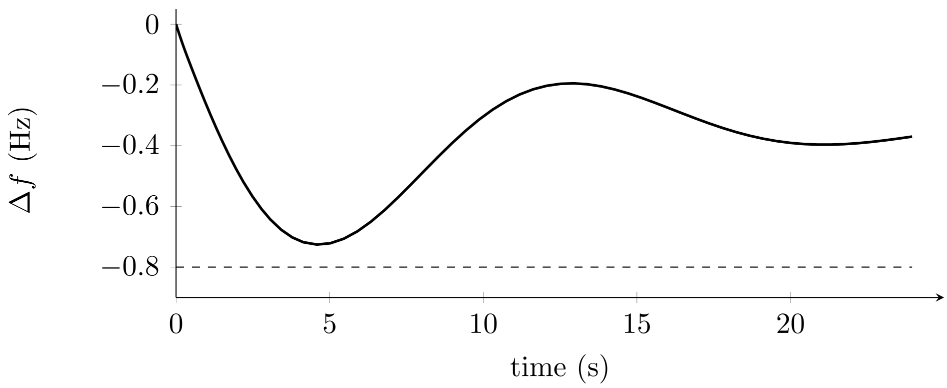

Figure 2.12: Dynamic simulation from an example SUC solution.

nadir was set to $\Delta f_{\max} = 0.8$Hz in the optimisation, demonstrating that the frequency nadir requirement is respected. The simulated RoCoF and q-s-s values are also within limits, 0.31Hz/s and 0.35Hz respectively. The conservativeness in nadir is driven by two factors: first, the analytical approximation in constraint (2.33), which is further analysed in Section 2.3.3; and second, the approximation of droop control for FR by an increasing ramp of power injection in (2.17) and (2.18). This increasing-ramp assumption was demonstrated by [23] to conservatively approximate any generic droop control. Therefore, even if a more complex control of frequency dynamics than that shown in Figure 2.11 were to be considered, the proposed security constraints would still respect the requirements, as long as the regulation for EFR being delivered by $\mathrm{T_s}$ and PFR being delivered by $\mathrm{T_g}$ is complied with.

2.3.3 Assessment of the proposed approximations

Three conservative approximations are proposed in this work to linearise the nadir constraint (2.33) while always guaranteeing frequency security: 1) a linear term approximating the effect of load damping on nadir, defined in (2.34); 2) the overestimation by using planes for inner-approximating the squared term in the left-hand side of (2.33), which is defined in (2.35); and 3) the binary expansion of $R_{\mathcal{G}}$ as described in (2.36). In this section, the conservativeness of these approximations is quantified, as well as their computational performance for different levels of accuracy of the approximations.

In order to assess the accuracy of the proposed linear damping term, inequality (2.33) is used to obtain system conditions that exactly meet the nadir requirement. Then, for these conditions the actual value of nadir is computed by numerically solving the swing equation (2.16). The same procedure is used for the case in which load damping is ignored, defined by constraint (2.27). The difference between the actual frequency nadir and the nadir requirement provides an indication on the conservativeness of this approximation. For (2.33) and (2.27), 3500 samples of system conditions that exactly meet the inequalities were obtained, for system conditions in the ranges $H \in [50, 400]$GWs, $R_{\mathcal{S}} \in [0, 400]$MW, $R_{\mathcal{G}} \in [500, 2500]$MW, $P_{\mathrm{L}} \in [1400, 1800]$MW and $\mathrm{P_D} \in [20, 60]$GW, corresponding to GB's 2030 system.

As shown in Table 2.2, the proposed approximation on load damping leads to a 6% conservativeness (0.05Hz) on average, while ignoring damping causes 25% conservativeness (0.19Hz). Even in the worst case, the proposed approximation only increases the requirement by 9% (0.07Hz), compared to 39% (0.31Hz) when load damping is ignored. Table 2.2 demonstrates that the linear approximation is slightly conservative but very close to the actual nadir requirement of $\Delta f_{\mathrm{nadir}} = 0.8$Hz. Note that implementing constraint (2.33) instead of (2.27) does not affect the computational time of the optimisation problem.

Table 2.2: Effective nadir requirement

	From constraint (2.33), linear approx. of damping	From constraint (2.27), neglecting damping
Mean nadir	0.75Hz	0.61Hz
Maximum nadir	0.79Hz	0.72Hz
Minimum nadir	0.73Hz	0.49Hz

The conservativeness of the second approximation, i.e. the overestimation due to using planes for inner-approximating the squared term in (2.33), is shown in Table 2.3 for different numbers of planes. These results were obtained again for $P_{\mathrm{L}} \in [1400, 1800]$MW and $R_{\mathcal{S}} \in [0, 400]$MW. There is a clear trend showing that using more planes reduces the conservativeness of the approximation but increases the computational time of the SUC. By increasing the number of planes from 2 to 4 and then to 8, the cost of frequency services (calculated after running the SUC as the total system operating cost net the energy cost) reduces by 0.4% and 0.7%, while the computational time is increased by 7% and 60%, respectively.

Table 2.3: Assessment of overestimating planes' approximation

	2 Planes (base case)	4 Planes	8 Planes
Mean overestimation in the entire range of $P_{\mathrm{L}}, R_{\mathcal{S}}$	0.72%	0.17%	0.04%
Maximum overestimation at any point in the range of $P_{\mathrm{L}}, R_{\mathcal{S}}$	1.25%	0.35%	0.09%
Increase in computational time	0%	7%	60%
Decrease in optimal cost of frequency services	0%	0.4%	0.7%

Table 2.4: Assessment of approximation due to binary expansion of $R_{\mathcal{G}}$

	12 bits (base case)	5 LSBs removed	10 LSBs removed
Precision achieved	1MW	32MW	1024MW
Decrease in computational time	0%	70%	97%
Increase in optimal cost of frequency services	0%	1%	49%

Regarding the binary expansion of $R_{\mathcal{G}}$, the precision is determined by the number of bits used. For the purpose of this thesis, a set of 12 bits, $\mathcal{L} = \{0, 1, \dots, 11\}$, is used as the base case, since the highest representable value of 4095MW is an acceptable upper bound for $R_{\mathcal{G}}$ in GB's 2030 system. From this base case, some of the Least Significant Bits (LSBs) are removed, in order to study the improvement in computational burden due to renouncing to some precision in the binary expansion. The results in Table 2.4 clearly show that a lower number of binary decision variables significantly reduces computational time for the optimisation with the drawback of increased conservativeness.

Since Stochastic Programming is a computationally demanding problem, a balance between accuracy in the optimal objective and computational efficiency is desired for the SUC-based simulations presented in coming sections. Therefore, 2 planes and 7 bits (5 LSBs removed) for the expansion of $R_{\mathcal{G}}$ are considered from now on. For future applications of these frequency-security constraints, different numbers of planes and bits can be chosen, depending on the time-requirements for solving the optimisation in each application.

2.3.4 Value of defining and optimising EFR as a distinct service

The proposed frequency-secured formulation can be used to achieve cost-effective operation of a low-carbon power system. In addition, it would also allow to identify the technologies and practices that would be most beneficial to the system, such as Battery Energy Storage Systems (BESS) providing EFR, or part-loading the largest generating units. The benefits from operating a system using this frequency-secured framework are not only economic but also environmental, as shown through case studies in this section.

Several case studies on the GB 2030 power system are carried out in this section to demonstrate the benefits of the proposed model, using the SUC introduced in Section 1.2.1. The characteristics of generation plants are included in Table 2.5. The minimum and maximum demand are 20GW and 60GW, respectively. A pumped storage unit with 10GWh capacity, 2.6GW rating and 75% round efficiency is also present in the system. Moreover, BESS with 1GWh capacity, 200MW rating and 90% efficiency is installed with the capability to provide EFR. Other system's parameters are: $\mathrm{T_s} = 0.5\mathrm{s}$, $\mathrm{T_g} = 10\mathrm{s}$, $\mathrm{D} = 0.5\%/\mathrm{Hz}$ and $\mathrm{P_L^{max}} = 1800\mathrm{MW}$. The dynamic-frequency requirements are set by National Grid regulation to $\Delta f_{\mathrm{max}} = 0.8\mathrm{Hz}$, $\Delta f^{\mathrm{ss}}_{\mathrm{max}} = 0.5\mathrm{Hz}$ and $\mathrm{RoCoF_{max}} = 0.5\mathrm{Hz/s}$ (corresponding to the expected relaxed RoCoF requirement). Synthetic inertia from wind turbines is only considered in Section 2.3.7.

Simulations were run in a twelve-core 3.5GHz Intel Xeon CPU with 64GB of RAM. The optimisations were solved with FICO Xpress 8.0, linked to a multi-threaded C++ application via the BCL interface. The duality gap for the MILPs was set to 0.1%. For the SUC, a scenario tree branching only in the current-time node was used, with net-demand quantiles of 0.005, 0.1, 0.3, 0.5, 0.7, 0.9 and 0.995. This approach using few quantiles was proven by [34] to provide similar results to more intricate structures, while significantly reducing the computational burden. The values for the quantiles were chosen to capture symmetrically the variance of the forecast error distribution, as well as its tails. Each SUC simulation corresponds to four months, in different seasons, of the operation of GB's 2030 system.

Table 2.5: Characteristics of thermal plants in GB's 2030 system

	Nuclear	CCGT	OCGT
Number of Units	4	100	30
Rated Power (MW)	1800	500	100
Min Stable Generation (MW)	1400	250	50
No-Load Cost c_g^{nl} (£/h)	0	4500	3000
Marginal Cost c_g^{m} (£/MWh)	10	47	200
Start-up Cost c_g^{st} (£)	N/A	10000	0
Start-up Time (h)	N/A	4	0
Min Up Time (h)	N/A	4	0
Min Down Time (h)	N/A	1	0
Inertia Constant H_g (s)	5	4	4
Max R_g deliverable (MW)	0	50	20
Emissions (tonCO_2/MWh)	0	0.394	0.557

This section presents the benefits from recognising the faster dynamics of EFR and optimising its provision in the scheduling process. Three different operating strategies for GB's power system are considered:

1. "Just PFR" (considered as the base-case strategy): EFR is not defined as a distinct service, as was the traditional practice. Therefore, the FR provided by BESS is considered as PFR.

2. "Fixed EFR": EFR is defined as service, but its provision is fixed throughout the year, reflecting the current practice in GB.

3. "Optimised EFR": EFR is defined and co-optimised along with PFR and inertia, using the model proposed in this thesis.

For all these strategies, the largest power infeed is kept constant to $P_{\mathrm{L}} = \mathrm{P}_{\mathrm{L}}^{\mathrm{max}}$. BESS of 200MW rating and 5h tank size are considered, for five cases of wind capacity corresponding to 0, 10, 20, 30 and 40GW.

Figure 2.13 displays the operational cost savings from strategies 2 and 3 referred to the base-case strategy 1, therefore showing the value of defining EFR as a distinct service and

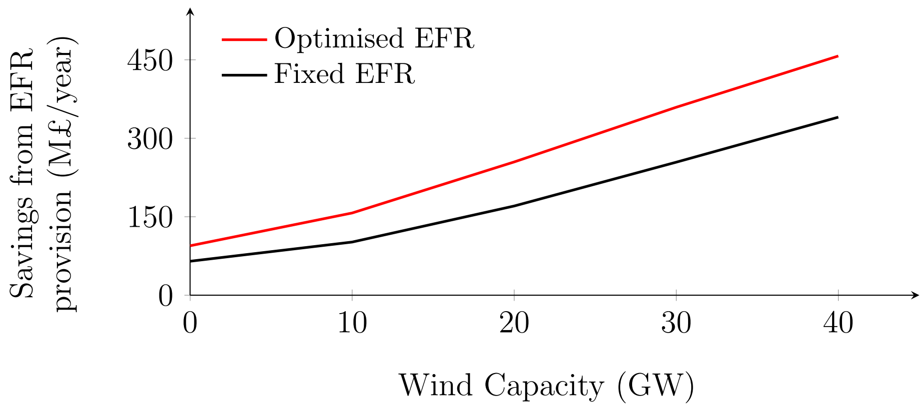

Figure 2.13: Annualised savings due to EFR provision from a 200MW-rated BESS, for two different operating strategies. Both strategies' savings are referred to the base-case in which the BESS provides just PFR.

optimising its provision, respectively. In strategy "Just PFR", the faster dynamics of EFR are not recognised in the optimisation and therefore the higher value of EFR is not taken into account, which justifies why the cost of frequency services is highest for this case in all wind-penetration scenarios.

As expected, the value of EFR in Figure 2.13 increases with increasing wind penetration, as the declining system inertia makes EFR more valuable. Furthermore, the savings from applying the proposed model to optimise EFR provision are higher than 33% for any level of wind penetration, when compared to just providing a fixed amount. The results demonstrate the need to not only recognise the faster dynamics of EFR but also optimise its provision.

The reason behind these results is that in the "Fixed EFR" strategy the full potential of EFR is still not recognised, as BESS are forced to provide 200MW of EFR at all times. Note that the provision of EFR from BESS is limited by the following constraint:

$$R_{\mathcal{S}} \leq \text{Max Discharge Rate} - \text{Discharge Rate} \tag{2.40}$$

Where the "Discharge Rate" would be negative if the BESS were charging. Therefore, in "Fixed EFR" the BESS can only charge or stay idle once the tank is full, because given that their capacity is of 200MW (i.e. Max Discharge Rate = 200MW), they are not allowed to discharge as their EFR provision would fall under 200MW.

The most efficient strategy is demonstrated to be "Optimised EFR" in Figure 2.13. The higher benefits from optimising EFR provision come from two aspects: by optimising EFR, a 200MW-BESS can provide up to 400MW of EFR at times; in addition, the BESS can provide other services such as energy arbitrage. These two aspects are better understood by looking at an example of the detailed operation of the BESS, as the one shown in Figure 2.14.

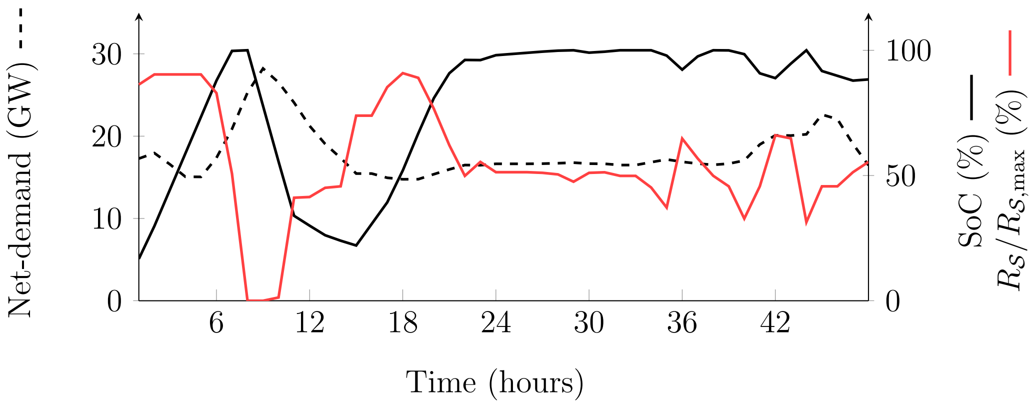

Figure 2.14: Two-day example of the operation of the power system.

Figure 2.14 presents a two-day period operation of BESS using strategy 3 : it displays the net-demand, the State of Charge (SoC) of the BESS, and the EFR scheduled as a percentage of the maximum EFR that could be provided, $R_{\mathcal{S},\max}$. Note that $R_{\mathcal{S},\max}$ takes the value of double the rating of the BESS, therefore $R_{\mathcal{S},\max} = 400$MW in this case; indeed an EFR of up to 400MW can be provided by the 200MW-BESS by swiftly shifting from fully charging to fully discharging, which would effectively increase power injection by twice the volume of the BESS. Therefore, an optimised provision of EFR allows BESS to provide a higher amount of EFR in periods of low net-demand (and therefore low inertia) as hours 4 and 18, which is achieved by scheduling the BESS to fully charge. On the other hand, when the system inertia is high (e.g. around hour 8), the BESS provides zero EFR while discharging.

Furthermore, the ability to shift between charging/discharging modes, when compared to the "Fixed EFR" strategy in which the BESS would be forced to stay idle in order to provide 200MW of EFR, also allows to take advantage of a synergy with energy costs. For low-net demand periods, EFR is more valuable while the cost of energy is generally lower, so charging the BESS in these periods is positive both from EFR and energy perspectives.

Finally, Figure 2.15 presents the extra savings from "Optimised EFR" provision over the "Fixed EFR" case. The volume of BESS is increased up to 900MW. These results show that the benefit from optimising EFR provision is very significant when a small volume of BESS is available, but reduces as the volume of BESS increases. For cases with more than 750MW BESS available, the provision of EFR is sufficient even for periods of low net-demand, leading to a very limited benefit of optimising its provision.

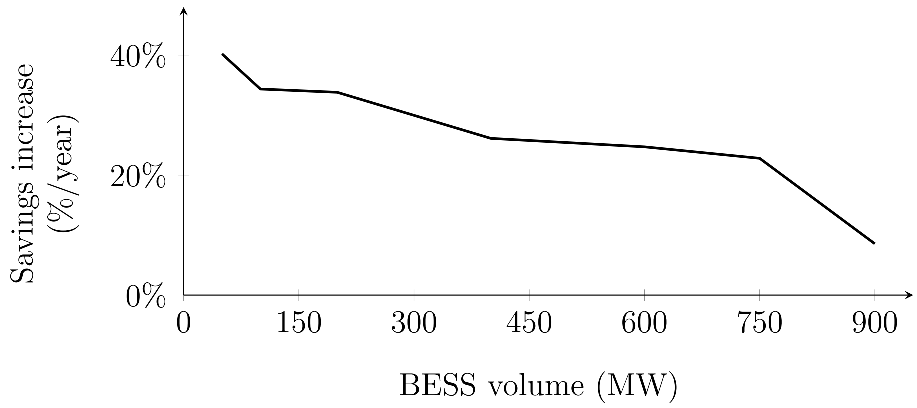

Figure 2.15: Increase in savings from strategy "Optimised EFR" with respect to strategy "Fixed EFR", for a 40GW-wind scenario.

2.3.5 Value of a dynamically-reduced largest power infeed

A lower largest-power-infeed, represented by a decreasing value of decision variable P_{L} in this formulation, effectively reduces the need for frequency services, as can be observed in the frequency-security constraints presented in Section 2.3.1. Although nuclear units provide low-cost, zero-emissions energy, the large capacity of each single unit becomes the key driver of the frequency-response requirement in GB. Under certain system's conditions, it may be cost-effective to reduce their power output in order to reduce the need for frequency services. Note that deloading nuclear units would be used as a preventive measure only when a low net-demand period is expected, since ramping capabilities of these types of units are typically limited, and therefore must be deloaded some time in advance.

Figure 2.16 shows the operating cost savings from a dynamically-reduced largest power

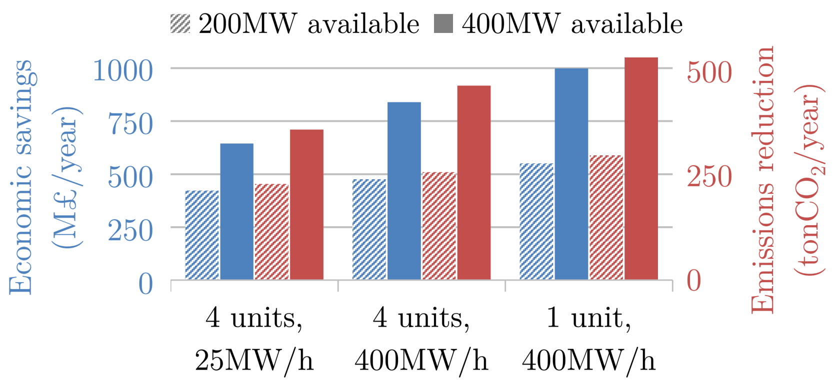

Figure 2.16: Economic and emissions savings due to nuclear deloading, for deloading availabilities of 200MW and 400MW in a 40GW-wind case.

infeed, with respect to the "Just PFR" strategy discussed in Section 2.3.4. A 40GW wind scenario is considered. Two different deloading capabilities are studied: 200MW and 400MW. The impact of the nuclear fleet's characteristics is analysed by considering 4 large units rated at 1.8GW and just 1 large unit. In addition, two extreme ramping rates of the units are considered, 25MW/h and 400MW/h. The results suggest that by allowing the deloading of nuclear units, considerable cost saving can be achieved. However, a higher number of large units and lower ramp rates reduce the savings, due to the fact that all large nuclear plants need to be deloaded in order to reduce the largest infeed, and the fact that it is more challenging for slower plants to lower their power outputs when required.

Furthermore, deloading nuclear units can reduce carbon emissions. Although this might seem contradictory, lowering the power production of large nuclear plants, which are carbon-free generators, reduces the need for frequency services and consequently less part-loaded conventional generators need to be online, allowing for more RES to be accommodated.

Note that the load factor of nuclear units would be reduced if the deloading strategy was adopted. Subsidies may need to be introduced to compensate for the lower power produced, so that the investment of nuclear providers could be recovered. Such subsidies would reduce the savings from this strategy.

2.3.6 Full co-optimisation of frequency services

The benefits of simultaneously optimising all four frequency services in the SUC are presented here. Two cases are considered: a "Low availability" case, corresponding to a 200MW-rated BESS and a maximum deloading of 200MW; and a "High availability" case, corresponding to a 600MW-rated BESS and a maximum deloading of 600MW. The largest power infeed is driven by 4 nuclear units rated at $P_L^{max} = 1.8$GW, with 100MW/h ramp rates. The results for both cases are presented in Figure 2.17, showing the cost savings from each case referred to the "Just PFR" strategy discussed in Section 2.3.4. The savings from this "Full optimisation" are compared to the savings from just EFR optimisation and just deloading optimisation.

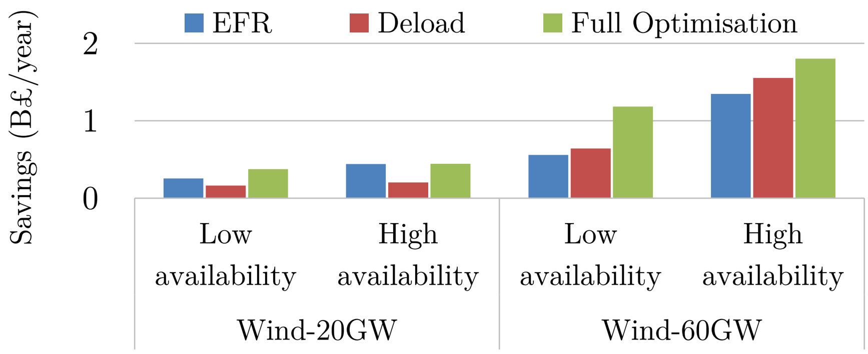

Figure 2.17: Annualised savings from optimising frequency services. The *EFR* strategy presents the savings from an optimised EFR provision, with no option to deload nuclear plants; the *Deload* strategy presents the savings from optimising the deloading option of large nuclear units, with no EFR availability in the system; finally, *Full Optimisation* considers the co-optimisation of both these services.

EFR shows to be more beneficial than deloading of nuclear units for the low-wind scenario, as EFR provision is free of cost in this framework but deloading nuclear units increases the cost of energy in low-wind scenarios, since the energy not produced by nuclear must be provided by more expensive thermal plants. However, for high wind penetration deloading becomes more valuable. In this scenario, the energy not provided from nuclear plants due to deloading is now provided by wind, free of cost. In addition, deloading nuclear plants is more valuable for securing post-fault frequency, as its delivery time is virtually zero while EFR takes T_s to be delivered.

Furthermore, the savings from the "Full Optimisation" strategy are significantly lower than the sum of savings from just EFR and just deloading optimisations, in the "High availability" cases. This result shows clear competition between these two services if there is a significant amount of both services available.

2.3.7 Impact of damping and SI in the value of frequency services

This section analyses the reduction of the value of EFR and nuclear deloading in the presence of higher load damping and synthetic-inertia (SI) provision from wind turbines. Figure 2.18 presents the impact of load damping on the benefits from introducing these two new frequency services. The savings from EFR and deloading are not significantly affected by higher damping when a limited amount of these services is available, but the savings become much more sensitive to damping if the availability of the services increases. This result suggests that increasing system damping would not affect the competitiveness of EFR and deloading but would instead reduce the required volume of services.

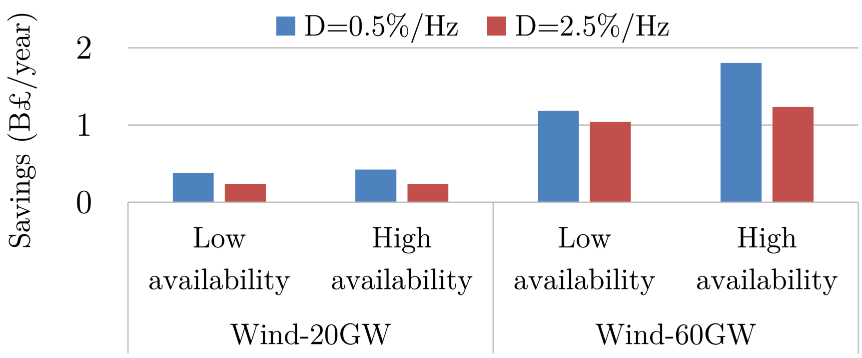

Figure 2.18: Impact of load damping on the savings from frequency services, for a *Full Optimisation* strategy.

Finally, Figure 2.19 displays the impact of SI provision from wind turbines on the value of other frequency services. The model developed in [54] for considering SI in a scheduling algorithm was integrated in the frequency-secured SUC proposed here. One of the main difficulties in modelling SI in the system level comes from the uncertainty in the number of wind turbines online for a given level of wind power generation. Here we assume the average number of online turbines as in [55], while considering two different inertia time-constants for

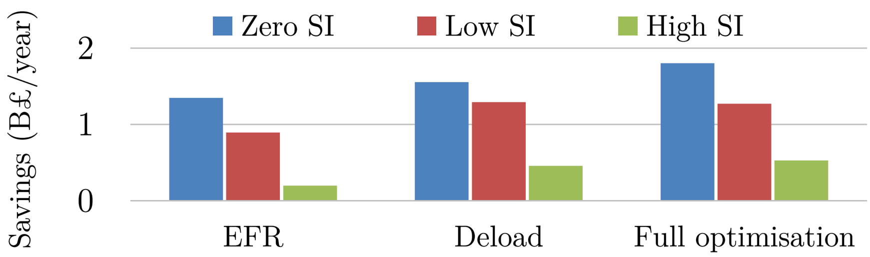

Figure 2.19: Impact of different levels of SI on the value of other frequency services, for a 60-GW-wind-capacity case and "High availability" of EFR and nuclear deloading.

individual wind turbines: in "Low SI" $H_W = 1.5$s, while in "High SI" $H_W = 5$s. The results in Figure 2.19, for a high-wind-penetration case of 60GW and the "High availability" case discussed in Section 2.3.6, suggest that the potential development of SI capability from RES needs to be taken into consideration when designing alternative frequency services. In the case with limited SI capability from wind turbines, there are still clear benefits from introducing the EFR and nuclear-deloading services, while in the case that wind turbines have a similar inertia time-constant to conventional plants, the benefits and need for alternative frequency services are limited.

In conclusion, the results in Figure 2.19 demonstrate that having access to a varied portfolio of frequency services that includes EFR and nuclear deloading is still valuable under moderate penetration of synthetic inertia from wind turbines (as the savings achieved in the "Low SI" case are significant), while the savings achieved from EFR and nuclear deloading are low in a "High SI" scenario.

2.3.8 Comparison of results in Stochastic and Deterministic UC

Here we compare the proposed frequency-constrained framework in both the SUC and a Deterministic UC. The "Full Optimisation" strategy presented before was used in a "Low Availability" case for frequency services (200MW-rated BESS and a maximum nuclear deloading of 200MW), while two wind-capacity cases were considered, of 20GW and 60GW. The Deterministic UC was run using a quantile of 0.98 for net-demand, as in [34]. The comparison of results from both UC approaches are presented in Table 2.6. This table shows the difference, in percentage, of several

Table 2.6: Comparison of results, from Deterministic UC over Stochastic UC

	Wind Capacity 20GW	Wind Capacity 60GW
Total Operating Cost	0.6%	1%
Wind Curtailment	0.9%	1.4%
Savings from EFR and Deload	-12%	-15%
Average H	5%	7%
Average $R_{\mathcal{S}}$	-4%	-5%
Average P_{L}	1%	2%

system magnitudes from the solution of the Deterministic UC with respect to the solution of the SUC.

Table 2.6 demonstrates that if the Deterministic UC is applied, the system operating cost and wind curtailment are both higher than for SUC. At the same time, the savings from the new frequency services, namely EFR and part-loading nuclear, are lower in Deterministic UC when compared to SUC. This is due to the fact that Deterministic UC tends to schedule a higher number of slow-start thermal generators (CCGTs) as shown in [34], implying a higher level of inertia than in SUC. The higher inertia makes EFR and Deloading less valuable to comply with the frequency constraints. Nevertheless, the savings obtained from co-optimising these services are still significant under a Deterministic UC: £320m/year for the 20GW-wind case and £980m/year for the 60GW-wind case.

2.4 Summary of findings

This chapter has presented the following studies and conclusions:

- A quantification of the value of inertia in a low-carbon electric grid. The value of inertia was analysed from three different points of view: the annual value for different scenarios of wind penetration, the instantaneous value for different demand-wind conditions, and the marginal value. The results show that significant savings in the operational cost of the system could be achieved if provision of extra inertia was incentivised, particularly for cases of high wind generation. These results support the idea proposed by [20] that an inertia market should be designed. In particular, an hourly inertia market needs to be developed as the results clearly demonstrate the time-varying value of inertia provision, depending on the different system's conditions. Under such a market framework, the results presented here would serve to inform both market operators and investors on provision of inertial response.

- A frequency-constrained UC in which a variable largest-possible-power-loss is explicitly modelled. This UC model has been used to analyse the potential operational benefits from deloading large nuclear generators in GB's system. These benefits, which have been demonstrated to be considerable, particularly in a high-wind-penetration scenario, are both economic and in terms of a reduction in carbon emissions. However, the savings are dependent of the rating of the largest plant in the system and the characteristics of the fleet that drives this $N-1$ requirement for frequency services.

- A co-optimisation of energy production along with every frequency service currently defined in any power system in the world: synchronous and synthetic inertia, PFR, EFR and a dynamically-reduced largest power infeed. Several case studies clearly demonstrate the benefits of introducing new frequency response services such as EFR. The results also highlight the importance of co-optimisation of alternative services to accurately capture their value.

Given these findings, the most relevant task for enhancing this modelling framework was identified as the co-optimisation of several FR products with distinct delivery times, other than just EFR and PFR, as such model would allow to recognise the different dynamics of providers, leading to a more efficient ancillary-services market. The model allowing to perform this co-optimisation is presented in Chapter 3.

Chapter 3

Optimal Portfolio of Distinct Frequency-Response Services and Marginal-Pricing Mechanisms

This chapter presents a model allowing to choose the optimal portfolio of Frequency Response (FR) providers from any finite number of FR services with distinguished characteristics, such as different delivery times and activation delays. In addition, we propose a marginal-pricing scheme for frequency services, which is shown to incentivise faster provision of FR.

While most of existing energy markets rely on Linear Programming, for example through DC Optimal Power Flow, the frequency-security constraints deduced in this chapter are formulated as a Mixed-Integer Second-Order Cone Program (MISOCP). Second-Order Cones (SOCs) are the highest class of conic optimisation problems that can be efficiently solved to global optimality in a mixed-integer formulation using commercial solvers [56]. Therefore, an MISOCP formulation is suitable for being implemented in a scheduling algorithm that needs binary variables to model the on/off state of the generators, such as the Unit Commitment.

This chapter is based on journal papers [2] and [3].

3.1 Introduction

A reduced level of system inertia due to renewable integration increases the need for cost-effective provision of ancillary services, such as Frequency Response. To tackle the declining system inertia, FR services with faster delivery have been introduced by system operators [31]. However, a fundamental question yet to be answered is how to optimise the portfolio of FR services from providers with diverse characteristics under different system conditions. References [23–26, 30] aggregate the response from all FR providers uniformly, therefore only allowing to consider a single FR service. References [1, 57] co-optimise the two FR services defined in the UK up to date, namely Enhanced Frequency Response (EFR) delivered by one second after the outage, and Primary Frequency Response (PFR) delivered ten seconds after the outage. The only work that integrates different dynamics from generic FR providers is [27], by considering an affine conservative approximation of the frequency dynamics until reaching the nadir.

Furthermore, the impact of FR activation delays on frequency stability has been studied in several recent publications, while it has not been considered in any of the above works. The authors in [58] analysed the impact of FR delays in post-fault frequency dynamics, by conducting a sensitivity analysis using dynamic simulations. Reference [59] considered the delays in the FR dynamics of battery storage, while [60] focused on the FR dynamics from demand-side response. The work in [61] developed a delay heuristic that estimates the post-fault frequency excursion. However, no study has yet analysed the economic impact of delays on FR markets.

A day-ahead market for FR services has recently been envisioned by National Grid [62]. Although the scope of this market is to provide FR independently of the energy market, cost efficiency would be significantly enhanced by using simultaneous clearing of energy and FR [63], as well as by introducing novel products such as extra inertia and a reduced largest-loss. Rewarding inertia provision has been demonstrated by several studies [8,20] to provide significant economic benefits to the system, and a synchronous-inertial-response product has been recently introduced by EirGrid in Ireland [64]. Optimally scheduling the largest possible loss has also been shown to achieve both economic and emission savings [9, 48].

In this context, some studies have focused on analysing market design for frequency services. The two-part paper [20, 65] considered a single FR service, Primary Frequency Response (PFR), while the work in [21] and [66] included also Enhanced Frequency Response (EFR). Previous works mainly apply regression techniques to obtain linear frequency-security constraints based on dynamic-simulation data [20, 65] or system operational data [21]. From the linear constraints, they developed a marginal pricing mechanism for FR services. On the other hand, the authors in [66] linearised an originally non-linear constraint in order to clear a market considering both the EFR and PFR services. Regarding a market for inertia, reference [20] used a similar approach for its proposed market for PFR, by fitting heuristic linear constraints from simulation data and applying a marginal-pricing scheme to the linear constraint. Reference [67] only focused on pricing inertia from the RoCoF constraint, for which an analytical linear formulation can be obtained.

In the available literature, system inertia has been assumed either fixed in the optimisation of FR [21, 23] or fully controllable by the UC [1, 25]. In fact, a considerable amount of inertia contribution is available from demand (references [68] and [69] estimated that demand in GB provides on average 1.75s of inertia), but this inertia is not controllable and can only be forecasted: assuming a central authority clearing a pool market using a frequency-secured UC, the inertia from demand can only be forecasted with certain accuracy. Given the risk aversion of system operators, it is necessary to explicitly model such uncertainty, in addition to the uncertainty associated with renewable generation.

Given this background, this chapter develops an efficient frequency-constrained optimisation framework that recognises and appropriately values the different dynamics of FR services. The contributions are four-fold:

1. We propose closed-form conditions to optimise, for the first time, any finite number of FR services with diverse dynamics while considering any combination of activation delays. The proposed frequency constraints are formulated as an MISOCP, which can be efficiently solved by taking advantage of the recent development of conic optimisation software.

2. We propose a marginal pricing scheme for frequency services (multi-speed FR, inertia and a reduced largest-loss), based on duality theory applied to the MISOCP formulation that we deduce for guaranteeing post-fault frequency security. This pricing scheme allows to optimally value the different dynamics of FR providers, as well as appropriately value a reduced largest loss.

3. The uncertainty associated with the inertia contribution from the demand side is explicitly modelled in the optimisation problem through chance constraints. A convex reformulation of the chance constraints allows maintaining the problem as an MISOCP.

4. We demonstrate the effectiveness and applicability of this frequency-secured framework through several relevant case studies. These studies demonstrate the economic benefits of recognising multi-speed FR, and that our proposed pricing scheme for frequency services puts in place the right incentives: FR providers are incentivised to provide faster FR because they are rewarded according to their speed of delivery, and RES generators are incentivised to provide frequency services (such as synthetic inertia).

Regarding the immediate practical applicability of the proposed model, this would be of particular interest for a system such as Great Britain (GB), an island where the low-inertia problem is more acute than in continental grids. The system operator National Grid is currently designing a new suite of frequency response products, which are envisioned to be modelled in the same way as proposed in this Chapter, i.e. as a power-increase ramp in combination with an activation delay [70]. Furthermore, an auction to competitively procure inertia was held at the beginning of 2020 [71]. Therefore, the frequency-secured formulation presented here would allow the system operator to optimally clear the ancillary services auctions, instead of pre-defining a volume of response to be procured through each separate auction, as is current practice.

3.2 Closed-form conditions for secure post-fault frequency dynamics

In this section we deduce the closed-form conditions for frequency security, that allow to map the sub-second dynamics of transient frequency to any desired time-scale, such as the typical minutes to hour resolution of a UC. Frequency security is respected if sufficient inertia and FR services are available at the time of the power outage to contain and recover the system frequency.

The conditions for a secure post-fault frequency evolution can be deduced from solving the swing equation [14]:

$$\frac{2(H+H_{\mathrm{D}})}{f_0}\cdot\frac{\mathrm{d}\Delta f(t)}{\mathrm{d}t}=\mathrm{FR}(t)-P_{\mathrm{L}} \tag{3.1}$$

Eq. (3.1) assumes the loss of the largest power infeed, therefore representing the $N-1$ reliability requirement. Load damping has been neglected as in [23], a common assumption since the damping level is expected to be significantly reduced in future power systems that are increasingly dominated by power electronics. Nevertheless, if some amount of load damping was present in the system, the frequency-security constraints proposed in this section would still hold, although they would enforce a tighter feasible region, as the support from load damping to contain the frequency drop would not be accounted for.

The system inertia is aggregated from the inertia provided by all devices, including thermal generators and certain loads, and it includes two components: H is the controllable term in the UC optimisation, as it is a decision variable which depends on the generators that are scheduled to be online; on the other hand, H_{D} is the inertia contribution from demand, which is assumed here to be non-controllable but can be forecasted for time-periods in the near future. The largest possible power outage P_{L} can be considered as a decision variable, which would involve part-loading a large generating unit or interconnector [1, 9].

Function $\mathrm{FR}(t)$ in (3.1) represents the frequency control for Frequency Response, a power injection from several system devices following the outage. We model this function to consider $|\mathcal{S}|$ different FR services, in which each FR service is associated with a characteristic delivery time, therefore allowing to recognise diverse dynamics in FR delivery from different providers:

$$
\mathrm{FR}(t) = \begin{cases}
\sum_{s\in\mathcal{S}} \frac{R_s}{\mathrm{T}_s} \cdot t & \text{if } t \le \mathrm{T}_1 \qquad (3.2.1) \\
R_1 + \sum_{s=2}^{|\mathcal{S}|} \frac{R_s}{\mathrm{T}_s} \cdot t & \text{if } \mathrm{T}_1 < t \le \mathrm{T}_2 \qquad (3.2.2) \\
\qquad \cdots & \\
\sum_{s=1}^{|\mathcal{S}|-1} R_s + \frac{R_{|\mathcal{S}|}}{\mathrm{T}_{|\mathcal{S}|}} \cdot t & \text{if } \mathrm{T}_{|\mathcal{S}|-1} < t \le \mathrm{T}_{|\mathcal{S}|} \qquad (3.2.|\mathcal{S}|) \\
\sum_{s\in\mathcal{S}} R_s & \text{if } t > \mathrm{T}_{|\mathcal{S}|} \qquad (3.2.(|\mathcal{S}|+1))
\end{cases}
$$

The delivery time T_s of a service s is the time by which full FR capacity for the service is delivered. Piecewise function (3.2) models the delivery of FR from each provider s as ramping up during the interval $t \in (0, \mathrm{T}_s]$, and constant for $t > \mathrm{T}_s$. This approach, proposed in [23] for a single FR service, is guaranteed to conservatively approximate any controller proportional to frequency deviation, as we further demonstrate in Section 3.4. Note that FR services are ordered from service 1 up to service $|\mathcal{S}|$ in increasing delivery time, i.e. service FR_1 is the fastest and service $\mathrm{FR}_{|\mathcal{S}|}$ is the slowest.

3.2.1 Deducing frequency-security constraints

By solving (3.1), the three constraints that guarantee a secure post-fault frequency evolution can be obtained. The RoCoF constraint is deduced following National Grid's standard [37], which established that the level of system inertia must be sufficient to limit the highest instantaneous RoCoF at $t = 0$:

$$|\mathrm{RoCoF}(t=0)| = \frac{P_\mathrm{L} \cdot f_0}{2(H + H_\mathrm{D})} \leq \mathrm{RoCoF}_\mathrm{max} \tag{3.3}$$

For frequency to stabilise eventually after the fault, the amount of FR available must be at least equal to the power outage. In other words, the steady-state constraint is obtained by setting RoCoF to zero in (3.1) and considering that every FR service has been fully delivered:

$$\sum_{s \in \mathcal{S}} R_s \geq P_\mathrm{L} \tag{3.4}$$

Finally, in order to respect all three frequency security requirements, the frequency nadir must be guaranteed to be above Δf_max. Since $\mathrm{FR}(t)$ defined in (3.2) is a piecewise function, the nadir constraint depends on the time-interval when the nadir occurs. For the nadir to take place in a given time-interval $t \in [\mathrm{T}_{n-1}, \mathrm{T}_n)$, the two following conditions must be met:

$$\left(\sum_{i=1}^{n-1} R_i + \sum_{j=n}^{|\mathcal{S}|} R_j \cdot \frac{\mathrm{T}_{n-1}}{\mathrm{T}_j} \leq P_\mathrm{L} \right) \quad \text{and} \quad \left(\sum_{i=1}^{n} R_i + \sum_{j=n+1}^{|\mathcal{S}|} R_j \cdot \frac{\mathrm{T}_n}{\mathrm{T}_j} > P_\mathrm{L} \right) \tag{3.5}$$

Condition (3.5) states that the power injected from FR becomes greater than the power loss P_L not before T_{n-1} and no later than T_n. Before T_{n-1}, only the fastest $n-1$ FR services have been fully delivered, while the rest are still ramping up; after T_n, the n^th service has been fully delivered as well.

The solution of (3.1) for $t \in [\mathrm{T}_{n-1}, \mathrm{T}_n)$ is:

$$\Delta f(t) = \frac{f_0}{2(H + H_{\mathrm{D}})} \left[\sum_{j=n}^{|\mathcal{S}|} \frac{R_j}{2\mathrm{T}_j} \cdot t^2 + \sum_{i=1}^{n-1} R_i \left(t - \frac{\mathrm{T}_i}{2} \right) - P_{\mathrm{L}} \cdot t \right] \tag{3.6}$$

The time within $t \in [\mathrm{T}_{n-1}, \mathrm{T}_n)$ at which nadir is exactly reached is given by setting RoCoF to zero in (3.1) for that given time interval:

$$t_{\mathrm{nadir}} = \frac{P_{\mathrm{L}} - \sum_{i=1}^{n-1} R_i}{\sum_{j=n}^{|\mathcal{S}|} R_j / \mathrm{T}_j} \tag{3.7}$$

By substituting (3.7) into (3.6), the condition for respecting the nadir requirement can be deduced:

$$|\Delta f_{\mathrm{nadir}}| = |\Delta f(t = t_{\mathrm{nadir}})| \leq \Delta f_{\mathrm{max}} \tag{3.8}$$

Finally, expanding the expression in (3.8) and enforcing the conditions for t_{nadir} to occur during time-interval $t \in [\mathrm{T}_{n-1}, \mathrm{T}_n)$, the nadir constraint is obtained as:

if $\left(\sum_{i=1}^{n-1} R_i + \sum_{j=n}^{|\mathcal{S}|} R_j \frac{\mathrm{T}_{n-1}}{\mathrm{T}_j} \leq P_{\mathrm{L}} \right)$ and $\left(\sum_{i=1}^{n} R_i + \sum_{j=n+1}^{|\mathcal{S}|} R_j \frac{\mathrm{T}_n}{\mathrm{T}_j} > P_{\mathrm{L}} \right)$ then enforce:

$$\underbrace{\left(\frac{H + H_{\mathrm{D}}}{f_0} - \sum_{i=1}^{n-1} \frac{R_i \cdot \mathrm{T}_i}{4\Delta f_{\mathrm{max}}} \right)}_{= x_1} \underbrace{\sum_{j=n}^{|\mathcal{S}|} \frac{R_j}{\mathrm{T}_j}}_{= x_2} \geq \frac{(P_{\mathrm{L}} - \sum_{i=1}^{n-1} R_i)^2}{4\Delta f_{\mathrm{max}}} \tag{3.9}$$

As one must consider the possibility of nadir occurring at any time $t \in \left[0, \mathrm{T}_{|\mathcal{S}|}\right)$ (note that the nadir must occur before $\mathrm{T}_{|\mathcal{S}|}$, as otherwise the steady-state constraint (3.4) would not hold), $|\mathcal{S}|$ different nadir constraints must be defined, corresponding to each time-interval $[\mathrm{T}_{\text{s-1}}, \mathrm{T}_{\text{s}})$ $\forall s \in \mathcal{S}$. Only one constraint will be enforced, which is the constraint for which the if-statement in (3.9) is met. Note that conditional statements in optimisation can be implemented using a big-M formulation with auxiliary binary decision variables [72].

Constraints (3.9) are non-linear but are in fact rotated SOCs, therefore convex constraints as x_1 and x_2 in (3.9) are non-negative. SOC Programming generalises Linear Programming, and recently developed interior-point methods allow to efficiently solve these types of conic optimisation problems to global optimality [56]. Furthermore, SOC Programs are the highest class of conic problems whose mixed-integer counterpart can be solved to global optimality using commercial optimisation packages. Since the nadir constraints in (3.9) introduce binary variables for implementing the conditional statements, the resulting optimisation problem is an MISOCP.

In conclusion, constraints (3.3), (3.4) and (3.9) guarantee frequency security in a power system, while considering the dynamics of any finite number $|\mathcal{S}|$ of different FR providers.

Clarification using a particular case

To better illustrate the procedure for obtaining these conditions, consider the following case with three FR-services, where the aggregated system Frequency Response, $\mathrm{FR}(t)$ in (3.1), is defined as:

$$\mathrm{FR}(t) = \begin{cases} \left(\dfrac{R_1}{\mathrm{T}_1} + \dfrac{R_2}{\mathrm{T}_2} + \dfrac{R_3}{\mathrm{T}_3}\right) \cdot t & \text{if } t \leq \mathrm{T}_1 \quad (3.10.1) \\ R_1 + \left(\dfrac{R_2}{\mathrm{T}_2} + \dfrac{R_3}{\mathrm{T}_3}\right) \cdot t & \text{if } \mathrm{T}_1 < t \leq \mathrm{T}_2 \quad (3.10.2) \\ R_1 + R_2 + \dfrac{R_3}{\mathrm{T}_3} \cdot t & \text{if } \mathrm{T}_2 < t \leq \mathrm{T}_3 \quad (3.10.3) \\ R_1 + R_2 + R_3 & \text{if } t > \mathrm{T}_3 \quad (3.10.4) \end{cases}$$

Since three distinct FR services are considered for $\mathrm{FR}(t)$ in (3.10), the time when the nadir occurs will depend on the total amount of FR delivered by each service, i.e. it will depend on the value of R_1, R_2 and R_3. As R_1, R_2 and R_3 will be decision variables in any optimisation problem which minimises the cost of frequency services, it is impossible to know exactly when the nadir will occur before solving the optimisation, and therefore every possibility for nadir must be considered beforehand.

Let's start by assuming that the nadir happens in the first time-interval defined in (3.10), i.e. the time-interval when $t \leq \mathrm{T}_1$. The power equilibrium that takes place at the nadir must then happen in that first time-interval, which means that the following condition holds:

$$R_1 + R_2 \cdot \frac{\mathrm{T}_1}{\mathrm{T}_2} + R_3 \cdot \frac{\mathrm{T}_1}{\mathrm{T}_3} > P_{\mathrm{L}} \tag{3.11}$$

The time within this first time-interval at which nadir is exactly reached is given by solving the swing equation (3.1) for that particular time-interval and setting RoCoF to zero:

$$t_{\text{nadir}} = \frac{P_{\text{L}}}{R_1/\text{T}_1 + R_2/\text{T}_2 + R_3/\text{T}_3} \tag{3.12}$$

One last step is necessary for obtaining the constraint which guarantees nadir security in this first time-interval $t \in [0, \text{T}_1]$, and it involves obtaining the expression for frequency deviation during that time-interval. This can be done by solving (3.1) for $t \in [0, \text{T}_1]$:

$$|\Delta f(t)| = \frac{f_0}{2H}\left(P_{\text{L}} \cdot t - \sum_{i=1}^{3} \frac{R_i}{2\text{T}_i} \cdot t^2\right) \tag{3.13}$$

Lastly, by substituting $t = t_{\text{nadir}}$ into (3.13) using the expression in (3.12), the value of frequency deviation at the nadir can be deduced:

$$|\Delta f(t = t_{\text{nadir}})| = \frac{f_0}{4H} \cdot \frac{(P_{\text{L}})^2}{R_1/\text{T}_1 + R_2/\text{T}_2 + R_3/\text{T}_3} \tag{3.14}$$

In conclusion, by limiting this maximum frequency deviation at the nadir to be below the requirement established by the system operator, i.e. enforcing $|\Delta f(t = t_{\text{nadir}})| \leq \Delta f_{\text{max}}$, the constraint for respecting nadir security is obtained. This constraint takes the form:

$$\frac{H}{f_0} \cdot \left(\frac{R_1}{\text{T}_1} + \frac{R_2}{\text{T}_2} + \frac{R_3}{\text{T}_3}\right) \geq \frac{(P_{\text{L}})^2}{4\Delta f_{\text{max}}} \tag{3.15}$$

Remember that in order to obtain (3.15) we have assumed that the nadir happens during the first time interval for FR(t), which means that condition (3.11) holds. However, the nadir could also occur during any other time-interval defined in (3.10): time-interval 2 where $t \in (\text{T}_1, \text{T}_2]$ or time-interval 3 where $t \in (\text{T}_2, \text{T}_3]$. The nadir constraints that would apply if the nadir happened in any of these time-intervals can be deduced by following the same mathematical procedure described above for time-interval 1. Therefore, all following constraints, along with the conditions for each of them to be enforced, must be implemented in an optimisation problem to guarantee nadir security:

if $\quad R_1 + R_2\frac{\text{T}_1}{\text{T}_2} + R_3\frac{\text{T}_1}{\text{T}_3} > P_{\text{L}} \quad$ then enforce:

$$\frac{H}{f_0} \cdot \left(\frac{R_1}{\text{T}_1} + \frac{R_2}{\text{T}_2} + \frac{R_3}{\text{T}_3}\right) \geq \frac{(P_{\text{L}})^2}{4\Delta f_{\text{max}}} \tag{3.16}$$

else if $\quad R_1 + R_2 + R_3\frac{\mathrm{T}_2}{\mathrm{T}_3} > P_\mathrm{L} \quad$ then enforce:

$$\left(\frac{H}{f_0} - \frac{R_1\mathrm{T}_1}{4\Delta f_\mathrm{max}}\right) \cdot \left(\frac{R_2}{\mathrm{T}_2} + \frac{R_3}{\mathrm{T}_3}\right) \geq \frac{(P_\mathrm{L} - R_1)^2}{4\Delta f_\mathrm{max}} \tag{3.17}$$

else enforce:

$$\left(\frac{H}{f_0} - \frac{R_1\mathrm{T}_1 + R_2\mathrm{T}_2}{4\Delta f_\mathrm{max}}\right) \cdot \frac{R_3}{\mathrm{T}_3} \geq \frac{(P_\mathrm{L} - R_1 - R_2)^2}{4\Delta f_\mathrm{max}} \tag{3.18}$$

The first condition states that the power equilibrium happens before T_1, when none of the three FR services have finished ramping up by the nadir; the second condition states that the power equilibrium happens after T_1 but before T_2, then only FR_1 has finished ramping up by the nadir; finally, the third condition states that the power equilibrium happens after T_2, then both FR_1 and FR_2 have finished ramping up (note that the nadir must always take place before the slowest FR service finishes ramping up, as otherwise it would be impossible to reach a power equilibrium and frequency would drop indefinitely). These conditional constraints (3.16), (3.17) and (3.18), which are only enforced if their associated condition is met, can be implemented in an optimisation problem with the use of auxiliary binary variables, refer to [72] and [73] for further details.

3.2.2 Considering activation delays in certain FR services

In Section 3.2.1, every FR service is considered in (3.2) to start ramping up at the very moment of the power outage. Those FR services would therefore react to any deviation from nominal frequency in the grid, not necessarily caused by the loss of a large power infeed. Here we generalise the model to account for some FR services which start providing FR some time after the power outage:

$$\mathrm{FR}_i(t) = \begin{cases} 0 & \text{if } t \leq \mathrm{T}_{\mathrm{del},i} & (3.19.1) \\ \dfrac{R_i}{\mathrm{T}_i} \cdot (t - \mathrm{T}_{\mathrm{del},i}) & \text{if } \mathrm{T}_{\mathrm{del},i} < t \leq \mathrm{T}_i & (3.19.2) \\ R_i & \text{if } t > \mathrm{T}_i & (3.19.3) \end{cases}$$

The FR service defined in (3.19) is activated $\mathrm{T}_{\mathrm{del},i}$ seconds after the fault, a delay which can be driven by either the frequency deadband of a droop control or the communication delay of an

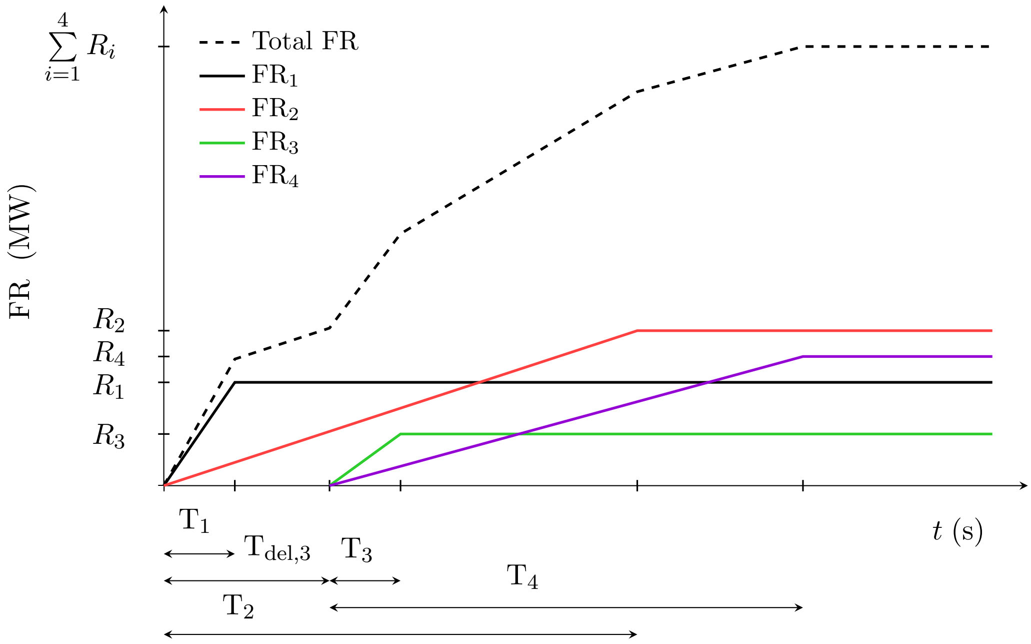

Figure 3.1: Time evolution of four distinct FR services: the first two start ramping up at the very moment of the power outage (which occurs at $t = 0$) and the other two have an activation delay. Note that $\mathrm{T}_{\mathrm{del},4} = \mathrm{T}_{\mathrm{del},3}$ in this case. The total system FR(t) as defined in eq. (3.1) is given by the dashed line.

activation signal sent to the FR provider. For the following deductions in this section, FR(t) as defined in (3.2) may now include FR services with an activation delay as the one defined in (3.19). An example considering four FR services is included in Figure 3.1, where services FR_1 and FR_2 start ramping up at the very moment of the fault (the fault is assumed to happen at $t = 0$) while services FR_3 and FR_4 have an activation delay.

The RoCoF and steady-state constraints constraints, (3.3) and (3.4), remain unchanged while the nadir constraints must be updated if some FR services have an activation delay. Following the same procedure as in Section 3.2.1, the swing equation is solved for the different time-intervals, yielding the following nadir constraint:

$$\underbrace{\left(\frac{H + H_{\mathrm{D}}}{f_0} - \sum_{k\in\mathcal{K}} \frac{R_k(\mathrm{T}_k + 2\mathrm{T}_{\mathrm{del},k})}{4\Delta f_{\max}} + \sum_{l\in\mathcal{L}} \frac{R_l \cdot \mathrm{T}_{\mathrm{del},l}^2/\mathrm{T}_l}{4\Delta f_{\max}}\right)}_{=y_1} \underbrace{\sum_{l\in\mathcal{L}} \frac{R_l}{\mathrm{T}_l}}_{=y_2} \geq \underbrace{\frac{(P_{\mathrm{L}} - \sum_{k\in\mathcal{K}} R_k + \sum_{l\in\mathcal{L}} R_l \cdot \mathrm{T}_{\mathrm{del},l}/\mathrm{T}_l)^2}{4\Delta f_{\max}}}_{=y_3^2} \tag{3.20}$$

Note that if every FR service starts ramping up exactly when the fault occurs, i.e. $\mathrm{T}_{\mathrm{del},k} = \mathrm{T}_{\mathrm{del},l} = 0\ \ \forall k \in \mathcal{K}, \forall l \in \mathcal{L}$, (3.20) reduces to (3.9). Therefore, (3.20) generalises (3.9) allowing to consider any combination of activation delays for FR services. The problem defined is still an MISOCP, since (3.20) is a rotated SOC. In a similar fashion as in (3.9), as many nadir constraints as intervals defined by the piecewise FR(t) must be included, along with the corresponding conditional statements for nadir to occur in that interval. For the example in Figure 3.1, each time-interval corresponds to each of the segments shown in the x-axis.

Clarification using a particular case

Consider the case of two distinct frequency services with also distinct activation delays:

$$\mathrm{FR}(t) = \begin{cases} 0 & \text{if } t \leq \mathrm{T}_{\mathrm{del},1} & (3.21.1) \\ \dfrac{R_1}{\mathrm{T}_1} \cdot (t - \mathrm{T}_{\mathrm{del},1}) & \text{if } \mathrm{T}_{\mathrm{del},1} < t \leq \mathrm{T}_1 & (3.21.2) \\ R_1 & \text{if } \mathrm{T}_1 < t \leq \mathrm{T}_{\mathrm{del},2} & (3.21.3) \\ R_1 + \dfrac{R_2}{\mathrm{T}_2} \cdot (t - \mathrm{T}_{\mathrm{del},2}) & \text{if } \mathrm{T}_{\mathrm{del},2} < t \leq \mathrm{T}_2 & (3.21.4) \\ R_1 + R_2 & \text{if } t > \mathrm{T}_2 & (3.21.5) \end{cases}$$

The RoCoF and q-s-s constraints for this case are still (3.3) and (3.4). The nadir constraints can be deduced following the same procedure as in Section 3.2.1: obtain the analytical expression for t_{nadir} for each of the time intervals defined in (3.21), solve the swing equation (3.1) for each of these time-intervals, and finally substitute the expression for t_{nadir} in the just obtained solution for swing equation. Following these steps, the conditional nadir constraints for this case are:

if $\quad R_1 > P_{\mathrm{L}} \quad$ then enforce:

$$\left(\frac{H}{f_0} + \frac{R_1 \cdot \mathrm{T}_{\mathrm{del},1}^2 / \mathrm{T}_1}{4\Delta f_{\max}} \right) \cdot \frac{R_1}{\mathrm{T}_1} \geq \frac{(P_{\mathrm{L}} + R_1 \cdot \mathrm{T}_{\mathrm{del},1}/\mathrm{T}_1)^2}{4\Delta f_{\max}} \tag{3.22}$$

else enforce:

$$\left(\frac{H}{f_0} - \frac{R_1(\mathrm{T}_1 + 2\mathrm{T}_{\mathrm{del},1})}{4\Delta f_{\max}} + \frac{R_2 \cdot \mathrm{T}_{\mathrm{del},2}^2 / \mathrm{T}_2}{4\Delta f_{\max}} \right) \cdot \frac{R_2}{\mathrm{T}_2} \geq \frac{(P_{\mathrm{L}} - R_1 + R_2 \cdot \mathrm{T}_{\mathrm{del},2}/\mathrm{T}_2)^2}{4\Delta f_{\max}} \tag{3.23}$$

Note that nadir will never happen at time-interval 1 in (3.21) because there is no FR delivered during that interval, so it is impossible to reach a power equilibrium. Nadir will also not happen in time-interval 3, because function $\mathrm{FR}(t)$ is constant during that time-interval. Therefore only time-intervals 2 and 4 in (3.21) have been considered for deducing (3.22) and (3.23).

Both constraints (3.22) and (3.23) are SOCs, and therefore the frequency-secured optimisation problem is still and MISOCP, due to the binary variables introduced by the conditional statements that enforce either (3.22) or (3.23).

3.2.3 Uncertainty in the inertia contribution from demand

In this section we propose chance constraints that allow to take into account the inertia contribution from demand subject to forecasting errors, therefore reducing the need for other frequency services such as inertia from thermal generators or FR. The inertia from demand, H_{D}, is considered as a random variable for which a forecast is available, along with a distribution on the forecasting error. In order to account for this uncertainty in the frequency-security conditions deduced in Sections 3.2.1 and 3.2.2, we modify the RoCoF and nadir constraints to become chance constraints, i.e. constraints that must be met above a predefined probability. Here we provide an exact convex reformulation of the non-convex chance constraints, to allow the system operator to limit the risk of violating each frequency constraint. The error in inertia forecasting is assumed to follow a Gaussian distribution (but any log-concave probability density function still makes the following deductions valid):

$$H_{\mathrm{D}} \sim \mathcal{N}(\mathrm{H}_{\mu}, \sigma^2) \tag{3.24}$$

The chance constraint for meeting the RoCoF requirement is given by the following non-convex constraint, based on (3.3):

$$\mathbf{P}\left(H_{\mathrm{D}} \geq \frac{P_{\mathrm{L}} \cdot f_0}{2 \cdot \mathrm{RoCoF}_{\max}} - H \right) \geq \eta \tag{3.25}$$

Note that H is a decision variable since it is the inertia contribution from the generators scheduled to be online in the UC, and therefore H is not subject to uncertainty.

Chance constraint (3.25) contains a convex constraint in the form $\mathbf{P}\left(g(H_{\mathrm{D}}) \leq 0\right) \geq \eta$, where function $g(H_{\mathrm{D}})$ is:

$$g(H_{\mathrm{D}}) = -(H_{\mathrm{D}} + H) + \frac{P_{\mathrm{L}} \cdot f_0}{2\mathrm{RoCoF}_{\max}} \tag{3.26}$$

Function $g(H_{\mathrm{D}})$ describes a linear transformation of random variable H_{D}, therefore it also follows a normal distribution [74]:

$$g(H_{\mathrm{D}}) \sim \mathcal{N}\Bigg(\underbrace{-(\mu + H) + \frac{P_{\mathrm{L}} \cdot f_0}{2 \cdot \mathrm{RoCoF}_{\max}},}_{=\mu_g}\ \sigma^2\Bigg) \tag{3.27}$$

As shown in [75], by making use of the log-concave property of the normal distribution for the random variable H_{D}, one can notice that the non-convex chance constraint (3.25) is equivalent to:

$$\Phi\left(\frac{-\frac{P_{\mathrm{L}} \cdot f_0}{2 \cdot \mathrm{RoCoF}_{\max}} + H + \mathrm{H}_\mu}{\sigma}\right) \geq \eta \tag{3.28}$$

Therefore, the exact linear reformulation of the RoCoF chance constraint (3.25) is:

$$H + \mathrm{H}_\mu - \Phi^{-1}(\eta)\sigma \geq \frac{P_{\mathrm{L}} \cdot f_0}{2 \cdot \mathrm{RoCoF}_{\max}} \tag{3.29}$$

The chance constraint for the nadir requirement, using the notation in (3.20), is:

$$\mathbf{P}\left[\left(\frac{H + H_{\mathrm{D}}}{f_0} + y_1\right) y_2 \geq y_3^2\right] = \mathbf{P}\left[h(H_{\mathrm{D}}) \leq 0\right] \geq \alpha \tag{3.30}$$

Where function $h(H_{\mathrm{D}})$ is given by:

$$h(H_{\mathrm{D}}) = -\left(\frac{H + H_{\mathrm{D}}}{f_0} + y_1\right) y_2 + y_3^2 \tag{3.31}$$

Function $h(H_{\mathrm{D}})$ is linear with respect to the random variable H_{D}, therefore it also follows a normal distribution [74]:

$$h(H_\mathrm{D}) \sim \mathcal{N}\Bigg(\underbrace{-\left[\frac{H+\mathrm{H}_\mu}{f_0}+y_1\right]y_2+y_3^2}_{=\mu_g},\ \underbrace{\sigma^2\left[\frac{y_2}{f_0}\right]^2}_{=\sigma_g^2}\Bigg) \tag{3.32}$$

Again making use of the log-concave property of the normal distribution, (3.30) becomes:

$$\Phi\left(\frac{0-\mu_g}{\sigma_g}\right) \geq \alpha \tag{3.33}$$

Expanding and rearranging (3.33):

$$\left(\frac{H+\mathrm{H}_\mu-\Phi^{-1}(\alpha)\sigma}{f_0}+y_1\right)y_2 \geq y_3^2 \tag{3.34}$$

Constraint (3.34) is a rotated SOC, therefore it provides a convex reformulation of the chance constraint (3.30), using the notation for the linear expressions y_1, y_2 and y_3 from (3.20). As in (3.20), any combination of distinct FR services with or without activation delays can be considered.

3.3 Marginal-pricing scheme for frequency services

In this section we propose a settlement mechanism which assigns shadow prices to the different frequency services so that an efficient market equilibrium can be obtained. This settlement is based on maximization of social welfare using strong duality.

The optimisation problem defined by the frequency-security constraints contains integer variables, and therefore strong duality does not hold: the solution of the dual optimisation problem, used to obtain shadow prices, is not equal to the solution of the primal problem (refer to [56] for more details on duality in optimisation). The sources of integrality are two: 1) H, since inertia is a discrete magnitude dependent on the on/off state of thermal generators; and 2) Binary variables introduced by the conditional statements for the nadir constraints, as in (3.22) and (3.23). Here we propose a methodology to overcome these issues and allow to define prices for the different frequency services.

Regarding inertia, the approach proposed in [20] is adopted, consisting on relaxing the integer decision variable to a continuous one. Although this approach would not lead to a feasible dispatch, a parallel optimisation maintaining the integrality of H would be run, giving the optimal dispatch. The relaxed problem would then give the market settlement allowing to price inertia as a service.

For the auxiliary binary variables in the nadir conditional statements, the following approach is proposed: first, the original MISOCP is run, which chooses the optimal time for nadir to occur by enforcing only one of the nadir constraints associated with a particular time-interval; then, a new optimisation is run, including only the nadir constraint that was chosen in the previous step and removing any binary variables, therefore yielding a convex SOCP formulation. Using this approach, strong duality holds for the resulting convex problem.

The price of each frequency service can be obtained from the Karush Kuhn Tucker (KKT) conditions of the frequency-constrained optimisation problem. The price-term for each service corresponding to the RoCoF (3.3) and q-s-s (3.4) constraints is immediately obtained from the dual variable of each constraint, since they are linear. These constraints appear in the Lagrangian with their corresponding Lagrange multipliers:

$$\lambda_{\mathrm{R}}\left(\frac{P_{\mathrm{L}} \cdot f_0}{\mathrm{RoCoF}_{\max}} - 2 \cdot H\right) \tag{3.35}$$

$$\lambda_{\mathrm{qss}}[P_{\mathrm{L}} - (R_1 + R_2)] \tag{3.36}$$

For the deduction of the price-terms associated with the nadir constraint in this section, the two FR services with activation delays considered in Section 3.2.2 are also considered. This is because that case allows to present the most general pricing scheme needed, corresponding to nadir happening in time-interval 4 of (3.21): the nadir constraint enforced is then (3.23), for which service FR_1 has finished ramping up while service FR_2 is still ramping up. Therefore, any service that has finished ramping up by the nadir can be priced in the same way as FR_1 in this example, while any service still ramping up can be priced as FR_2.

Before deducing the pricing terms associated with constraint (3.23), it must first be reformulated to be expressed in standard SOC form [76]:

$$\left\| \begin{bmatrix} \frac{1}{f_0} & \frac{-\mathrm{T}_1-\mathrm{T}_{\mathrm{del},1}}{4\Delta f_{\max}} & \frac{\mathrm{T}_{\mathrm{del},2}^2/\mathrm{T}_2}{4\Delta f_{\max}} - \frac{1}{\mathrm{T}_2} & 0 \\ 0 & \frac{-1}{\sqrt{\Delta f_{\max}}} & \frac{\mathrm{T}_{\mathrm{del},2}/\mathrm{T}_2}{\sqrt{\Delta f_{\max}}} & \frac{1}{\sqrt{\Delta f_{\max}}} \end{bmatrix} \begin{bmatrix} H \\ R_1 \\ R_2 \\ P_\mathrm{L} \end{bmatrix} \right\| \\ \leq \begin{bmatrix} \frac{1}{f_0} & \frac{-\mathrm{T}_1-\mathrm{T}_{\mathrm{del},1}}{4\Delta f_{\max}} & \frac{\mathrm{T}_{\mathrm{del},2}^2/\mathrm{T}_2}{4\Delta f_{\max}} + \frac{1}{\mathrm{T}_2} & 0 \end{bmatrix} \begin{bmatrix} H \\ R_1 \\ R_2 \\ P_\mathrm{L} \end{bmatrix} \tag{3.37}$$

This constraint appears in the Lagrangian with its respective vector multipliers:

$$\lambda_1 \left(\frac{H}{f_0} - R_1 \frac{\mathrm{T}_1 + \mathrm{T}_{\mathrm{del},1}}{4\Delta f_{\max}} + R_2 \left[\frac{\mathrm{T}_{\mathrm{del},2}^2/\mathrm{T}_2}{4\Delta f_{\max}} - \frac{1}{\mathrm{T}_2} \right] \right) + \lambda_2 \left(\frac{P_\mathrm{L} - R_1}{\sqrt{\Delta f_{\max}}} + R_2 \frac{\mathrm{T}_{\mathrm{del},2}/\mathrm{T}_2}{\sqrt{\Delta f_{\max}}} \right) \\ - \mu \left(\frac{H}{f_0} - R_1 \frac{\mathrm{T}_1 + \mathrm{T}_{\mathrm{del},1}}{4\Delta f_{\max}} + R_2 \left[\frac{\mathrm{T}_{\mathrm{del},2}^2/\mathrm{T}_2}{4\Delta f_{\max}} + \frac{1}{\mathrm{T}_2} \right] \right) \tag{3.38}$$

The following constraint must be included in the dual problem to comply with the KKT condition for dual feasibility, due to using vector dual variables for the SOC:

$$\left\| \begin{matrix} \lambda_1 \\ \lambda_2 \end{matrix} \right\| \leq \mu \tag{3.39}$$

The KKT stationarity condition is given by the gradient of the Lagrangian. Then, by differentiating the Lagrangian with respect to each frequency service, the corresponding price is obtained:

- The price of H would be:

$$\underbrace{\frac{\mu - \lambda_1}{f_0}}_{\text{nadir}} + \underbrace{2\lambda_\mathrm{R}}_{\text{RoCoF}} \tag{3.40}$$

- The price of P_L is:

$$-\underbrace{\frac{\lambda_2}{\sqrt{\Delta f_\mathrm{max}}}}_{\text{nadir}}\underbrace{-\frac{\lambda_\mathrm{R}\cdot f_0}{\mathrm{RoCoF}_\mathrm{max}}}_{\text{RoCoF}}\underbrace{-\lambda_\mathrm{qss}}_{\text{q-s-s}} \tag{3.41}$$

  Note that the price for P_L would be negative since a larger loss would increase the cost for ancillary-service provision.

- The price of an FR service which has finished ramping up by nadir (as FR_1 in this example) is given by:

$$\underbrace{\frac{\lambda_2}{\sqrt{\Delta f_\mathrm{max}}}-(\mu-\lambda_1)\frac{\mathrm{T}_1+\mathrm{T}_\mathrm{del,1}}{4\Delta f_\mathrm{max}}}_{\text{nadir}}\underbrace{+\lambda_\mathrm{qss}}_{\text{q-s-s}} \tag{3.42}$$

  Therefore the value of the service decreases with increasing delivery time and increasing delay. In other words, the service becomes less valuable as its dynamics are slower.

- The price of FR services still ramping up by the nadir (as FR_2 in this example) is given by:

$$\underbrace{(\mu+\lambda_1)\frac{1}{\mathrm{T}_2}+(\mu-\lambda_1)\frac{\mathrm{T}^2_\mathrm{del,2}/\mathrm{T}_2}{4\Delta f_\mathrm{max}}-\lambda_2\frac{\mathrm{T}_\mathrm{del,2}/\mathrm{T}_2}{\sqrt{\Delta f_\mathrm{max}}}}_{\text{nadir}}\underbrace{+\lambda_\mathrm{qss}}_{\text{q-s-s}} \tag{3.43}$$

The pricing methodology proposed in this section applies to any convex optimisation problem which includes the frequency-security constraints deduced in Section 3.2, including the case in which the energy and FR markets are cleared simultaneously.

3.3.1 Discussion on uplift

The inherent non-convexities in power systems, where the commitment decision of thermal units is forcibly a binary variable, makes it impossible to apply duality theory even to price energy in electricity markets. This issue has been studied in the literature and several approaches have been proposed to overcome this challenge and obtain marginal prices for energy [77]:

- Dispatchable model, where the commitment decision of thermal units is relaxed from binary to continuous, as used in the present thesis.

- Restricted model, which consist on first running the original mixed-integer problem, then running a second optimisation relaxing the commitment decision but using equality constraints to force the commitment variables to take the same value as in the solution of the original, mixed-integer problem. Some studies have observed that this model can lead to high volatility of energy prices [76].

- Convex hull approach, which consists on substituting the original mixed-integer problem by its convex hull, i.e. the tightest possible convex relaxation of the original problem. The authors in [77] argue that this approach provides the smallest make-whole payments, while computing the convex hull of a problem is a very computationally-intensive task.

This is still an active area of research, as no method has been proven to be superior in all instances for the pricing of "uplift" (some very recent publications on the matter are available [78]). The term "uplift" refers to the payments that must be made to certain generators in order to compensate for the negative revenue that they might obtain at times, given that the energy prices only support the optimal solution in the simplified, convex model where they are derived from, but not in the original non-convex model that more accurately represents the real power system.

Since the pricing of uplift is inherently related to the non-convexities in a power system and not just related to inertia, it is out of the scope of the present thesis to study uplift in detail. Therefore, we have opted to use the dispatchable model for allowing to price inertia, as was proposed in [20]. However, our pricing formulation could also be applied if any of the other methods for pricing uplift is considered. Future work should study the implications of other uplift-pricing models for the co-optimisation of energy and frequency services.

3.4 Validation and applicability of the frequency-security constraints

The frequency-security constraints obtained in Section 3.2 are purely mathematical deductions from the swing equation (3.1), and hence guaranteed to provide the security region entailing no approximation. However, the assumptions for function $\mathrm{FR}(t)$ in (3.2) are conservative, as considering detailed frequency controls in the swing equation would impede to solve it algebraically, and therefore no closed-form frequency-security conditions could be obtained. In this section we demonstrate that the assumptions for FR(t) do indeed underestimate an actual frequency droop control, a demonstration based on comparing FR(t) with an actual dynamic simulation to which we feed the solution of a frequency-constrained optimisation.

For the validation of the dynamic model for post-fault frequency, a generic case including four FR services has been considered: two FR services with no activation delay, FR_1 and FR_2, with delivery times $\mathrm{T}_1 = 3$s and $\mathrm{T}_2 = 10$s; an FR service, FR_3, with $\mathrm{T}_{\mathrm{del},3} = 0.5$s and $\mathrm{T}_3 = 5$s; and another FR service, FR_4, with $\mathrm{T}_{\mathrm{del},4} = 1$s and $\mathrm{T}_4 = 8$s. An operating point exactly meeting the nadir constraint (3.20) was fed into a dynamic simulation in MATLAB/Simulink, for which the dynamics of FR providers are modelled as in Figure 3.2. The operating condition exactly meeting the nadir is $P_{\mathrm{L}} = 1.8$GW, $H = 180$GWs, $R_1 = 0.2$GW, $R_2 = 0.98$GW, $R_3 = 0.5$GW, $R_4 = 0.6$GW. A damping term of 0.15GW/Hz was added to the dynamic simulation, in order to analyse the impact of neglecting such support in the frequency constraints.

The results of the dynamic simulation are shown in Figure 3.3 and Figure 3.4. The nadir is of 0.72Hz, indeed above the $\Delta f_{\max} = 0.8$Hz requirement. Although the nadir constraint

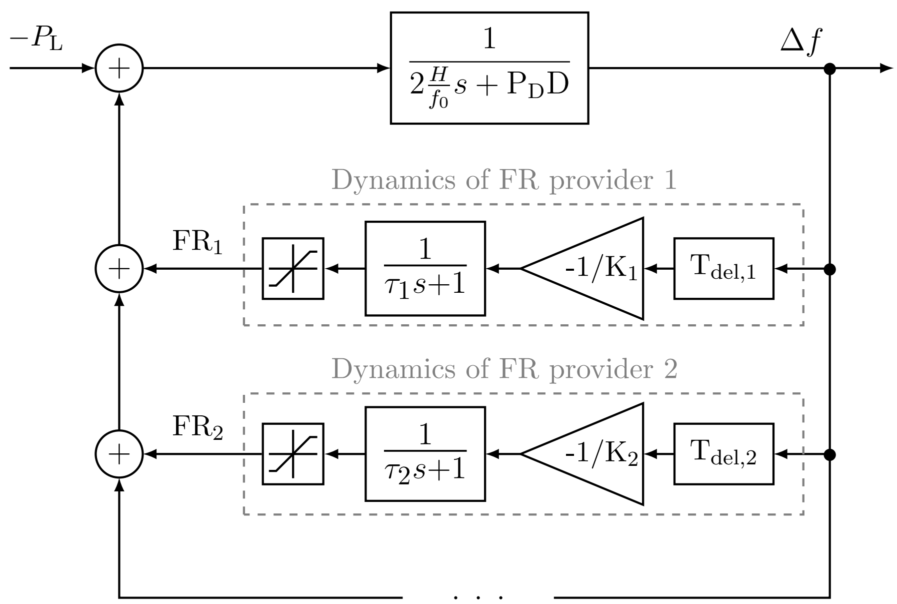

Figure 3.2: Block diagram for the simulation of the system frequency dynamics.

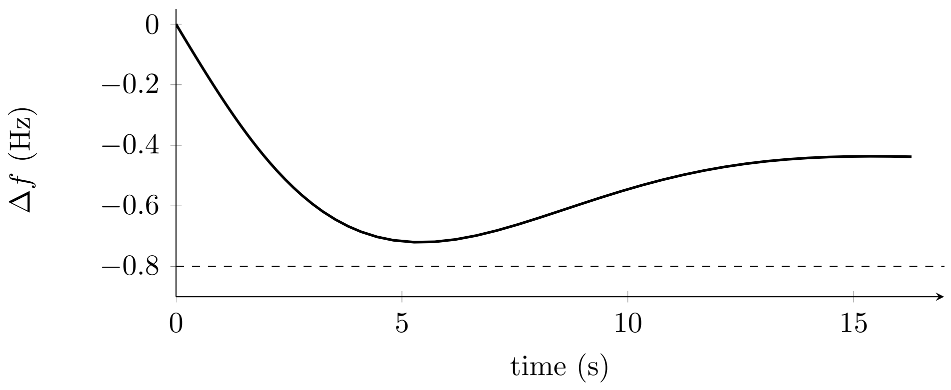

Figure 3.3: Post-fault frequency deviation from the dynamic simulation.

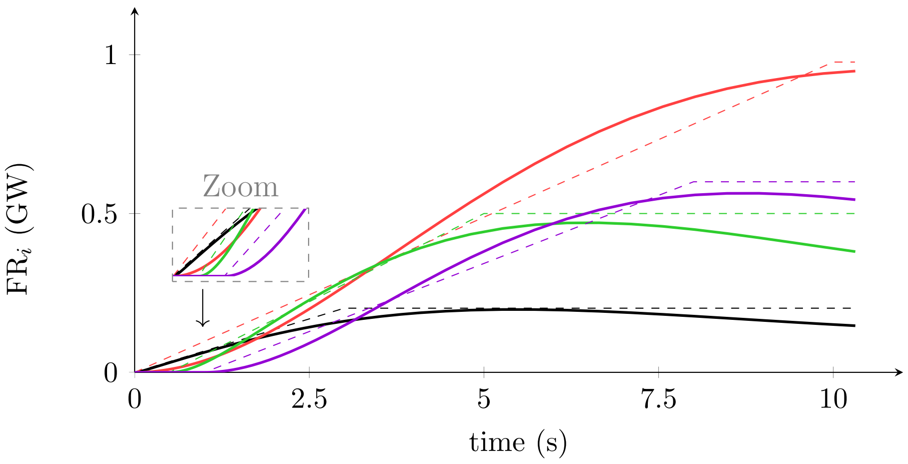

Figure 3.4: Time-evolution of FR obtained from the dynamic simulation considering the four different providers: FR_1 and FR_2 do not have an activation delay (black and red lines), while FR_3 and FR_4 have a delay (green and purple lines). The dashed lines represent the FR profile for each provider assumed in (3.2).

was binding for this system condition, the 0.08Hz conservativeness in the simulation is due to neglecting the damping support and the linear-ramp assumption for FR delivery in (3.2).

The validation of the frequency constraints has been performed for a particular system condition simply to illustrate the appropriateness of the proposed model. Even for contingencies of different sizes, this model guarantees post-fault frequency security as long as the ramps for FR are appropriately chosen to represent the frequency controls: the linear-ramp assumption for FR delivery in (3.2) can conservatively approximate a generic FR dynamics, such as the droop control in Figure 3.2, as was demonstrated by [23].

3.4.1 Applicability to system scheduling and dispatch

The frequency-security constraints deduced in this thesis can be used to solve the scheduling of a power grid while guaranteeing that enough inertia and FR will be available in the event of an outage. After the commitment solution is fixed, and therefore the inertia level is decided, the system operator could then send the order to the chosen providers for frequency response to adjust their frequency control: in the case of droop-controlled generators, the droop gains would be changed to guarantee the agreed FR deliverable by the specified time after a fault; in the case of converter-based devices (such as battery storage or smart loads), their fast power injections are similar to ramps controlled by activation signals, so their FR dynamics would closely match the ones considered in eq. (3.19) without further tuning.

Before solving the frequency-constrained scheduling, the system operator could gather information from all devices willing to provide frequency response: these providers would have to submit the fastest delivery time that the device can comply with under any possible system condition (i.e. any level of inertia combined with contingency size), which for the case of generators would likely come from their ramp limitations. With this information, the system operator would solve the frequency-secured UC, and after that would inform FR providers of the chosen level of inertia and contingency size so that their frequency controls can be tuned appropriately.

This proposed approach is consistent with current practice in Great Britain (and to the best of our knowledge, in other power systems in the world), which simply establishes that a particular service such as Primary Frequency Response must be fully delivered 10 seconds following a contingency. PFR providers have to guarantee delivery of the agreed amount of FR by this time, no matter the size of the contingency.

While FR is expected to be increasingly delivered by converter-based devices, which therefore would entail no conservativeness in the dispatch of FR using the constraints proposed here, if in a given system most of the providers of FR are droop-controlled generators, future work could be oriented towards reducing conservativeness in the FR solution. That is, studying ways in which full potential of FR delivery can be extracted by more precisely mapping the ramp parameters considered in the frequency constraints (T_s and $\mathrm{T}_{\mathrm{del},s}$) to the droop dynamics. This mapping would need to be done before solving the frequency-secured UC, when the inertia and contingency size are not yet known, so that the FR provider can submit appropriate dynamic parameters to the system operator before the frequency-secured scheduling is solved.

3.5 Case studies: demonstrating the applicability of the marginal-pricing scheme

In this section we carry out several frequency-secured Economic Dispatch (ED) and Unit Commitment (UC) optimisations, to demonstrate the applicability and implications of our proposed marginal-pricing methodology for frequency services. These optimisation problems, formulated as MISOCPs due to the conditional nadir constraints, were implemented in YALMIP [79], an optimisation modelling layer for MATLAB, while the low-level numerical computations were solved by calling commercial solver Gurobi. The code used for solving these examples is available in this link: https://github.com/badber/MultiFR_optimisation.

In these studies the different generators submit a bid for providing energy to the market operator, and the market clearing consists on minimising total system costs. There is no explicit bid for inertia or FR provision. The frequency-security requirements are set to $\mathrm{RoCoF}_{\mathrm{max}} = 1\mathrm{Hz/s}$ and $\Delta f_{\mathrm{max}} = 0.8\mathrm{Hz}$.

3.5.1 Value of single-speed FR

This section demonstrates that if there are no distinct speeds for FR, the pricing scheme for the single FR service is equivalent to that of reserve: generators simply recover their opportunity cost. This study is based on Example 6.7 in [63], which demonstrates that by using the dual variable from the reserve constraint in a simultaneous clearing of the energy and reserve markets, all the generators would recover the opportunity cost from limiting their power output due to providing reserve.

To illustrate this point, we run a single-time-period ED, simultaneously clearing the energy and FR markets. The optimisation problem is formulated as:

$$\min \quad \sum_{g\in\mathcal{G}} \mathrm{c}_g^{\mathrm{m}} \cdot P_g \tag{3.44}$$

$$\text{s.t.} \quad \sum_{g\in\mathcal{G}} P_g = \mathrm{P_D} \tag{3.45}$$

$$0 \leq P_g \leq \mathrm{P}_g^{\max} \qquad \forall g \in \mathcal{G} \tag{3.46}$$

$$0 \leq R_g \leq \mathrm{R}_g^{\max} \qquad \forall g \in \mathcal{G} \tag{3.47}$$

$$0 \leq R_g \leq \mathrm{P}_g^{\max} - P_g \quad \forall g \in \mathcal{G} \tag{3.48}$$

RoCoF constraint

Nadir constraints

q-s-s constraint

Constraint (3.45) enforces the power balance, (3.46) enforce generation limits, (3.47) enforce FR-provision limits, and (3.48) limits FR provision to be below the headroom of each generator.

The characteristics of generators participating in the energy and FR markets are given in Table 3.1. All generators willing to provide FR are assumed to provide Primary Frequency Response with a delivery time of 10s, which was the only FR service defined by National Grid in Great Britain until 2016. The largest possible outage is driven by the largest single plant, the nuclear unit, therefore setting $P_{\mathrm{L}} = \mathrm{P}_{\mathrm{L}}^{\max} = 100$MW. Note that there are 5 units of Generators type 1, therefore each of them has a rating of 80MW. Similarly, 5 units of Generators type 2 are available, with a 60MW-rating each.

Table 3.1: Characteristics of thermal generators

	Nuclear	Gen. type 1	Gen. type 2
Power range (MW)	100-100	0-400	0-300
Number of Units	1	5	5
FR capacity (MW)	0	225	175
Energy bid (£/MWh)	15	17	18
Inertia constant (s)	6	6	6
FR delivery time (s)	N/A	10	10

Some further clarifications on Table 3.1: for the sake of simplicity, we choose zero Minimum Stable Generation (MSG) for all generators, to better illustrate the pricing of FR services (zero MSG was also used in Example 6.7 in [63]). Also for clarity, we consider fixed system inertia; however, the co-optimisation of inertia and FR is possible with our model, and will be demonstrated in a UC example in Section 3.5.5.

Since both types of generators 1 and 2 in Table 3.1 have the same FR delivery-time of 10s, the nadir constraint is:

$$R_1 \geq \frac{(P_\mathrm{L})^2 \cdot \mathrm{T}_1 \cdot f_0}{4\Delta f_{\mathrm{max}} \cdot H} = 372\mathrm{MW} \tag{3.49}$$

Which is equivalent to a fixed reserve requirement, such as Reserve $\geq$ 372MW.

The results for a low-demand case of $\mathrm{P_D} = 250\mathrm{MW}$ are presented in Table 3.2:

Table 3.2: Solution of the frequency-secured ED for the system in Table 3.1, for a low-demand case of $\mathrm{P_D} = 250\mathrm{MW}$.

	Nuclear	Gen. type 1	Gen. type 2
Power produced (MW)	100	150	0
FR provided (MW)	0	197	175
Revenue from energy (£)	1700	2550	0
Revenue from FR (£)	0	0	0
Profit (£)	200	0	0
Energy price (£/MWh)	17		
FR price (£/MW)	0		

The energy price has been calculated using the dual variable of the power-balance constraint (3.45), and the FR price comes from the dual variable of (3.49). Profit has been calculated assuming a competitive market in which energy bids are equal to marginal costs.

In this low-demand case, since FR is provided for free and all the energy can be provided by the cheapest Generators type 1, the price for FR is of £0/MW. However, if the demand increases to reach $\mathrm{P_D} = 400\mathrm{MW}$, the clearing prices change:

Table 3.3: Solution of the frequency-secured ED for the system in Table 3.1, for a high-demand case of $P_D = 400$MW.

	Nuclear	Gen. type 1	Gen. type 2
Power produced (MW)	100	203	97
FR provided (MW)	0	197	175
Revenue from energy (£)	1800	3654	1746
Revenue from FR (£)	0	197	175
Profit (£)	300	400	175
Energy price (£/MWh)	18		
FR price (£/MW)	1		

Now that the demand has increased, Generators type 2 start providing energy, so that Generators type 1 can still provide 197MW of FR (because the FR provision from Generators type 2 is capped at 175MW). The price of FR becomes £1/MW while the price of energy is now of £18/MW, so Generators type 1 are indifferent to providing FR or selling more energy: if they are part-loaded to provide FR, they recover the opportunity cost of not providing as much energy as they could.

This study has demonstrated that if a single FR service is defined, as was common practice in Great Britain until recently, the same principles as for reserve pricing could be applied, since there was no significant difference between the single-speed FR and reserve. However, the following section will demonstrate the need for a marginal-pricing scheme tailored for FR if multi-speed FR services are to be recognised by the operator.

3.5.2 Value and incentives for multi-speed FR

The case study presented here will demonstrate the difference between marginal-pricing for reserve and marginal-pricing for FR when more than one FR service is available.

Now let's consider the same system as in Section 3.5.1, but assuming that Generators type 1 can actually provide FR in 7s, corresponding to a "fast PFR" service that some gas plants could provide [80]. These Generators type 1 then increase their energy bid to £19/MWh due to providing this faster FR service (they then become the most expensive generators):

Table 3.4: Characteristics of thermal generators. The only different parameters with respect to Table 3.1 are given in bold font.

	Nuclear	Gen. type 1	Gen. type 2
Power range (MW)	100-100	0-400	0-300
Number of Units	1	5	5
FR capacity (MW)	0	225	175
Energy bid (£/MWh)	15	**19**	18
Inertia constant (s)	6	6	6
FR delivery time (s)	N/A	**7**	10

The results for a demand of $\mathrm{P_D}$ = 400MW are presented in Table 3.5:

Table 3.5: Solution of the frequency-secured ED for the system in Table 3.4, for a demand of $\mathrm{P_D}$ = 400MW.

	Nuclear	Gen. type 1	Gen. type 2
Power produced (MW)	100	50.6	249.4
FR provided (MW)	0	225	50.6
Revenue from energy (£)	1900	961.4	4738.6
Revenue from FR (£)	0	315	50.6
Profit (£)	400	315	300
Energy price (£/MWh)	19		
$\mathrm{FR_1}$ price (£/MW)	1.4		
$\mathrm{FR_2}$ price (£/MW)	1		

After solving the ED optimisation, one can verify that the enforced nadir constraint in this case is:

$$\frac{R_1}{\mathrm{T_1}} + \frac{R_2}{\mathrm{T_2}} \geq \frac{(P_\mathrm{L})^2 \cdot f_0}{4\Delta f_{\mathrm{max}} \cdot H} \tag{3.50}$$

Simplifying the previous constraint:

$$1.4 \cdot R_1 + R_2 \geq 372\mathrm{MW} \tag{3.51}$$

These results show that Generators type 2 are compensated for their part-loading by the payment for $\mathrm{FR_2}$, therefore they recover their opportunity cost. On the other hand, Generators type 1 increase their revenue from providing the faster service $\mathrm{FR_1}$ than if they were fully loaded to sell more energy. This demonstrates that fast provision of FR is incentivised under the proposed marginal-pricing scheme: FR providers can make a profit from providing faster

FR, not simply recover the opportunity cost. Otherwise, there would be no incentive for FR providers to achieve faster delivery of FR. This is the key difference between reserve and FR: the delivery time of FR is of critical importance (as it defines the FR ramping-up capability), while for reserve it is not necessary to ramp up in a matter of seconds, and therefore delivery time can be ignored. The delivery time of FR is reflected in the marginal pricing for FR that we propose. Therefore our methodology puts the right incentives in place to reduce whole system costs, as generators are incentivised to provide faster FR and that in turn benefits the whole system.

3.5.3 Incentive for reducing FR activation delays

Here we study the impact of an activation delay in the value of an FR service, for which we use the same system as in Table 3.4 but considering that service FR_1 now has a 0.4s delay, i.e. $\mathrm{T}_{\mathrm{del},1} = 0.4$s. For a graphical description of activation delays, see Figure 3.1.

The results for a demand of $\mathrm{P_D} = 400$MW are presented in Table 3.6:

Table 3.6: Solution of the frequency-secured ED for the system in Table 3.4, for a demand of $\mathrm{P_D} = 400$MW. Service FR_1 has a 0.4s activation delay in this case.

	Nuclear	Gen. type 1	Gen. type 2
Power produced (MW)	100	143.5	156.5
FR provided (MW)	0	225	143.5
Revenue from energy (£)	1900	2726.5	2973.5
Revenue from FR (£)	0	222.7	143.5
Profit (£)	400	222.7	300
Energy price (£/MWh)	19		
FR_1 price (£/MW)	0.99		
FR_2 price (£/MW)	1		

The enforced nadir constraint in this case is:

$$\left(\frac{H}{f_0} + \frac{R_1 \cdot \mathrm{T}_{\mathrm{del},1}^2/\mathrm{T}_1}{4\Delta f_{\max}}\right) \cdot \left(\frac{R_1}{\mathrm{T}_1} + \frac{R_2}{\mathrm{T}_2}\right) \geq \frac{(P_\mathrm{L} + R_1 \cdot \mathrm{T}_{\mathrm{del},1}/\mathrm{T}_1)^2}{4\Delta f_{\max}} \tag{3.52}$$

The price of service FR_1 has dropped to £0.99/MW, making FR_1 less valuable than FR_2 although the delivery time of FR_2 is still longer than T_1, but FR_2 still has no delay. Due to the 0.4s activation delay, the profit of Generators type 1 has decreased by 29% compared to the results in Table 3.5, which demonstrates how FR providers are incentivised to reduce their activation delay with our marginal-pricing methodology.

3.5.4 Value of a reduced largest-loss

Now we analyse the value of a "reduced largest-loss": the value from part-loading the nuclear unit in order to reduce the need for FR. Note that this value of P_{L} is set by the power output of the nuclear unit in this system, since the nuclear plant drives the largest power infeed.

Table 3.7: Characteristics of thermal generators. The only different parameter with respect to Table 3.4 is given in bold font.

	Nuclear	Gen. type 1	Gen. type 2
Power range (MW)	**90**-100	0-400	0-300
Number of Units	1	5	5
FR capacity (MW)	0	200	150
Energy bid (£/MWh)	15	19	18
Inertia constant (s)	6	6	6
FR delivery time (s)	N/A	7	10

Table 3.8: Solution of the frequency-secured ED for the system in Table 3.7, for a high-demand case of $\mathrm{P_D} = 400\mathrm{MW}$.

	Nuclear	Gen. type 1	Gen. type 2
Power produced (MW)	93	7	300
FR provided (MW)	0	225	0
Revenue from energy (£)	1767	133	5700
Revenue from reduced-P_{L} (£)	28	-	-
Revenue from FR (£)	0	186.8	0
Profit (£)	400	186.8	300
Energy price (£/MWh)	19		
Reduced-P_{L} price (£/MW)	4		
$\mathrm{FR_1}$ price (£/MW)	0.83		
$\mathrm{FR_2}$ price (£/MW)	0.58		

The largest possible outage P_{L} can now be reduced by part-loading the nuclear unit, as shown in Table 3.7: although this unit provides the cheapest energy, by part-loading it a lower amount of FR is needed, and therefore lower overall system costs in the simultaneous clearing of the energy and FR markets may be achieved.

The nadir constraint enforced in this case is:

$$H \cdot \left(\frac{R_1}{\mathrm{T}_1} + \frac{R_2}{\mathrm{T}_2} \right) \geq \frac{(P_\mathrm{L})^2 \cdot f_0}{4 \Delta f_{\max}} \tag{3.53}$$

The results in Table 3.8 demonstrate that large nuclear units would recover their opportunity cost from being part-loaded, since the price for this service obtained from the vector dual-variables of the SOC constraint (3.53) is £4/MW, which is the difference between the energy price and the nuclear's energy bid. Generators type 1 still make a profit from providing fast FR in 7s.

A note of caution is necessary, since the payment for a reduced loss might introduce a perverse incentive for large units. To illustrate this point, let's now consider a case for which the marginal-value of a reduced-P_L is actually higher than the opportunity cost for the nuclear unit due to being part-loaded.

Table 3.9: Characteristics of thermal generators. The only different parameter with respect to Table 3.7 is given in bold font.

	Nuclear	Gen. type 1	Gen. type 2
Power range (MW)	**95**-100	0-400	0-300
Number of Units	1	5	5
FR capacity (MW)	0	200	150
Energy bid (£/MWh)	15	19	18
Inertia constant (s)	6	6	6
FR delivery time (s)	N/A	7	10

Consider the system in Table 3.9, for which the results of the ED are provided in Table 3.10: all the part-loading allowed is used in this case, so the nuclear unit would make a higher profit from part-loading than if it were to sell all the energy possible. If the nuclear unit would collect the price of this "reduced-loss" service, a perverse incentive would be created: the nuclear plant could benefit by making things worse for the whole system, i.e. by aiming for a high MSG that would increase the need for frequency services. One way of doing so would be for example to submit a higher-than-truthful MSG to the system operator.

Table 3.10: Solution of the frequency-secured ED for the system in Table 3.9, for a high-demand case of $P_D = 400$MW.

	Nuclear	Gen. type 1	Gen. type 2
Power produced (MW)	95	19.3	285.7
FR provided (MW)	0	225	14.3
Revenue from energy (£)	1805	366.7	5428.3
Revenue from reduced-P_L (£)	35.5	-	-
Revenue from FR (£)	0	315	14.3
Profit (£)	415.5	315	300
Energy price (£/MWh)	19		
Reduced-P_L price (£/MW)	7.1		
FR_1 price (£/MW)	1.4		
FR_2 price (£/MW)	1		

This unwanted incentive can be avoided if the nuclear unit only gets compensated for the opportunity cost of not selling all available power in the energy market, instead of being compensated from the marginal value of P_L. The value of this opportunity cost can be easily calculated from the difference between the marginal price for energy and the marginal cost of the nuclear unit. By collecting this revenue, nuclear units do not need to receive an out-of-market payment, since they would recover their high investment just as planned (as they were conceived as must-run units providing base load at all times) but never make a perverse profit.

Note that the value of nuclear part-loading in a real system would be limited by the ramp rates of the nuclear fleet, since typically a large nuclear unit would have to be part-loaded several hours in advance, as shown in our previous work [1]. We have limited ourselves to a single-period market clearing in these examples for the sake of clarity, but the marginal-pricing formulation presented here could be directly applied to a multi-period market clearing.

3.5.5 Value and incentives for inertia

In this section we run several frequency-constrained UCs, so that the co-optimisation of inertia along with other frequency services can be analysed. System inertia is inherently related to the commitment state of thermal generators, and can be calculated with the following expression:

$$H = \sum_{g\in\mathcal{G}} \mathrm{H}_g \cdot \mathrm{P}_g^{\max} \cdot y_g - \mathrm{P}_{\mathrm{L}}^{\max} \cdot \mathrm{H}_{\mathrm{L}} \tag{3.54}$$

Which considers that the largest unit won't contribute to system inertia after an outage.

The formulation of the single-period UC with frequency constraints used here is as follows:

$$\min \quad \sum_{g\in\mathcal{G}} \mathrm{c}_g^{\mathrm{nl}} \cdot y_g + \mathrm{c}_g^{\mathrm{m}} \cdot P_g \tag{3.55}$$

$$\text{s.t.} \quad \sum_{g\in\mathcal{G}} P_g + \mathrm{P_R} - P_{\mathrm{R}}^{\mathrm{curt}} = \mathrm{P_D} \tag{3.56}$$

$$y_g \cdot \mathrm{P}_g^{\mathrm{msg}} \le P_g \le y_g \cdot \mathrm{P}_g^{\max} \qquad \forall g \in \mathcal{G} \tag{3.57}$$

$$0 \le R_g \le y_g \cdot \mathrm{R}_g^{\max} \qquad \forall g \in \mathcal{G} \tag{3.58}$$

$$0 \le R_g \le \mathrm{P}_g^{\max} - P_g \qquad \forall g \in \mathcal{G} \tag{3.59}$$

$$0 \le P_{\mathrm{R}}^{\mathrm{curt}} \le \mathrm{P_R} \tag{3.60}$$

RoCoF constraint

Nadir constraints

q-s-s constraint

Constraint (3.56) enforces the power balance, (3.57) enforce generation limits, (3.58) enforce FR-provision limits, (3.59) limits FR provision to be below the headroom of each generator, and constraint (3.60) limits RES curtailment to be below RES generation. In this UC we consider the economic inefficiencies of a part-loaded generator through their MSG ($\mathrm{P}_g^{\mathrm{msg}}$) and no-load cost ($\mathrm{c}_g^{\mathrm{nl}}$), as explained in Section 1.2.1.

As explained in Section 3.3, the procedure to apply the marginal-pricing scheme and overcome the integrality of the UC is: 1) Solve the Mixed-Integer Second-Order Cone UC; 2) Solve again, relaxing the commitment decision for generators from binary to continuous and enforcing only the nadir constraint chosen in step 1, so that the problem becomes convex and therefore marginal prices can be computed. The marginal prices can be obtained for the dual variables of the problem in step 2, while the feasible operating solution is given by the original MISOCP problem in step 1.

Table 3.11: Characteristics of thermal generators.

	Nuclear	Gen. type 1	Gen. type 2
Power range per unit (MW)	1800-1800	250-500	75-150
Number of Units	1	30	30
No-load cost c_g^{nl} (£)	0	500	500
Marginal cost c_g^{m} (£/MWh)	10	95	50
Inertia constant (s)	5	5	5
FR delivery time (s)	N/A	7	10

Table 3.12: Solution of the frequency-secured UC for the system in Table 3.11, for a demand case of $P_D = 24$GW and a low-RES-generation case of $P_R = 10$GW.

	Nuclear	Gen. type 1	Gen. type 2
Online units	1	24	30
Power produced (GW)	1.8	7.7	4.5
FR provided (GW)	0	4.3	0
Operating cost (£k)	18	743.5	240
Revenue from energy (£k)	172.4	737.6	431
Profit from energy (£k)	154.4	-5.9	191
Total revenue (£k)	172.8	743.4	431.9
Total profit (£k)	154.8	-0.1	191.9
Energy price (£/MWh)	95.79		
Inertia price (£/MWs)	0.041		
FR_1 price (£/MW)	0.79		
FR_2 price (£/MW)	0.55		
RES accommodated (GW)	10GW (0GW curtailed)		

The details of the system used for these case studies are shown in Table 3.11. The solution of the frequency-secured UC for a low-RES-generation case is given in Table 3.12. RES are assumed to have a zero marginal cost (i.e. c_g^{m}=£0/MWh).

The enforced nadir constraint in these cases is:

$$H \cdot \left(\frac{R_1}{\mathrm{T}_1} + \frac{R_2}{\mathrm{T}_2} \right) \geq \frac{(P_{\mathrm{L}})^2 \cdot f_0}{4\Delta f_{\max}} \tag{3.61}$$

These results illustrate that the prices for frequency services would be small in a low-RES-generation condition, since the thermal units are online to cover the net demand (demand minus

RES-generation) and therefore frequency services become a by-product of energy production. It is interesting to notice that a make-whole payment would be necessary for Generators type 1, and this make-whole payment would be much higher if generators were not compensated for inertia and FR (the difference in make-whole payments can be obtained from comparing the profit from energy with the total profit). Although pricing uplift, which is the cause for make-whole payments, is out of the scope of this work, this example demonstrates that remunerating generators for these ancillary services would reduce the amount of make-whole payments, a conclusion that was also reached in [65].

Table 3.13: Solution of the frequency-secured UC for the system in Table 3.11, but considering that the inertia constant of Gen. type 2 is increased to 6s. The demand level is set to $P_D = 24$GW and a low-RES-generation case of $P_R = 10$GW is considered, same as for the results shown in Table 3.12.

	Nuclear	Gen. type 1	Gen. type 2
Online units	1	24	30
Power produced (GW)	1.8	7.7	4.5
FR provided (GW)	0	4.1	0
Operating cost (£k)	18	743.5	240
Revenue from energy (£k)	172.4	737.7	431.1
Profit from energy (£k)	154.4	-5.8	191.1
Total revenue (£k)	172.8	743.4	432.2
Total profit (£k)	154.8	-0.1	192.2
Energy price (£/MWh)	95.80		
Inertia price (£/MWs)	0.039		
FR_1 price (£/MW)	0.81		
FR_2 price (£/MW)	0.56		
RES accommodated (GW)	10GW (0GW curtailed)		

Now let's analyse the incentives for higher inertia provision, by increasing the inertia constant of Generators type 2 to 6s. This study is of relevance to investors in new thermal generation units, who could manufacture turbines with higher inertia if operating revenues increased sufficiently. Retro-fitting existing thermal units to increase their inertia is unlikely to be feasible.

The results in Table 3.13 show that Generators type 2 slightly increase their revenue due to increasing their inertia constant, but this increase is indeed very small, of roughly 0.1% of the total profit. However, the incentives for inertia provision will become clear in a high-RES-generation case, for which the results are presented in Table 3.14:

Table 3.14: Solution of the frequency-secured UC for the system in Table 3.11, for a demand case of $P_D = 24$GW and a high-RES-generation case of $P_R = 18$GW.

	Nuclear	Gen. type 1	Gen. type 2
Online units	1	17	27
Power produced (GW)	1.8	4.25	2.05
FR provided (GW)	0	4.25	2
Operating cost (£k)	18	412.2	116
Revenue from energy (£k)	0	0	0
Profit from energy (£k)	-18	-412.2	-116
Total revenue (£k)	41.4	413.1	166.7
Total profit (£k)	23.4	0.9	50.7
Energy price (£/MWh)	0		
Inertia price (£/MWs)	4.6		
FR_1 price (£/MW)	51.2		
FR_2 price (£/MW)	35.9		
RES accommodated (GW)	15.9GW (2.1GW curtailed)		

Note that in this high-RES-generation case the price of energy drops to £0/MWh due to RES curtailment, since the next MWh of energy could be provided by RES for free. Therefore, all the operating cost of the system is related to the cost of frequency services. The price of inertia has increased by more than a factor 100 compared to the low-RES condition in Table 3.12, while the prices of FR_1 and FR_2 have increased by a factor 65.

Table 3.14 also shows that all generating units are operating at MSG, which illustrates the main driver for RES curtailment in a low-inertia system: since thermal generators providing inertia and FR must be online generating at least MSG, the sum of MSG-energy from all these sources results in RES curtailment of an equivalent value. Regarding the need for a make-whole payment for Generators type 1, it has been completely eliminated by the compensation for inertia and FR.

Let's again increase the inertia constant of Generators type 2 to 6s, to understand the incentives for higher inertia provision:

Table 3.15: Solution of the frequency-secured UC for the system in Table 3.11, but considering that the inertia constant of Gen. type 2 is increased to 6s. The demand level is set to $P_D = 24$GW and a high-RES-generation case of $P_R = 18$GW is considered, same as for the results shown in Table 3.14.

	Nuclear	Gen. type 1	Gen. type 2
Online units	1	16	28
Power produced (GW)	1.8	4	2.1
FR provided (GW)	0	4	2.1
Operating cost (£k)	18	388	119
Revenue from energy (£k)	0	0	0
Profit from energy (£k)	-18	-388	-119
Total revenue (£k)	39.6	388.4	188.8
Total profit (£k)	21.6	0.4	69.8
Energy price (£/MWh)	0		
Inertia price (£/MWs)	4.4		
FR_1 price (£/MW)	53.1		
FR_2 price (£/MW)	37.1		
RES accommodated (GW)	16.1GW (1.9GW curtailed)		

The profit for Generators type 2 has increased by 38% due to increasing their inertia constant by 1s. Furthermore, RES curtailment has been reduced by 0.2GW due to this extra inertia, when compared to the results in Table 3.14.

In conclusion, our pricing scheme promotes higher provision of inertia, which can greatly increase the revenue for generators during high-RES-generation conditions. In turn, the whole system would benefit from a lower RES curtailment, which would reduce overall costs. This also promotes investment in RES that provide services such as synthetic inertia, as they could achieve a revenue even during periods of RES curtailment when the energy price drops to £0/MWh, potentially eliminating the need for subsidies for renewables since the uncertainty in revenues for RES would be reduced.

3.6 Case studies: understanding the value of multi-speed FR through SUC

In order to highlight the importance of co-optimising the provision of distinct FR services, as well as to understand the value of different services under diverse system conditions, several case studies were carried out in the SUC presented in Section 1.2.1, with the frequency-security constraints deduced in Section 3.2 implemented. The characteristics of the GB 2030 system considered are given in Section 1.2.2. A 10GWh pump-storage unit is included, with 2.6GW rating and 75% round efficiency, corresponding to the Dinorwig plant in GB. Battery Energy Storage Systems (BESS) with 90% efficiency and a 5h tank are also present, with a capacity of 200MW.

Simulations spanning one year of operation were run, with frequency-security requirements of $\mathrm{RoCoF}_{\max} = 0.5\mathrm{Hz/s}$ and $\Delta f_{\max} = 0.8\mathrm{Hz}$, while $\mathrm{P}_{\mathrm{L}}^{\max} = 1.8\mathrm{GW}$. The quantiles for the SUC were set to 0.005, 0.1, 0.3, 0.5, 0.7, 0.9 and 0.995.

3.6.1 Importance of defining and co-optimising new FR services

Creating new FR services involves a trade-off between improved market efficiency and increased market complexity. A fundamental question that needs to be answered is "*How many and which new FR services should be defined?*" While previous models [1, 57] only allow to co-optimise up to two distinct FR services, here we show the benefits of optimising additional FR services by applying the proposed frequency-secured formulation, which can efficiently co-optimise any number of FR services. This section therefore focuses on quantifying the value in defining new FR services using the GB 2030 system, while the results give insight on the benefits that new services would bring to any different system.

In this section, some Combined-Cycle Gas Turbines (CCGTs) are assumed to provide FR in less than 10s, corresponding to a "fast PFR" service that some gas plants could provide [80]. The generation mix in Table 2.5 is considered, and from the total number of CCGTs, 70% are assumed to provide PFR in 10s, 20% have the capability of providing FR in 7s and the 10%

remaining have the capability of providing FR in 5s. Four different cases for FR services are defined:

- Base case: only EFR and PFR are defined by the system operator, as is current practice in the UK. Therefore, all CCGTs are considered to provide PFR even if some of them can actually achieve faster FR dynamics. EFR is provided by the BESS.
- Case 1: a new FR service is defined, FR_2, delivered in 7s (i.e. $\mathrm{T}_2 = 7\mathrm{s}$), therefore the CCGTs with the capability of providing FR in 5s and 7s can provide this FR_2.
- Case 2: a new FR service FR_2 is defined with $\mathrm{T}_2 = 5\mathrm{s}$, therefore the CCGTs with the capability of providing FR in 5s can provide this FR_2, while the CCGTs with the capability of providing FR in 7s will provide PFR.
- Case 3: two new FR services are defined, FR_2 with $\mathrm{T}_2 = 5\mathrm{s}$ and FR_3 with $\mathrm{T}_3 = 7\mathrm{s}$. This allows to fully extract the value of the different dynamics in FR-provision available.

For each of these cases, two different wind-capacity levels are considered: 40GW and 60GW. For the CCGTs providing FR in less than 10s, the marginal cost is increased by £0.01/MWh to £46.01/MWh, just so that they are slightly penalised in the optimisation due to providing a more valuable service FR service than the CCGTs simply providing PFR. The nuclear units are assumed to be fully loaded, therefore $P_\mathrm{L} = \mathrm{P}_\mathrm{L}^\mathrm{max} = 1.8\mathrm{GW}$.

The results are presented in Figure 3.5, showing the benefits of the three cases referred to the base case. It is interesting to note that Case 2 shows higher benefits than Case 1: by having only 10% of the CCGTs providing FR in 5s in Case 2 (all other CCGTs are assumed to provide PFR in 10s), higher savings can be achieved than in Case 1, where 30% of the CCGTs provide FR in 7s (20% with the capability of providing FR in 7s plus 10% with the capability of 5s). The results clearly demonstrate the complex task of defining new services, which will be a trade-off between the FR speed of delivery and the amount of provision. Finally, Case 3 shows the benefits from taking full advantage of fast-FR from CCGTs, by defining two new FR services with delivery times of 5s and 7s. For all cases, the savings increase with wind penetration, as higher wind capacity implies lower inertia available from thermal generators, and therefore recognising fast FR services becomes more valuable.

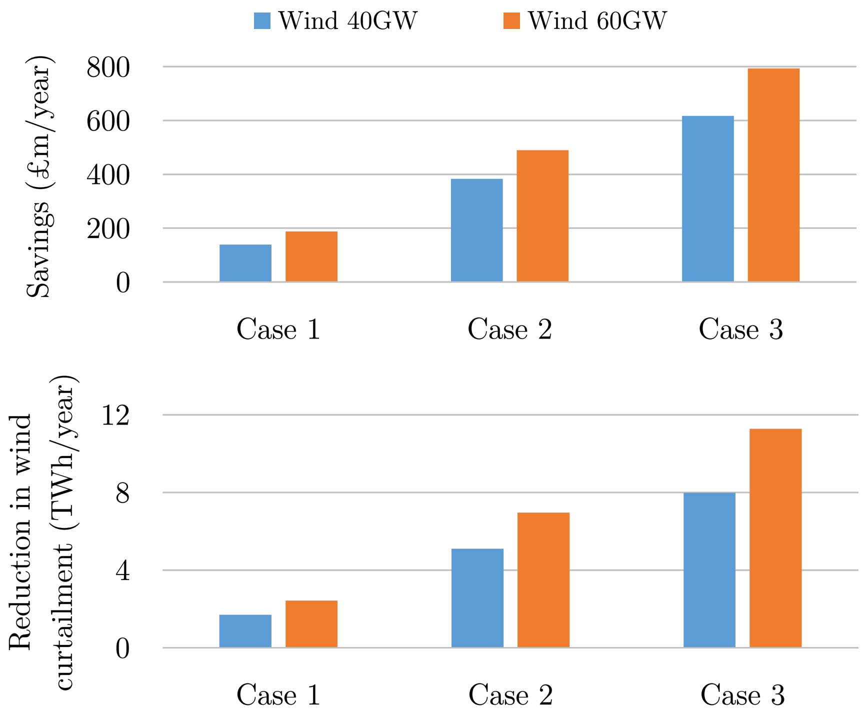

Figure 3.5: Benefits of defining new FR services, in terms of economic savings and reduction in wind curtailment.

Note that the benefits of co-optimising fast FR services are not only in terms of cost, but also in reduced wind curtailment, as shown in Figure 3.5: by defining the new FR services, a lower number of thermal generators need to stay online simply for providing inertia and FR, and therefore more wind power can be accommodated. The wind-curtailment reduction in Figure 3.5 is again referred to the base case, for which wind curtailment was of 31.86TWh/year for the 40GW-wind-capacity scenario (which means a 26.36% of wind energy curtailed) and of 79.97TWh/year for the 60GW-wind-capacity (44.10% wind energy curtailed).

Finally, Figure 3.6 presents the load factor for the different CCGT types for the same simulations mentioned above: the load factor of CCGTs providing "fast FR" is higher than that of CCGTs providing PFR, for every case considered. This difference in load factors increases with wind penetration, and it is explained by the fact that at wind capacities of 40GW or 60GW, CCGTs are often not needed to provide energy but to provide frequency services instead (inertia and FR) instead. Since fast FR is a significantly more valuable service than regular PFR, the CCGTs providing this fast FR are prioritised in the scheduling. As thermal plants need to be online generating at least Minimum Stable Generation in order to provide frequency

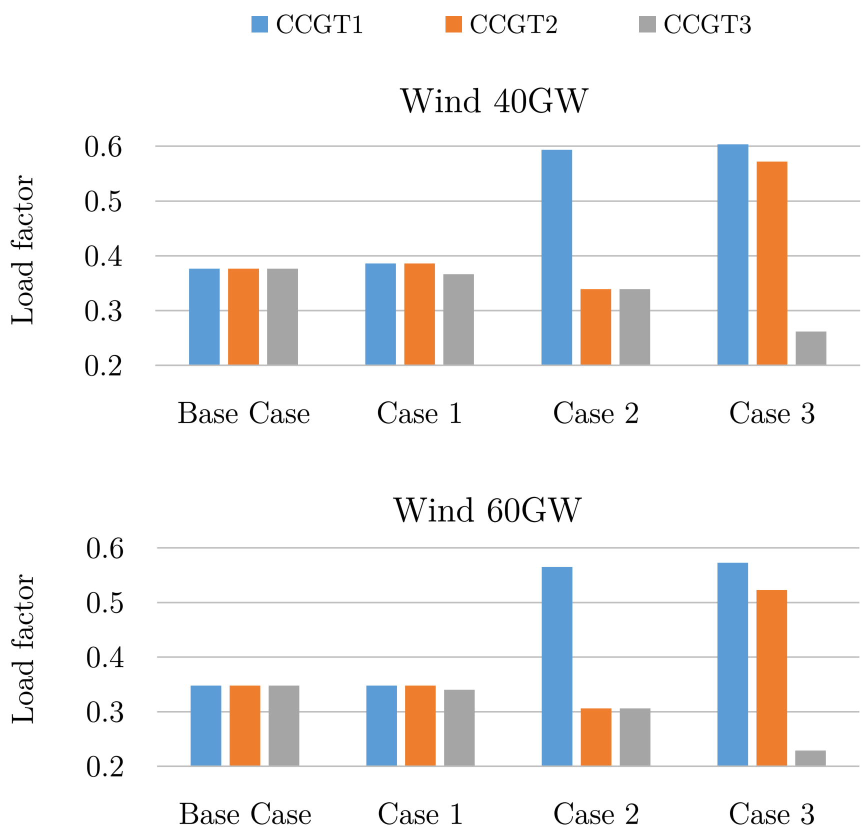

Figure 3.6: Average load factor of the CCGTs with different dynamics for FR provision: "CCGT1" have the capability of providing FR in 5s, "CCGT2" in 7s and "CCGT3" in 10s.

services, that is the reason behind the higher load factor seen for these units.

As an example of the computational efficiency of the proposed formulation, the simulation for Cases 1 and 2 took roughly 2h50min to run. Note that this simulation represents a whole year of operation of the GB 2030 system, for the computationally intensive Stochastic-UC problem. The SUC optimisations were solved with FICO Xpress 8.0 in a 3.5GHz Intel Xeon CPU with twelve cores and 64GB of RAM, and the duality gap for the MISOCPs was set to 0.5%. Case 3, in which four FR services are defined and therefore an additional binary decision variable is needed for the conditional statements in the nadir constraints (3.9), took 5h10min to run. Therefore, although defining more FR services increases the computation time of the system scheduling, it is still manageable for the burdensome SUC problem.

3.6.2 Impact of the availability of frequency services on the benefits from defining new services

The previous section has demonstrated that the value of new FR services will depend on the speed of delivery of these services, but another factor must be taken into account: the availability of frequency services, i.e. the number of units/providers that can deliver each FR service. In order to analyse such impact, we consider that one new FR service has been created, and study the following variations:

- The new FR_2 service is provided by 5%, 10%, 20%, 30% and 40% of the total CCGTs.
- Same as the previous case, but nuclear units are allowed to part-load 400MW from their rated power (note that nuclear part-loading is co-optimised along with every other frequency service).

Furthermore, wind penetrations of 40GW and 60GW are considered, as well as delivery times for FR_2 of $T_2 = 7s$ and $T_2 = 5s$. The "base case" is the same as in Section 3.6.1, where all CCGTs provide PFR.

The results are presented in Figure 3.7, which shows that the benefits from defining a new FR_2 service highly depend on the mix of providers: the savings can be limited if only 5% of the CCGTs can provide FR_2, particularly if there is already 400MW of nuclear part-loading available and $T_2 = 7s$ (savings of £55m/year for a 40GW-wind scenario). The first case titled "No nuclear part-loading" shows increasing savings with respect to the base case when more units can deliver the new FR_2 service, but a saturation effect is also present: when the new FR_2 service defined has a $T_2 = 7s$, going beyond 20% of the CCGTs providing this FR_2 does not further increase savings, while the saturation occurs at 30% of the CCGTs if the new FR_2 service is delivered with $T_2 = 5s$. Moreover, the results for the second case titled "400MW nuclear part-loading" show reduced savings for all scenarios of percentage of CCGTs providing FR_2, wind penetration level, and delivery time for FR_2: this is due to a reduced need for fast FR services when the output level of the largest units (the nuclear units for the GB system) is co-optimised along with FR. In other words, there would exist competition between the "part-loading nuclear" service and fast FR.

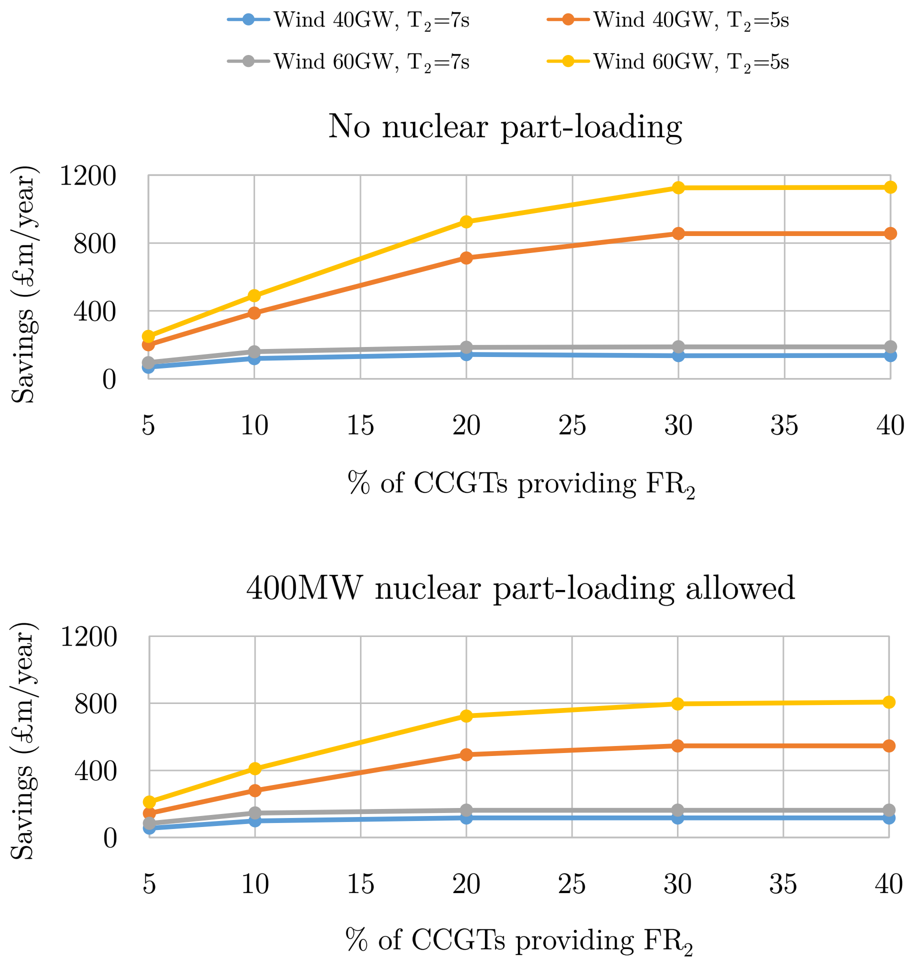

Figure 3.7: Impact of the mix of frequency-services' providers on the savings from defining a new FR service.

In conclusion, these results demonstrate that the system operator should conduct a survey to check how many providers can potentially provide new fast FR services, before starting the process to change the market rules to define such FR services.

3.6.3 Impact of activation delays in FR provision

This section analyses the impact on system operating cost due to activation delays for the different FR services, i.e. the time after the power outage when the FR services are activated and start ramping up. The base case here assumes 30% of the CCGTs providing FR_2 with $T_2 = 5$s. Two different wind capacities are studied: 20GW and 60GW. Then, three cases of FR delays are considered:

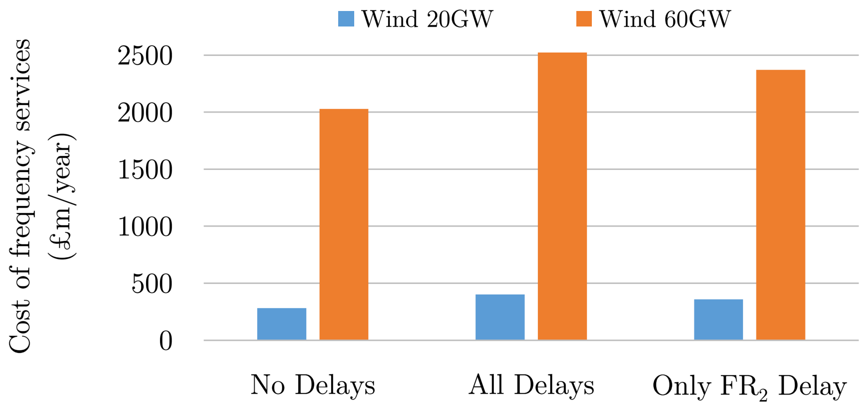

Figure 3.8: Impact of activation delays of FR services on the operational cost of the system.

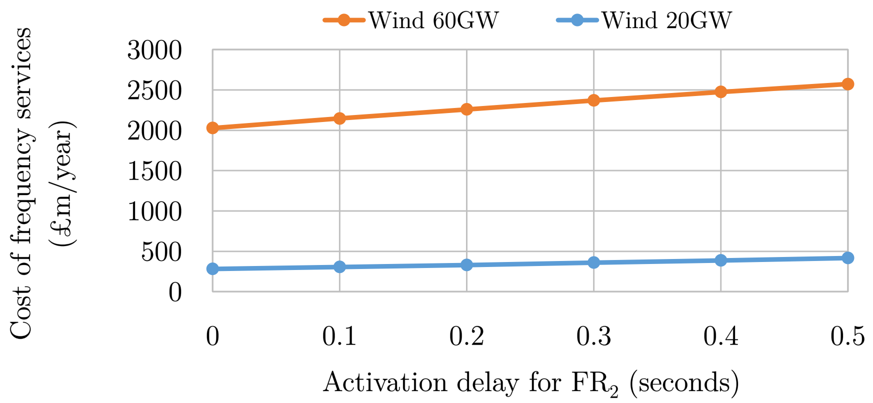

Figure 3.9: Sensitivity analysis for the impact of the activation delay in service FR_2 on the operational cost of the system.

- None of the FR services have an activation delay, therefore they all react to any deviation from nominal frequency.
- All three FR services have a 0.3s activation delay.
- EFR and PFR have no delay, but FR_2 has a 0.3s delay.

While the impact of FR delays on the frequency nadir has been studied through dynamic simulations in [58], no previous work has studied their impact on the system operating cost.

The results are presented in Figure 3.8, which shows the annual cost of frequency services for each case, that is, the cost related to providing inertia and the different types of FR. This "cost of frequency services" is calculated by taking the cost from the solution of the frequency-secured

SUC minus the cost of an SUC with no frequency constraints. By comparing the second case "All Delays" to the first one "No Delays", it is demonstrated that activation delays in the delivery of FR services can significantly reduce their value to the system. However, a 0s delay would mean reacting to any deviation from nominal frequency, which would likely have associated wear-and-tear for the device providing FR. This is particularly true for battery storage providing EFR, since the lifetime of the device can be greatly impacted from the frequent charge-discharge switching that would be caused by reacting to any frequency deviation. Finally, the third case "Only FR_2 delay" shows that by eliminating the delay in the provision of EFR and PFR, the system costs can be reduced by more than £150m/year for a 60GW-wind scenario.

The economic impact of activation delays for FR provision shown in Figure 3.8 is very significant for the 60GW-wind scenario, but this impact is limited for the 20GW-wind scenario. The reason behind it is the low-inertia level driven by the high-wind-penetration scenario of 60GW throughout the year: a reduced inertia greatly increases the need for alternative fast frequency services in order to comply with frequency-security constraints, therefore FR services that start contributing to restoring the power equilibrium at the very moment of the power outage become very valuable.

Finally, Figure 3.9 presents a sensitivity analysis for the activation delay in FR_2, for the case "Only FR_2 delay", demonstrating that a reduction of just 0.1s in $T_{del,2}$ can have a significant impact in annual system costs: reducing the delay from 0.3s to 0.2s would bring £111m/year savings, for the 60GW-wind scenario.

3.6.4 Role of forecast for inertia contribution from demand

In this section we study the system operating cost under different forecasting scenarios for the inertia contribution from the demand side. The base case here considers 30% of the CCGTs providing FR_2 with $T_2 = 7$s and a 40GW wind capacity. The system operator is assumed to require a 99% probability for the RoCoF and nadir constraints (3.29) and (3.34) to be fulfilled, i.e. $\alpha = \eta = 0.99$.

From this base-case, in which no inertia from demand is taken into account, we consider four further cases:

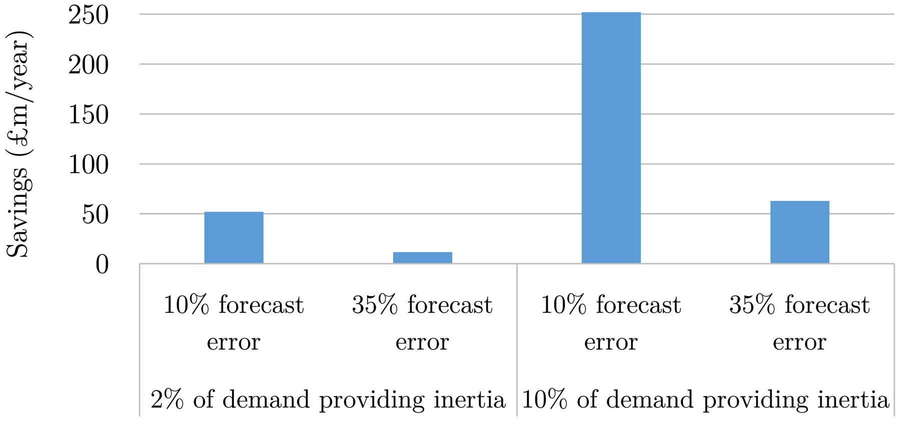

Figure 3.10: Savings from considering the inertia contribution from demand, under different percentages of demand providing inertia and different forecast errors.

- Of the total demand at each time-step in the SUC, 2% is assumed to provide inertia, with a forecast error of 10% (i.e. $\sigma = 0.1\mathrm{H}_\mu$).
- Same as the previous case, but with a forecast error of 35% (i.e. $\sigma = 0.35\mathrm{H}_\mu$).
- Of the total demand at each time-step, 10% is assumed to provide inertia, with a forecast error of 10%.
- Same as the previous case, but with a forecast error of 35%.

The inertia constant for demand is assumed to be 5s in all cases. The study in [68] estimated that 35% of demand would provide inertia on average (the authors demonstrated that demand in GB provides on average 1.75s of inertia, which is equivalent to 35% of demand providing inertia with an inertia constant of 5s), which is also consistent with the findings in [69] for the inertia provided by "residual sources" (synchronous demand and embedded generation). However, since [68] also warns that Variable Frequency Drives are expected to be more widely deployed in the demand side, which would in turn reduce inertia from demand, the studies in this thesis are chosen to be more conservative. We therefore consider only 2% and 10% of the demand to provide inertia, rather than 35%.

The results in Figure 3.10 demonstrate that considering the inertia contribution from demand can bring non-negligible economic savings to the system, more so if a higher percentage of the demand is contributing to inertia. Furthermore, the results highlight the importance of achieving an accurate forecast for the inertia contribution from demand: by reducing the forecast error

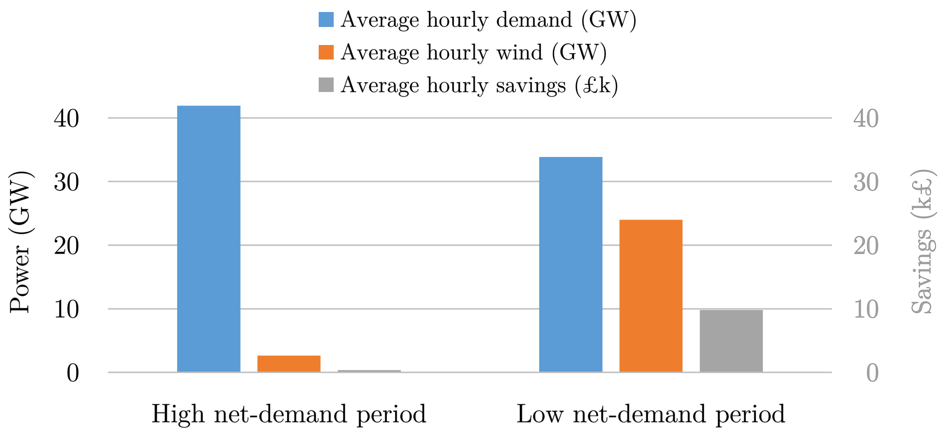

Figure 3.11: Average hourly savings due to considering the inertia contribution from the demand side, for two cases corresponding each to a 50-hour period.

from 35% to 10%, £190m/year additional savings can be obtained, for a case of 10% of demand contributing to inertia.

Furthermore, we analyse in Figure 3.11 the detailed operation of the system by considering two cases, each corresponding to a 50-hour period, but showing significantly different levels of net-demand (demand minus wind): a high net-demand period in January, and a low net-demand period in July.

The results in Figure 3.11, which consider that 2% of the demand provides inertia and the forecast error is of 10%, demonstrate how valuable inertia from demand becomes during low net-demand periods: the savings in the second period (average hourly savings of £9.8k) are significantly higher than in the first period (average hourly savings of £0.36k), although there is less inertia available from the demand side in the former. In the first case, the high net-demand implies that significant inertia from synchronous generators is already available (note that net-demand must be covered by online thermal generators), therefore extra inertia from the demand side is not very valuable in this case.

The results clearly demonstrate that market arrangements need to be in place not only to incentivise the demand side to provide inertia, but also to incentivise these inertia-providing loads to consume during periods when low net-demand is expected.

3.7 Summary of findings

This chapter has presented the following studies and conclusions:

- A frequency-secured formulation in MISOCP form has been introduced, that allows to consider any finite number of FR providers, as well as any combination of activation delays for the different FR services. This is the first time that a convex formulation generalising Linear Programming has been used to guarantee frequency stability. Case studies of frequency-secured SUC have demonstrated the importance of new FR services for achieving cost-efficiency in power systems with significant renewable penetration, while highlighting the difficulty in designing a multi-speed FR market that is both simple and cost effective.

- A marginal-pricing scheme for frequency services such as inertia, different types of FR and a reduced largest-loss has been proposed, allowing for the first time to appropriately value multi-speed response. Through several simple case studies, we demonstrate that this marginal-pricing methodology puts in place the right incentives: providers have been shown to be incentivised to increase their inertia and achieve faster delivery of FR, as they are rewarded according to their speed of delivery. In addition, this methodology could promote investment in RES that provide frequency services, as they could collect revenue even during times of RES curtailment. We further demonstrate that large nuclear units would recover their opportunity cost from being part-loaded, but we also warn against possible perverse incentives and how to mitigate them.

Regarding future work, an efficient way to integrate the approximation for the support of load damping introduced in Chapter 2 into the multi-speed FR model presented in this chapter should be studied. Such a model would allow the co-optimisation of all possible frequency services that could be defined in a power system.

Chapter 4

Beyond the Uniform-Frequency Model: Conditions for Regional Frequency Security

This chapter discusses the phenomenon of distinct regional frequencies recently observed in some power systems. We first study the causes through dynamic simulations and then develop the mathematical model describing this behaviour. Then, techniques to solve the model are discussed, demonstrating that the post-fault frequency evolution in any given region is equal to the frequency evolution of the Centre Of Inertia considered in previous chapters plus certain inter-area oscillations.

This finding leads to the deduction of conditions for guaranteeing frequency security in all regions of such power systems, a deduction performed using a mixed analytical-numerical approach that combines theoretical mathematical analysis with regression methods on simulation samples. The proposed constraints are linear and allow the co-optimisation of all frequency services available. Although some conservative steps are taken to deduce these linear constraints, i.e. steps that tighten the feasible region, we demonstrate that the conservativeness introduced is not significant for practical purposes in a power system.

The work presented here is the first reported mathematical framework that guarantees frequency security in a multi-region system.

4.1 Introduction

In previous chapters we have considered the uniform frequency model, represented by the swing equation: all generators are considered to move coherently as a single lumped mass (Centre Of Inertia concept) and load damping is represented by a single constant. The frequency of the COI can be calculated as [81]:

$$f_{\mathrm{COI}} = \frac{\sum_{\forall g \in \mathcal{G}} \mathrm{H}_g \cdot \omega_g}{2\pi \sum_{\forall g \in \mathcal{G}} \mathrm{H}_g} \tag{4.1}$$

The frequency of the COI is therefore a weighted average of the rotational speeds of all synchronous machines in the system, where the rotational speed of each machine is weighted by the ratio of total system inertia that the machine provides.

While the uniform frequency model provided a precise representation of frequency dynamics in systems dominated by thermal units, recent studies have shown that the Centre Of Inertia representation can be inaccurate in modern grids, in which RES are typically located in remote areas far from load centres, creating a non-uniform distribution of inertia. This non-uniform inertia distribution causes distinct regional frequencies as can be observed in Figure 4.1, obtained from the dynamic simulation of a two-region system where a generation outage occurs in region 2.

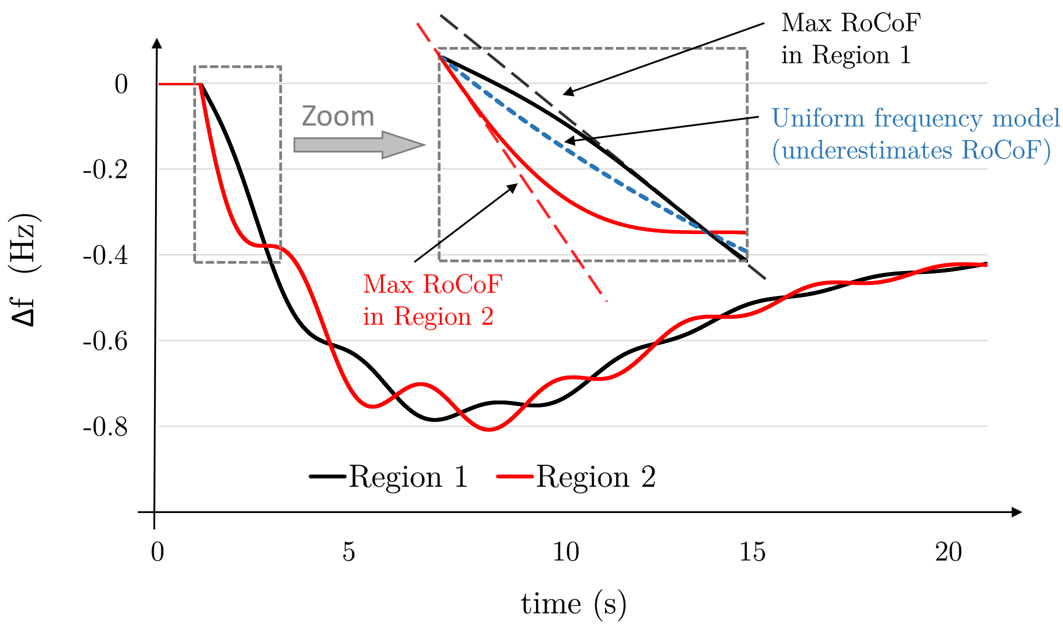

Figure 4.1: Frequency dynamics in a 2-region system after a power outage in region 2.

These geographical discrepancies in frequency have been observed after frequency events in recent years by utilities all over the world. Several recent publications and reports [82–85] highlight this issue, and some propose remedies from a control perspective. The authors in [86] propose a method for optimal placement of virtual inertia based on minimising deviation from nominal frequency after an outage; while that is a meaningful objective function in control theory, it does not apply to a frequency-constrained economic optimisation, since frequency deviation that does not violate any dynamic-security limit is safe from a scheduling point of view. The authors in [87] perform probabilistic frequency-stability analysis from dynamic simulations of systems with heterogeneous distributions of inertia, while reference [88] developed a simple algebraic formula for accurately estimating frequency in any of the grid's buses, which is claimed to significantly decrease the computation of dynamic simulations. However, to date no work has deduced conditions for regional frequency security. Such deduction is done in the present thesis, by obtaining conditions expressed in the form of inequality constraints which could be implemented in optimisation routines.

From a frequency-security perspective, Figure 4.1 illustrates the dangers of considering the Centre of Inertia (COI) model in systems with non-uniform inertia distribution: frequency constraints deduced from the swing equation would underestimate the actual need for frequency services, leading to higher regional RoCoF and lower regional nadirs than expected (note that the frequency of the COI evolves in between the frequencies of the two areas, which exhibit some inter-area oscillations). If the scheduling optimisation is not appropriately constrained to reflect the distinct regional frequencies, unexpected tripping of RoCoF relays and triggering of UFLS could take place, which in turn could cause cascading outages potentially leading to a blackout.

In this context, the present chapter focuses on extending the currently available frequency-constrained optimisation frameworks to account for the spatial variations in post-fault frequency dynamics. In order to do so, frequency constraints are deduced from a spatial swing model, which generalises the swing equation by considering N different regions in the grid coupled by ac transmission lines.

By solving this spatial swing model, constraints for guaranteeing regional frequency security can be obtained. Nevertheless, solving this model analytically is a challenging task, even impossible for the simplest systems as will be demonstrated in coming sections of this chapter. To overcome this difficulty, in this chapter we propose a mixed analytical-numerical method to obtain the constraints, using theoretical mathematical techniques combined with regression methods on simulation samples.

The key contributions of the work presented in this chapter are two-fold:

1. To the best of our knowledge, this is the first work to deduce conditions for regional frequency security in a power grid.

2. A linear formulation of the frequency-security constraints is provided to allow a computationally-efficient optimisation. This formulation allows the co-optimisation of distinct frequency services such as inertia, several forms of Frequency Response (FR), damping and a dynamically-reduced largest power infeed.

In principle, this model generalises all previous models presented in this thesis, since all the novel tools developed during this thesis so far will be included: a dynamically-reduced largest power infeed, multiple FR services and considering the support from load damping. However, since we also demonstrate in this chapter that it is not possible to obtain analytical solutions for frequency security conditions in an N-region system, some conservative approximations will be used to obtain the conditions in the form of convex constraints. Therefore, for systems in which the uniform frequency model still provides a good description of the frequency dynamics, the models developed in previous chapters of this thesis would likely provide a better solution.

4.2 Causes of distinct regional frequencies

Before undertaking the deduction of mathematical constraints that would guarantee regional frequency security, let's consider a simple example: the Great Britain (GB) system split in two areas, corresponding roughly to Scotland and England. Scotland has significant wind resources while most load centres are located in England, a fact that drives a non-uniform inertia distribution.

The two-region England-Scotland system was simulated in MATLAB/Simulink, using a mathematical model that will be discussed in Section 4.3. Simulations were run by changing the system operating condition, i.e. changing the inertia, load damping and frequency response in each region, the location of the generation outage (placed alternatively in Scotland and England) and the strength of the electrical interconnection between the regions (driven by the impedance of the connecting transmission corridors). This last parameter was the first shown to significantly affect the post-fault regional frequencies, as illustrated in Figure 4.2.

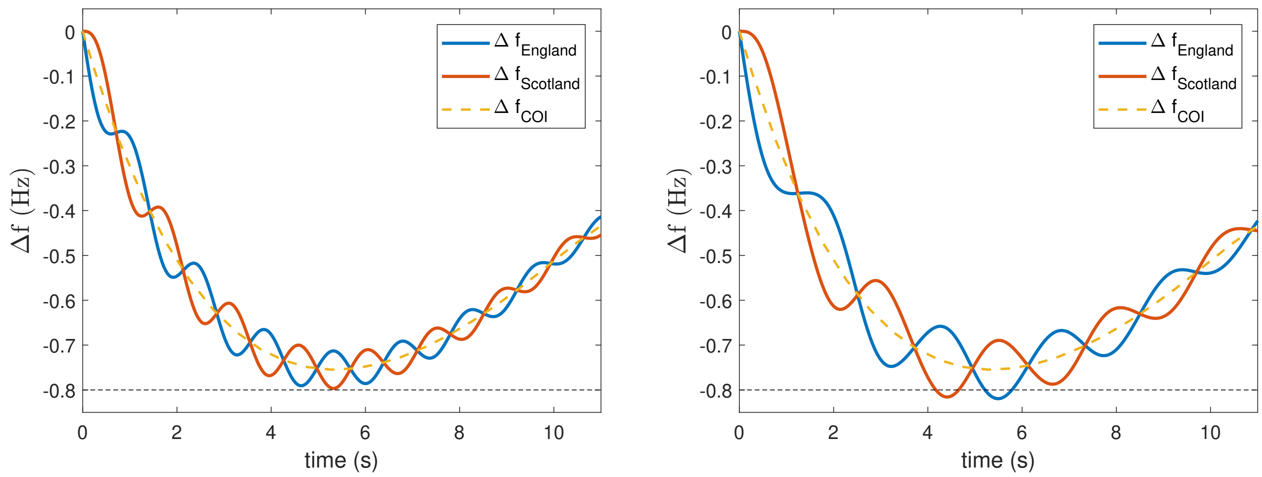

(a) $X_{i,j} = 40\Omega$ (b) $X_{i,j} = 100\Omega$

Figure 4.2: Impact of impedance of the transmission connection on the distinct regional frequencies. These cases consider a uniform inertia distribution, with both England and Scotland having the same inertia.

Both cases in Figure 4.2, which consider an even split of inertia, load damping and frequency response among England and Scotland, show a roughly equal Centre Of Inertia frequency (referred to as Δf_{COI} in the graphs); however, some inter-area oscillations can be observed in both Figs. 4.2a and 4.2b, while the amplitude of these oscillations is notably higher in the case in Figure 4.2b. These oscillations clearly increase the absolute value of the RoCoF and further deteriorate the frequency nadir, which drops below -0.8Hz in Figure 4.2b.

High-impedance transmission lines are closely related to renewables, since the best renewable sources, particularly wind, are typically located in remote areas far from load centres. This fact implies that the electrical connection between these renewable generators and the rest of the grid will necessarily be weak given its great length (unless reinforcement of the network through, for example, parallel circuits is chosen, but this approach involves high investment costs).

At this point a questions arises: given that existing transmission corridors have not significantly changed in recent years, and if anything have been reinforced, *why are system operators observing distinct regional frequencies in recent times, as reported in works such as [82–85]?* The answer is that there is a second cause for this phenomenon: these renewables located in remote regions also drive a non-uniform inertia distribution, as inertia in the regions dominated by renewable generation is very low.

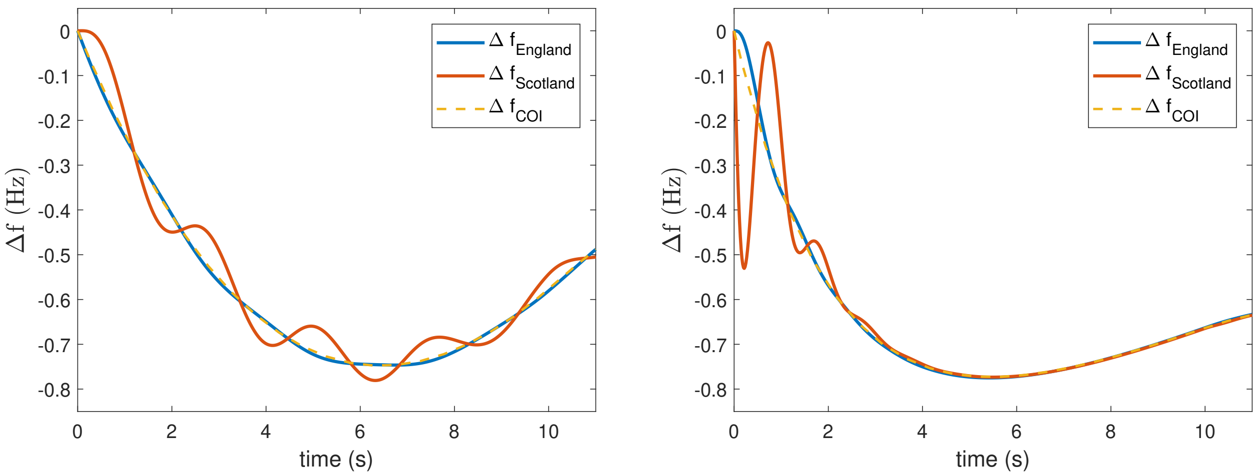

(a) 1.8GW generation loss in England

(b) 0.6GW generation loss in Scotland

Figure 4.3: Impact of fault location on the distinct regional frequencies. System inertia is unevenly distributed in these cases, with 90% located in England and 10% in Scotland.

Consider the examples in Figure 4.3, as these simulations show that regional frequencies become significant when there are gradients of inertia in the system, particularly so when the generation outage occurs in the low-inertia region: the 600MW loss in Scotland displayed in Figure 4.3b exhibits extreme RoCoF in that region during the first few seconds, while a 1.8GW loss in England shows a fairly similar behaviour to the Centre Of Inertia model. The observation of highest oscillations in the first instants after the fault, for a fault happening in the low-inertia region was also reported in [82] and [83].

In conclusion, the preliminary simulations conducted in this section have shown that the two main causes driving distinct regional frequencies are:

- A weak electrical interconnection, as it increases the amplitude of inter-area oscillations.
- A non-uniform distribution of inertia (i.e. a geographical gradient of inertia) combined with a generation outage in the low-inertia region.

Two options can be immediately identified to limit the impact of regional frequencies, guaranteeing that RoCoF and nadir requirements are respected: 1) improving the ac connection between the regions (note that using dc connections would effectively de-couple the regions for inertia purposes), although this would involve high investment costs; and 2) appropriately scheduling frequency services in each region, notably inertia and the largest possible loss.

The findings reported in this section are the reason for undertaking the work of deducing frequency-security constraints for multi-region systems, but no further assumption on the strength of the electrical connection or the inertia distribution is made in the remaining of this chapter. The impedance of the interconnection can be chosen in our model to match that of any particular system under study, while the location of inertia will be considered as a decision variable in our constraints.

4.3 Dynamic model for post-fault regional frequencies

This section describes the mathematical model of post-fault frequency evolution in multi-region systems, from which the conditions for regional frequency security will be obtained. The same nomenclature as in previous chapters is used, using index i for denoting that a particular variable or parameter corresponds to region i: for example, $\Delta f_i(t)$ corresponds to the post-fault frequency deviation in region i.

For now let's consider the simplest case of 2 regions, as the generalisation for N regions follows the same logic. The post-fault frequency in each region is described by this set of differential equations:

$$\begin{cases} 2H_1 \cdot \dfrac{\mathrm{d}\Delta f_1(t)}{\mathrm{d}t} + \mathrm{D}_1 \cdot \mathrm{P}_1^{\mathrm{D}} \cdot \Delta f_1(t) = \mathrm{FR}_1(t) - P_1^{\mathrm{L}} + \Delta\mathrm{P}_1^{\mathrm{import}}(t) & (4.2.1) \\ 2H_2 \cdot \dfrac{\mathrm{d}\Delta f_2(t)}{\mathrm{d}t} + \mathrm{D}_2 \cdot \mathrm{P}_2^{\mathrm{D}} \cdot \Delta f_2(t) = \mathrm{FR}_2(t) - P_2^{\mathrm{L}} + \Delta\mathrm{P}_2^{\mathrm{import}}(t) & (4.2.2) \end{cases}$$

Eqs. (4.2) can be described as two coupled swing equations, in which the coupling term is the ac power exchange between regions. The coupling term $\Delta\mathrm{P}_i^{\mathrm{import}}(t)$ represents the deviation from the steady state power being imported to region i. That is, before the outage there was a certain amount of power being imported to region i; after the outage, the amount of power imported changes following the laws of energy conservation, so that a frequency equilibrium is restored in the whole network. $\Delta\mathrm{P}_i^{\mathrm{import}}(t)$ is the difference between the power imported after-outage and before-outage.

To obtain the mathematical description of the term $\Delta\mathrm{P}_i^{\mathrm{import}}(t)$, let's first consider the steady-state power transfer between 2 neighbouring buses, i and j. This steady-state power transfer is described by the following equation [14]:

$$\mathrm{P}_{i,j}^{\mathrm{transfer}} = \frac{\mathrm{V}_i \mathrm{V}_j}{\mathrm{X}_{i,j}} \cdot \sin(\delta_i - \delta_j) \tag{4.3}$$

Note that the line resistance is neglected as we consider $\mathrm{X}_{i,j} \gg \mathrm{R}_{\mathrm{i,j}}$ (a typical assumption in transmission lines), and that δ_i, δ_j are bus voltage phase-angles referred to the rotating frame, which rotates at synchronous speed (50Hz in Europe). Therefore, these phase angles δ_i, δ_j are time-invariant in steady state. The phase angles will however change in the event of a power outage in the system, as the rotating speed of the generators deviates from 50Hz while they release the kinetic energy stored in their rotating masses.

The deviation from the steady state power transfer between buses i, j after a fault can be calculated as:

$$\Delta\mathrm{P}_{i,j}^{\mathrm{transfer}}(t) = \mathrm{P}_{i,j}^{\mathrm{transfer}}(t) - \mathrm{P}_{i,j}^{\mathrm{transfer,\ ss}} = \frac{\mathrm{V}_i \mathrm{V}_j}{\mathrm{X}_{i,j}} \cdot \sin\Big(\delta_i(t) - \delta_j(t)\Big) - \frac{\mathrm{V}_i \mathrm{V}_j}{\mathrm{X}_{i,j}} \cdot \sin(\delta_i^{\mathrm{ss}} - \delta_j^{\mathrm{ss}}) \tag{4.4}$$

Linearising around the operating point $\delta_i = \delta_i^{\text{ss}}$, $\delta_j = \delta_j^{\text{ss}}$ [14]:

$$\Delta \mathrm{P}_{i,j}^{\text{transfer}}(t) = \frac{\mathrm{V}_i \mathrm{V}_j}{\mathrm{X}_{i,j}} \cdot \cos(\delta_i^{\text{ss}} - \delta_j^{\text{ss}}) \cdot \left[\Delta\delta_i(t) - \Delta\delta_j(t)\right] \tag{4.5}$$

where $\Delta\delta_i(t) = \delta_i(t) - \delta_i^{\text{ss}}$. We have assumed that the average voltage variation in the grid is small after the generation outage, an assumption also made in the literature [89, 90].

Now, in order to express the power imported by any region in terms of electric frequency $\Delta f(t)$ rather than phase angle $\Delta\delta(t)$, it's important to understand the relation between these two magnitudes:

$$\frac{\mathrm{d}\delta(t)}{\mathrm{d}t} = \frac{\mathrm{d}\theta_m(t)}{\mathrm{d}t} - \omega_s = \omega_m(t) - \omega_s = \Delta\omega(t) = 2\pi\Delta f(t) \tag{4.6}$$

Where δ is assumed to be expressed in radians and Δf in Hz. θ_m is the absolute angle of the synchronous generator, not referred to the rotating reference as δ is; ω_s is the synchronous rotational speed of the generators (equivalent to the 50Hz electrical frequency).

Note that this relationship still holds when considering phase-angle deviations from steady state, $\Delta\delta(t)$:

$$\frac{\mathrm{d}\Delta\delta(t)}{\mathrm{d}t} = \frac{\mathrm{d}\delta(t)}{\mathrm{d}t} - \cancelto{0}{\frac{\mathrm{d}\delta^{\text{ss}}}{\mathrm{d}t}} = \Delta\omega(t) = 2\pi\Delta f(t) \tag{4.7}$$

So the post-fault power imported by any region i can be expressed as:

$$\Delta \mathrm{P}_i^{\text{import}}(t) = -\sum_{j \in \mathcal{J}_i} \mathrm{T}_{i,j} \left[\int_0^t \Delta f_i(\tau) d\tau - \int_0^t \Delta f_j(\tau) d\tau\right] \tag{4.8}$$

Where $\mathcal{J}_i$ is the set of neighbour areas of area i. Note that a negative value of $\Delta \mathrm{P}_i^{\text{import}}(t)$ means that region i is exporting power to other regions. To make (4.8) and following expressions clearer, we have defined the electrical stiffness of the transmission line as [91]:

$$\mathrm{T}_{i,j} = 2\pi \cdot \frac{\mathrm{V}_i \mathrm{V}_j}{\mathrm{X}_{i,j}} \cdot \cos(\delta_i^{\text{ss}} - \delta_j^{\text{ss}}) \tag{4.9}$$

The generalization for N regions of the coupled swing equations, including the inter-region power transfer term, can be done using the same logic. The model for post-fault frequency deviation in a system with N regions is then:

$$\begin{cases} 2H_1 \cdot \dfrac{\mathrm{d}\Delta f_1(t)}{\mathrm{d}t} + \mathrm{D}_1 \cdot \mathrm{P}_1^{\mathrm{D}} \cdot \Delta f_1(t) = \mathrm{FR}_1(t) - P_1^{\mathrm{L}} + \Delta \mathrm{P}_1^{\mathrm{import}}(t) & (4.10.1) \\ 2H_2 \cdot \dfrac{\mathrm{d}\Delta f_2(t)}{\mathrm{d}t} + \mathrm{D}_2 \cdot \mathrm{P}_2^{\mathrm{D}} \cdot \Delta f_2(t) = \mathrm{FR}_2(t) - P_2^{\mathrm{L}} + \Delta \mathrm{P}_2^{\mathrm{import}}(t) & (4.10.2) \\ \vdots & \\ 2H_n \cdot \dfrac{\mathrm{d}\Delta f_n(t)}{\mathrm{d}t} + \mathrm{D}_n \cdot \mathrm{P}_n^{\mathrm{D}} \cdot \Delta f_n(t) = \mathrm{FR}_n(t) - P_n^{\mathrm{L}} + \Delta \mathrm{P}_n^{\mathrm{import}}(t) & (4.10.n) \end{cases}$$

where $\Delta \mathrm{P}_i^{\mathrm{import}}(t)$ is modelled as in (4.8).

The set of integro-differential equations (4.10) is the extension of the single-bus swing equation to consider distinct regions, and therefore allows to consider geographical gradients in frequency within a power system. The power system is modelled as a set of regions that do not swing coherently but are connected through synchronous ac transmission lines. This model generalizes the uniform frequency model, as (4.10) reduces to the single-bus swing equation if the impedance of the transmission lines tends to zero.

4.3.1 Solving the dynamic model: two-region case

This section discusses how to obtain a solution for $\Delta f_1(t)$ and $\Delta f_2(t)$ in a two-region system as defined by (4.2). Without loss of generality and for the sake of simplicity, we consider a single frequency-response service, PFR:

$$\begin{cases} 2H_1 \cdot \dfrac{\mathrm{d}\Delta f_1(t)}{\mathrm{d}t} + \mathrm{D}_1 \cdot \mathrm{P}_1^{\mathrm{D}} \cdot \Delta f_1(t) = \mathrm{PFR}_1(t) - P_1^{\mathrm{L}} + \Delta \mathrm{P}_1^{\mathrm{import}}(t) & (4.11.1) \\ 2H_2 \cdot \dfrac{\mathrm{d}\Delta f_2(t)}{\mathrm{d}t} + \mathrm{D}_2 \cdot \mathrm{P}_2^{\mathrm{D}} \cdot \Delta f_2(t) = \mathrm{PFR}_2(t) - P_2^{\mathrm{L}} + \Delta \mathrm{P}_2^{\mathrm{import}}(t) & (4.11.2) \end{cases}$$

Where PFR is modelled as:

$$\mathrm{PFR}_i(t) = \begin{cases} \dfrac{R_i}{\mathrm{T_g}} \cdot t & \text{if } t \leq \mathrm{T_g} & (4.12a) \\ R_i & \text{if } t > \mathrm{T_g} & (4.12b) \end{cases}$$

In order to obtain an analytical solution for the set of integro-differential equations (4.11), we propose to first apply the Laplace transform so that a set of algebraic equations is obtained. Then, this set of algebraic equations can be solved analytically, and the inverse Laplace transform can be applied to obtain the solution in time domain.

Applying the Laplace transform to (4.11) we obtain:

$$\begin{cases} 2H_1 \cdot s\Delta F_1(s) + \mathrm{D}_1 \cdot \mathrm{P}_1^{\mathrm{D}} \cdot \Delta F_1(s) = \mathrm{PFR}_1(s) - \dfrac{P_1^{\mathrm{L}}}{s} + \Delta \mathrm{P}_1^{\mathrm{import}}(s) & (4.13.1) \\ 2H_2 \cdot s\Delta F_2(s) + \mathrm{D}_2 \cdot \mathrm{P}_2^{\mathrm{D}} \cdot \Delta F_2(s) = \mathrm{PFR}_2(s) - \dfrac{P_2^{\mathrm{L}}}{s} + \Delta \mathrm{P}_2^{\mathrm{import}}(s) & (4.13.2) \end{cases}$$

where $\Delta F_i(s) = \mathscr{L}\{\Delta f_i(t)\}$ and $\Delta \mathrm{P}_i^{\mathrm{import}}(s)$ is given by:

$$\Delta \mathrm{P}_i^{\mathrm{import}}(s) = -\sum_{j \in \mathcal{J}_i} \mathrm{T}_{i,j} \frac{\Delta F_i(s) - \Delta F_j(s)}{s} \tag{4.14}$$

Considering that PFR is still ramping up, which is the period of interest for RoCoF and nadir purposes:

$$\mathrm{PFR}_i(s) = \frac{R_i}{\mathrm{T_g}} \cdot \frac{1}{s^2} \tag{4.15}$$

The set of algebraic equations (4.13) where the unknowns are $\Delta F_i(s)$ can be solved algebraically using any computer algebra system, which gives the following solution:

$$\Delta F_i(s) = \frac{\mathrm{C}_1 \cdot s^3 + \mathrm{C}_2 \cdot s^2 + \mathrm{C}_3 \cdot s + \mathrm{C}_4}{\mathrm{C}_5 \cdot s^5 + \mathrm{C}_6 \cdot s^4 + \mathrm{C}_7 \cdot s^3 + \mathrm{C}_8 \cdot s^2} \tag{4.16}$$

Where the constants C_j are all real numbers, which are functions of the system parameters that appear in (4.13) such as H_1, H_2, P_1^{L}, etc. These functions of system parameters are significantly convoluted as shown later in this section, hence the use of these generic constants C_j to represent them in a simple way.

In order to apply the inverse Laplace transform and then obtain the time-domain solution $\Delta f_i(t)$, (4.16) must be decomposed in partial fractions:

$$\Delta F_i(s) = \frac{\mathrm{C}_1'}{s^2} + \frac{\mathrm{C}_2'}{s} + \frac{\mathrm{C}_3' \cdot s^2 + \mathrm{C}_4' \cdot s + 1}{\mathrm{C}_5' \cdot s^3 + \mathrm{C}_6' \cdot s^2 + \mathrm{C}_7' \cdot s + 1} = \frac{\mathrm{C}_1'}{s^2} + \frac{\mathrm{C}_2'}{s} + \sum_{k=1}^{3} \frac{\mathrm{Z}_k}{s - \mathrm{z}_k} \tag{4.17}$$

Note that these constants C'_j are again generic functions of the system parameters but different to the C_j used in (4.16). Terms Z_k and z_k are generic complex numbers. The factorisation performed in (4.17) makes use of the **Fundamental Theorem of Algebra**, which states that every polynomial of degree n has n roots. The inverse Laplace transform of (4.17) gives the time-domain solution:

$$\Delta f_i(t) = \mathscr{L}^{-1}\left\{\Delta F_i(s)\right\} = \mathscr{L}^{-1}\left\{\frac{\mathrm{C}'_1}{s^2} + \frac{\mathrm{C}'_2}{s} + \sum_{k=1}^{3}\frac{\mathrm{Z}_k}{s-\mathrm{z}_k}\right\} = \mathrm{C}'_1\cdot t + \mathrm{C}'_2 + \sum_{k=1}^{3}\mathrm{Z}_k\cdot \mathrm{e}^{\mathrm{z}_k t} \quad (4.18)$$

To fully understand (4.18), let's consider the two possibilities for the roots of the last denominator in (4.17), z_k, : 1) All z_k are real; or 2) z_1 is real while z_2 and z_3 are complex conjugates. This conclusion comes from the **Complex Conjugate Root Theorem**, which states that if a polynomial in one variable with real coefficients (as is the case in (4.17)) has a complex root, then the conjugate is also a root. **Proposition**: for the range of values in a realistic power system, the third-order denominator in (4.17) has one real root and two complex conjugate roots, i.e. z_1 is real while z_2 and z_3 are complex conjugates in (4.17) and (4.18). The validity of this proposition is supported by the evidence reported in the literature [82–85] and in the dynamic simulations in Section 4.2, which show that the post-fault regional frequencies behave as the COI plus certain inter-area oscillations. As is shown in the next paragraphs, such dynamic behaviour corresponds to one real root and two complex conjugate roots for the denominator in (4.17).

Considering this proposition, the last term in (4.18) can be expressed as:

$$\begin{aligned}\sum_{k=1}^{3}\mathrm{Z}_k\cdot \mathrm{e}^{\mathrm{z}_k t} &= \mathrm{Z}_1\cdot \mathrm{e}^{\mathrm{z}_1 t} + \mathrm{Z}_2\cdot \mathrm{e}^{\mathrm{z}_2 t} + \overline{\mathrm{Z}_2}\cdot \mathrm{e}^{\overline{\mathrm{z}_2}t}\\ &= \mathrm{Z}_1\cdot \mathrm{e}^{\mathrm{z}_1 t} + (\mathrm{a}_2 + j\mathrm{b}_2)\cdot \mathrm{e}^{(\mathrm{a}_2+j\mathrm{b}_2)t} + (\mathrm{a}_2 - j\mathrm{b}_2)\cdot \mathrm{e}^{(\mathrm{a}_2-j\mathrm{b}_2)t}\\ &= \mathrm{Z}_1\cdot \mathrm{e}^{\mathrm{z}_1 t} + \mathrm{e}^{\mathrm{a}_2 t}\left[\mathrm{a}_2\left(\mathrm{e}^{j\mathrm{b}_2 t} + \mathrm{e}^{-j\mathrm{b}_2 t}\right) + j\mathrm{b}_2\left(\mathrm{e}^{j\mathrm{b}_2 t} - \mathrm{e}^{-j\mathrm{b}_2 t}\right)\right]\\ &= \mathrm{Z}_1\cdot \mathrm{e}^{\mathrm{z}_1 t} + \mathrm{e}^{\mathrm{a}_2 t}\left[\mathrm{a}_2\cdot 2\cos(\mathrm{b}_2 t) - \mathrm{b}_2\cdot 2\sin(\mathrm{b}_2 t)\right] \quad (4.19)\end{aligned}$$

where a_2 and b_2 are generic real numbers. Note that (4.19) shows that the last term in (4.18) corresponds to an exponential function plus certain oscillations in time-domain.

Since a third-order polynomial can be factorised algebraically (for example, using Cardano's formula), we now describe the procedure to do so. First, let's consider the explicit values for the generic constants C_j in (4.16) and C'_j in (4.17) for region 1 (the expression for region 2 is omitted but equivalent):

$$\Delta F_1(s) = \frac{-2H_2 P_1^{\mathrm{L}} \cdot s^3 + (\frac{2H_2R_1}{\mathrm{T_g}} - \mathrm{D}_2^{'} P_1^{\mathrm{L}})s^2 + (\frac{\mathrm{D}_2^{'}R_1}{\mathrm{T_g}} - P_1^{\mathrm{L}} \cdot \mathrm{T}_{1,2})s + \frac{R \cdot \mathrm{T}_{1,2}}{\mathrm{T_g}}}{4H_1H_2 \cdot s^5 + 2(\mathrm{D}_1^{'}H_2 + \mathrm{D}_2^{'}H_1)s^4 + (2H \cdot \mathrm{T}_{1,2} + \mathrm{D}_1^{'}\mathrm{D}_2^{'})s^3 + \mathrm{D}^{'}\mathrm{T}_{1,2} \cdot s^2} \tag{4.20}$$

Eq. (4.20) has been simplified using: $H = H_1 + H_2$, $R = R_1 + R_2$, $\mathrm{D}_i^{'} = \mathrm{D}_i \cdot \mathrm{P}_i^{\mathrm{D}}$ and $\mathrm{D}' = \mathrm{D}_1 \cdot \mathrm{P}_2^{\mathrm{D}} + \mathrm{D}_1 \cdot \mathrm{P}_2^{\mathrm{D}}$. Before applying the inverse Laplace transform and then obtain the time-domain solution $\Delta f_1(t)$, (4.20) must be decomposed in partial fractions as was done to obtain (4.17) from (4.16). An algebraic partial-fraction decomposition can be done using any computer algebra system such as MATLAB or Maple:

$$\Delta F_1(s) = \frac{R}{\mathrm{D}^{'}\mathrm{T_g} \cdot s^2} - \frac{2HR + \mathrm{D}^{'}\mathrm{T_g}P_1^{\mathrm{L}} - \frac{\mathrm{D}_2^{'}(R_1\mathrm{D}_2^{'} - R_2\mathrm{D}_1^{'})}{\mathrm{T}_{1,2}}}{(\mathrm{D}^{'})^2\mathrm{T_g} \cdot s}$$

$$+ \frac{\mathrm{C}_1^{''}s^2 + \mathrm{C}_2^{''}s + \mathrm{C}_3^{''}}{\mathrm{T_g}\mathrm{T}_{1,2}(\mathrm{D}^{'})^2[4H_1H_2 \cdot s^3 + 2(\mathrm{D}_1^{'}H_2 + \mathrm{D}_2^{'}H_1) \cdot s^2 + (2H \cdot \mathrm{T}_{1,2} + \mathrm{D}_1^{'}\mathrm{D}_2^{'}) \cdot s + \mathrm{D}^{'}\mathrm{T}_{1,2}]} \tag{4.21}$$

where:

$$\mathrm{C}_1^{''} = 4H_1H_2(P_1^{\mathrm{L}}\mathrm{T_g}\mathrm{T}_{1,2}\mathrm{D}^{'} + 2HR \cdot \mathrm{T}_{1,2} - R_1(\mathrm{D}_2^{'})^2 + R_2\mathrm{D}_1^{'}\mathrm{D}_2^{'}) \tag{4.22}$$

$$\mathrm{C}_2^{''} = 2[P_1^{\mathrm{L}}\mathrm{T_g}\mathrm{T}_{1,2}\mathrm{D}_2^{'}(H_1 - H_2)(\mathrm{D}_1^{'} + \mathrm{D}_2^{'}) + 2R \cdot \mathrm{T}_{1,2}(\mathrm{D}_2^{'}H_1^2 + \mathrm{D}_1^{'}H_2^2)$$
$$+ \mathrm{D}_1^{'}(\mathrm{D}_2^{'})^2(H_1R_2 - H_2R_1) + (\mathrm{D}_1^{'})^2\mathrm{D}_2^{'}H_2R_2 - (\mathrm{D}_2^{'})^3H_1R_1] \tag{4.23}$$

$$\mathrm{C}_3^{''} = 4H^2R(\mathrm{T}_{1,2})^2 + 2H \cdot \mathrm{D}^{'}P_1^{\mathrm{L}}\mathrm{T_g}(\mathrm{T}_{1,2})^2 - (\mathrm{D}_2^{'})^2\mathrm{T}_{1,2}[P_1^{\mathrm{L}}\mathrm{T_g}\mathrm{D}^{'} + 2H_1(2R_1 + R_2)]$$
$$+ 2\mathrm{D}_1^{'}\mathrm{D}_2^{'}\mathrm{T}_{1,2}(H_1R_2 + 2H_2R_1 + H_2R_2) - 2(\mathrm{D}_1^{'})^2\mathrm{T}_{1,2}H_2R_2 + \mathrm{D}_1^{'}(\mathrm{D}_2^{'})^2(R_2\mathrm{D}_1^{'} - R_1\mathrm{D}_2^{'}) \tag{4.24}$$

At this point, it is revealing to compare (4.21) with the partial-fraction decomposition of the uniform frequency model:

$$\Delta F_{\mathrm{COI}}(s) = \frac{R}{\mathrm{D}'\mathrm{T_g} \cdot s^2} + \frac{2HR + \mathrm{D}'\mathrm{T_g}P^{\mathrm{L}}}{(\mathrm{D}')^2\mathrm{T_g}} \left(\frac{1}{s + \frac{\mathrm{D}'}{2H}} - \frac{1}{s} \right) \tag{4.25}$$

By applying the inverse Laplace transform to (4.25), the $\frac{1}{s^2}$ term would give rise to a linear function in time-domain, the $\frac{1}{s}$ term to a constant in time-domain and the $\frac{1}{s+\frac{\mathrm{D}'}{2H}}$ term to an exponential function in time-domain:

$$\Delta f_{\mathrm{COI}}(t) = \frac{R}{\mathrm{D}'\mathrm{T_g}} \cdot t + \frac{2HR + \mathrm{D}'\mathrm{T_g}P^{\mathrm{L}}}{(\mathrm{D}')^2\mathrm{T_g}} \left(\mathrm{e}^{-\frac{\mathrm{D}'}{2H} \cdot t} - 1 \right) \tag{4.26}$$

By comparing (4.21) to (4.25), one can notice that the $\frac{1}{s^2}$ term is the same in both expressions, and the $\frac{1}{s}$ in (4.21) reduces to the one in (4.25) as $\mathrm{T}_{1,2}$ tends to infinity, i.e. the impedance of the interconnecting line tends to zero and therefore the two regions become effectively one. The comparison of the $\frac{1}{s+\frac{\mathrm{D}'}{2H}}$ term in (4.25) with the last fraction in (4.21) is not as straightforward, but the evidence reported in the literature and in the simulations conducted in Section 4.2 shed some light for the comparison: the post-fault frequency in a multi-region system exhibits the behaviour of the COI plus certain inter-area oscillations. This observation is consistent with (4.19), which demonstrates that the last term in (4.21) corresponds to an exponential function plus oscillations in time-domain. Therefore the exponential time-domain term rising from the $\frac{1}{s+\frac{\mathrm{D}'}{2H}}$ term in (4.25) is roughly equal to the exponential term in (4.19).

In conclusion, the deductions in this section have shown that for practical purposes in any realistic power system, the post-fault frequency evolution in a two-region system is of the form:

$$\Delta f_i(t) \approx \Delta f_{\mathrm{COI}}(t) + \mathrm{e}^{-\mathrm{a}_i t}\mathrm{A}_i \sin(\omega_i t + \phi_i) + \mathrm{C}_i \tag{4.27}$$

Note that the approximation in (4.27) lies in the COI term, as discussed in the paragraph above. Through simulations such as the ones reported in Section 4.2, it was verified that this approximation is almost perfect for several examples of interest in a realistic power system (i.e. every realistic operating condition setting the numerical values for inertia in each region, frequency response in each region, generation outage, etc.). This result is consistent with the multi-region post-fault frequency cases reported in the literature. The simulations conducted also showed that the approximation becomes slightly less accurate as the regions become more weakly linked, i.e. as the impedance of the interconnecting line increases.

The deductions in this section have allowed to obtain the *mathematical structure* of the post-fault frequency evolution in a two-region system, given by eq. (4.27). This expression will be used as an initial step to obtain conditions that guarantee frequency security in a two-region system, in Section 4.4.

Finally, it is worth noting that since the third-order denominator in (4.21) can be factorised analytically, in principle the exact expression that has been approximated in (4.27) could be obtained analytically. However, this is not done in this thesis for two reasons: 1) given that the expressions (4.21) through (4.24) are cumbersome, the solution would include highly non-linear functions which would make frequency-security constraints very inefficient for being implemented in optimisation routines (if even possible to obtain such constraints); and 2) deducing this analytical solution would only be possible for a two-region system, and not for a system with three or more regions, as is proved in the next section.

4.3.2 Solving the dynamic model: N-region case

This section discusses how to obtain a solution for every region's post-fault frequency, $\Delta f_i(t)$, in an N-region system as defined by (4.10). The Laplace transform of this set of differential eqs. (4.10) is given by:

$$\begin{cases} 2H_1 \cdot s\Delta F_1(s) + \mathrm{D}_1 \cdot \mathrm{P}_1^{\mathrm{D}} \cdot \Delta F_1(s) = \mathrm{PFR}_1(s) - \dfrac{P_1^{\mathrm{L}}}{s} + \Delta \mathrm{P}_1^{\mathrm{import}}(s) & (4.28.1) \\ 2H_2 \cdot s\Delta F_2(s) + \mathrm{D}_2 \cdot \mathrm{P}_2^{\mathrm{D}} \cdot \Delta F_2(s) = \mathrm{PFR}_2(s) - \dfrac{P_2^{\mathrm{L}}}{s} + \Delta \mathrm{P}_2^{\mathrm{import}}(s) & (4.28.2) \\ \vdots & \\ 2H_n \cdot s\Delta F_n(s) + \mathrm{D}_n \cdot \mathrm{P}_n^{\mathrm{D}} \cdot \Delta F_n(s) = \mathrm{PFR}_n(s) - \dfrac{P_n^{\mathrm{L}}}{s} + \Delta \mathrm{P}_n^{\mathrm{import}}(s) & (4.28.\mathrm{n}) \end{cases}$$

where $\Delta \mathrm{P}_i^{\mathrm{import}}(s)$ is given by (4.14). The solution for a generic region i of this set of algebraic eqs. is:

$$\Delta F_i(s) = \frac{\mathrm{C}_1}{s^2} - \frac{\mathrm{C}_2}{s} + \frac{\text{polynomial in } s \text{ of degree } 2 \cdot N - 2}{\text{polynomial in } s \text{ of degree } 2 \cdot N - 1} \tag{4.29}$$

In order to apply the inverse Laplace transform to (4.29) and then obtain the time-domain solution $\Delta f_i(t)$, the last term in (4.29) must be decomposed in partial fractions. However, since it is not possible to algebraically factorise polynomials of degree higher than four as proved by the **Abel–Ruffini Theorem**, it is not possible to decompose in partial fractions the last term in (4.29). Therefore, it is not possible to obtain an analytical solution in time-domain for $\Delta f_i(t)$ for a general power system with N regions, i.e. a system with three or more regions.

Proposition: for the range of values in a realistic power system, the denominator of the last term in (4.29) always has one real root and $2N - 2$ complex conjugate roots. This proposition makes use of the Fundamental Theorem of Algebra and the Complex Conjugate Roots theorem, see the previous Section 4.3.1 discussing two-region systems for more details. This proposition is consistent with the studies reported in the literature [82–85], which show post-fault frequencies behaving as the COI plus certain inter-area oscillations.

Therefore, although no analytical solution can be obtained for $\Delta f_i(t)$ for a general system with N regions, the proposition mentioned above gives information about the *mathematical structure* of $\Delta f_i(t)$, in a similar fashion as was deduced in Section 4.3.1 for a two-region system.

As discussed in Section 4.3.1, the real root of the denominator in of the last term in (4.29) gives rise to an exponential in time-domain, which added to the first two terms in (4.29) corresponds to the post-fault frequency of the COI; the $2N - 2$ complex conjugate roots give rise to $N - 1$ oscillations in time-domain, as was discussed for the two complex conjugate roots of the two-region system considered in Section 4.3.1. Therefore, the solution for the post-fault frequency evolution of any region i in an N-region system is:

$$\Delta f_i(t) \approx \Delta f_{\mathrm{COI}}(t) + \sum_{j=1}^{N-1} \mathrm{e}^{-\mathrm{a}_j t} \mathrm{A}_j \sin(\omega_j t + \phi_j) + \mathrm{C}_j \tag{4.30}$$

As for the the two-area system considered in Section 4.3.1, simulations showed that the approximation in (4.30) becomes slightly less accurate as the regions become more weakly linked.

4.4 Conditions for frequency security: two-region case

By solving the set of integro-differential eqs. (4.11) one could obtain the expression for $\Delta f_i(t)$ and use it to deduce the conditions for respecting RoCoF, nadir and q-s-s in region i, following a similar procedure to the one used in Chapters 2 and 3 of this thesis. However, we have shown in Section 4.3.1 that it is impractical to analytically obtain the expression for $\Delta f_i(t)$: it is theoretically possible (since it would involve factorising a third-order polynomial), but the resulting function for $\Delta f_i(t)$ would be highly nonlinear and therefore impractical for deducing frequency-security constraints.

Nevertheless, in this section we propose a method to obtain semi-analytical constraints for guaranteeing regional frequency security. To illustrate this method, let's start by remembering that the time-evolution of frequency deviation in any of the two regions, $\Delta f_i(t)$, is of the form:

$$\Delta f_i(t) \approx \Delta f_{\mathrm{COI}}(t) + \mathrm{e}^{-\mathrm{a}_i t}\mathrm{A}_i \sin(\omega_i t + \phi_i) + \mathrm{C}_i \tag{4.31}$$

as we have demonstrated in Section 4.3.1. In (4.31), $\Delta f_{\mathrm{COI}}(t)$ is the frequency deviation of the Centre Of Inertia, which was deduced in Section 4.3.1:

$$\Delta f_{\mathrm{COI}}(t) = \left(\frac{P^{\mathrm{L}}}{\mathrm{D}\cdot\mathrm{P^D}} + \frac{2H\cdot R}{\mathrm{T_g}\cdot\left(\mathrm{D}\cdot\mathrm{P^D}\right)^2} \right) \left(\mathrm{e}^{-\frac{\mathrm{D}\cdot\mathrm{P^D}}{2H}t} - 1 \right) + \frac{R\cdot t}{\mathrm{T_g}\cdot\mathrm{D}\cdot\mathrm{P^D}} \tag{4.32}$$

Eq. (4.31) therefore gives valuable insight on the *mathematical structure* of the solution for $\Delta f_i(t)$, but it is not possible to analytically obtain the coefficients a_i, A_i and ω_i. Using the information provided by (4.31), we propose to use a numerical approach to estimate the coefficients a_i, A_i and ω_i. This approach would consist on numerically solving the set of differential eqs. (4.10) for several possible operating points of a power system (therefore considering only plausible values for H_1, H_2, P_{L} and the rest of the system variables), and using a regression technique on the solution samples to estimate the coefficients a_i, A_i and ω_i.

In summary, this mixed analytical-numerical approach goes as far as possible using analytical techniques and completes the task of obtaining frequency-security constraints by using numerical techniques to estimate the remaining parameters that cannot be obtained analytically. This method is driven by the two following goals: 1) to always guarantee frequency security, therefore becoming conservative if necessary, rather than under-conservative, although always trying to be as least conservative as possible; and 2) to obtain convex constraints that would provide computational efficiency for the optimisation problem in which they would eventually be implemented.

4.4.1 RoCoF constraint: analytical deduction

Taking into consideration (4.31) the RoCoF in region i is:

$$\mathrm{RoCoF}_i(t) = \mathrm{RoCoF}_{\mathrm{COI}}(t) + \mathrm{RoCoF}_{\mathrm{oscillations}_i}(t) \tag{4.33}$$

where $\mathrm{RoCoF}_{\mathrm{oscillations}_i}(t)$ is the derivative of the attenuated oscillations in (4.31):

$$\mathrm{RoCoF}_{\mathrm{oscillations}_i}(t) = \pm e^{-\mathrm{a}_i t}\mathrm{A}_i[\omega\cos(\omega t + \phi_i) - \mathrm{a}_i \sin(\omega t + \phi_i)] \tag{4.34}$$

Since this $\mathrm{RoCoF}_{\mathrm{oscillations}_i}(t)$ is a non-convex function, then $\mathrm{RoCoF}_i(t)$ in eq. (4.33) is also a non-convex function and therefore it is not possible to obtain its global maximum analytically. We make use of the following inequality to come up with a conservative estimation of this maximum for $\mathrm{RoCoF}_i(t)$:

$$\sup\{\mathrm{RoCoF}_i(t) \mid t \geq 0\} \leq \sup\{\mathrm{RoCoF}_{\mathrm{COI}}(t) \mid t \geq 0\} + \sup\{\mathrm{RoCoF}_{\mathrm{oscillations}_i}(t) \mid t \geq 0\} \tag{4.35}$$

The $\sup\{\mathrm{RoCoF}_{\mathrm{oscillations}_i}(t) \mid t \geq 0\}$ cannot be analytically obtained, because $\mathrm{RoCoF}_{\mathrm{oscillations}_i}(t)$ is a non-convex function as mentioned before, but it can be overestimated by:

$$\sup\{\mathrm{RoCoF}_{\mathrm{oscillations}}(t) \mid t \geq 0\} \leq \mathrm{A}_i \cdot \omega \tag{4.36}$$

Expression (4.36) has been obtained by neglecting the attenuation term $e^{-\mathrm{a}_i t}$, therefore assuming that the oscillations are not attenuated.

In conclusion, the constraints that guarantee the RoCoF to be within specified limits in a two-region system are:

$$|\mathrm{RoCoF}_1| = \frac{P^{\mathrm{L}}}{2(H_1 + H_2)} + \mathrm{A}_1 \cdot \omega_1 \leq \mathrm{RoCoF}_{\max} \tag{4.37a}$$

$$|\mathrm{RoCoF}_2| = \frac{P^{\mathrm{L}}}{2(H_1 + H_2)} + \mathrm{A}_2 \cdot \omega_2 \leq \mathrm{RoCoF}_{\max} \tag{4.37b}$$

where A_i and ω_i are dependent on the operating condition of the system, i.e. are functions of H_i, P_i^{L}, etc. These functions can be estimated by using a regression on samples obtained from dynamic simulations of the system described by (4.11). We propose to fit a function into these samples that yields linear RoCoF constraints, which is explained in the next section.

4.4.2 RoCoF constraint: numerical estimation

As explained in Section 4.3.1, it would be impractical to deduce an analytical function for the parameters of the inter-area oscillations appearing in eqs. (4.37), i.e. parameters A_i and ω_i. Therefore, we propose to do a numerical estimation of these parameters, which allows to obtain linear RoCoF constraints for each region. Using this approach, constraints (4.37) become:

$$\frac{P^{\mathrm{L}}}{2(H_1 + H_2)} + \frac{\mathrm{m}_1 H_1 + \mathrm{m}_2 H_2 + \mathrm{m}_3 P^{\mathrm{L}} + \mathrm{m}_4 \mathrm{D}_1 \mathrm{P}_1^{\mathrm{D}} + \mathrm{m}_5 \mathrm{D}_2 \mathrm{P}_2^{\mathrm{D}} + \mathrm{m}_6 R_1 + \mathrm{m}_7 R_2 + \mathrm{m}_8}{2(H_1 + H_2)} \leq \mathrm{RoCoF}_{\max} \tag{4.38}$$

The procedure for estimating the oscillation parameters A_i and ω_i numerically (i.e. finding the right value for the constant terms ‘m’) is described in Algorithm 1, while an implementation of this algorithm using MATLAB and Simulink is freely available in this link:
https://github.com/badber/TwoRegion_Frequency.

Algorithm 1 generates a number of feasible operating points for the power system, that exactly respect the regional RoCoF limit: dynamic simulations are run for a number of operating points, and samples that just barely respect the RoCoF requirement are recorded. Finally, a regression is run on these samples to find the right values for terms ‘m’ in eq. (4.38). Some further explanation on Algorithm 1:

- Algorithm 1 starts by considering a system operating point that just barely respects the COI frequency stability (i.e. that neglects the inter-area oscillations), as described in lines 3 through 7. Parameter ‘k^*’ in line 4 refers to the condition for respecting the COI

Algorithm 1 Numerical estimation of A_i and ω_i for the regional RoCoF constraint

Input: range of possible operating conditions for the power system
Output: estimation of A_i and ω_i for each condition (i.e. value of terms 'm' in eq. 4.38)
1: **for** several feasible values of P_{L} **do**
2: **for** several splits of D among the regions **do**
3: $H_{\mathrm{total}} = P_{\mathrm{L}}/(2 \cdot \mathrm{RoCoF}_{\mathrm{max}})$
4: $R_{\mathrm{total}} = H_{\mathrm{total}}/k^*$
5: **if** $R_{\mathrm{total}} < P_{\mathrm{L}} - \mathrm{D} \cdot \mathrm{P_D} \cdot \Delta f_{\mathrm{max}}$ **then**
6: $R_{\mathrm{total}} = P_{\mathrm{L}} - \mathrm{D} \cdot \mathrm{P_D} \cdot \Delta f_{\mathrm{max}}$
7: **end if**
8: **for** several splits of R_{total} among the regions **do**
9: **for** several splits of H_{total} among the regions **do**
10: run dynamic simulation (e.g. Simulink)
11: **while** RoCoF in the region $>$ $\mathrm{RoCoF}_{\mathrm{max}}$ **do**
12: $H_{\mathrm{total}} = H_{\mathrm{total}} +$ slight increase
13: run dynamic simulation
14: **end while**
15: estimate A_i and ω_i numerically (e.g. function 'estimate_oscillation.m')
16: record system operating state (H_1, H_2, P_{L}, ...) as features for the regression
17: record the estimated '$\mathrm{A}_i \cdot \omega_i$' as labels for the regression
18: **end for**
19: **end for**
20: **end for**
21: **end for**
22: run a regression using the recorded features and labels (e.g. using 'Rocof_regression.m')

nadir requirement, described in eq. (2.7). The 'if' statement on line 5 guarantees that the quasi-steady-state requirement is respected.

- The reason for starting from a system operating point that just barely respects the COI frequency stability is to iteratively reach an operating point precisely at the regional RoCoF security boundary, using the loop in lines 11 through 14. Using only samples at the RoCoF security boundary allows to obtain a more accurate regression for '$\mathrm{A}_i \cdot \omega_i$', as explained later in this section and illustrated in Figure 4.4.

- The several 'for' loops included in the algorithm have the goal of generating samples that consider several possible splits of the system magnitudes (H, R, D...) among the regions. This allows to obtain a wide range of system operating points, covering appropriately the space of feasible operating points of the power system.

The last line in Algorithm 1 applies a regression to estimate the values of '$\mathrm{A}_i \cdot \omega_i$', as this is the expression that needs to be estimated in eqs. (4.37). The system operating points are used as features for the regression, which then will provide the values of terms 'm' in eq. (4.38). A conservative regression is used, so as to guarantee that the resulting constraints will lead to a frequency-stable operating point in every circumstance, with the tradeoff of a tighter frequency-security region if the security boundary is far from being linear. Nevertheless, as will be demonstrated in Section 4.4.3, this tradeoff is not significant for practical purposes in a power system.

The conservative regression can be computed solving the following constrained optimisation:

$$\min_{\theta} \quad \frac{1}{2}\left\|X \cdot \theta - y\right\|^2 \tag{4.39}$$

$$\text{s.t.} \quad X \cdot \theta \geq y \tag{4.40}$$

Where y are the regression labels, X are the regression features and θ is the vector of the regression parameters (in this case, $\theta = [\mathrm{m}_1, ..., \mathrm{m}_8]$ for eq. 4.38). The above optimisation problem simply defines a constrained least-squares regression, which forces the resulting regression to be above all training samples contained in vector y: in this case, the regression is forced to overestimate the regional RoCoF caused by the inter-area oscillation, i.e. by term '$\mathrm{A}_i \cdot \omega_i$' in eqs. (4.37).

As explained before, Algorithm 1 only uses samples close to the frequency-security boundary to train the conservative regression (i.e. samples that barely respect the $\mathrm{RoCoF_{max}}$ limit within the region). To illustrate the importance of training the conservative regression using only samples that fall very close to the frequency-security boundary, consider Figure 4.4: as a conservative above-all-samples regression is used, training it only with samples close to the security boundary avoids an overly-conservative RoCoF constraint. Note that this Figure 4.4 is for illustration purposes only, as it has been generated by considering the COI nadir limit in eq. (2.7): since the analytical expression for that limit can be obtained, it is possible to visually understand the advantage of using appropriate samples when tying to estimate the boundary through a regression.

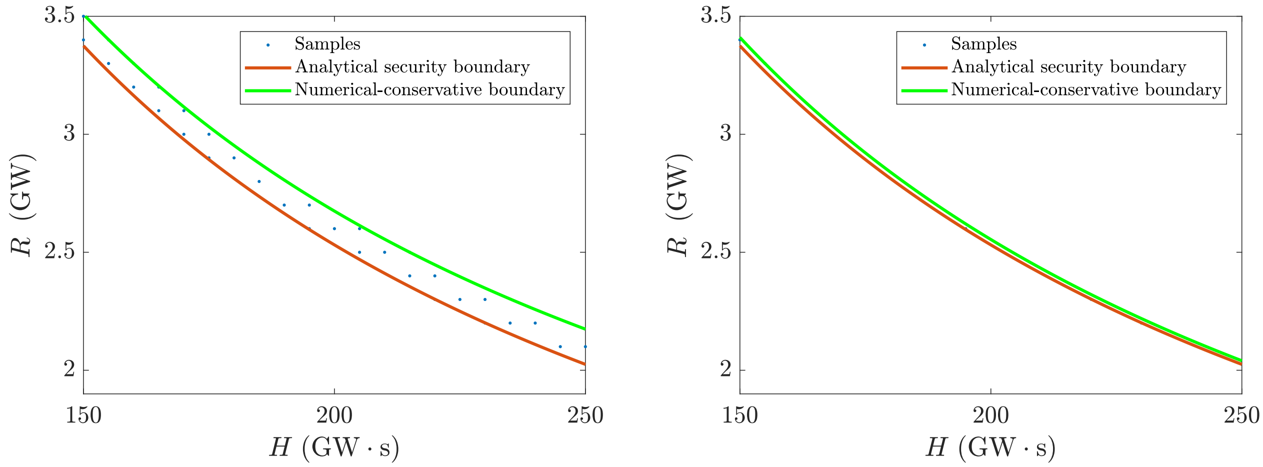

(a) Using samples within 0.05Hz of the the nadir security boundary.

(b) Using samples within 0.01Hz of the the nadir security boundary.

Figure 4.4: Importance of using samples close to the actual security boundary when estimating the boundary using a regression.

4.4.3 Applicability of the resulting RoCoF constraint

In this section we demonstrate that the resulting RoCoF constraints do indeed respect the $\text{RoCoF}_{\text{max}}$ limit in each region, while achieving a very small degree of conservativeness.

In order to assess how the resulting RoCoF constraints for each region perform, a number of system operating states was generated that exactly meet the RoCoF constraint in each region (i.e. that exactly meet constraint 4.38). Then, each system operating point was fed into a dynamic simulation to compute the actual RoCoF that would occur for that operating point. The comparison of the computed RoCoF and the predicted RoCoF using constraint (4.38) in each region is presented in Table 4.1.

Table 4.1: Assessment of conservativeness in regional RoCoF constraints

	Region 1	Region 2 (faulted)
Mean overestimation of RoCoF	0.04Hz/s	0.001Hz/s
Max overestimation of RoCoF	0.05Hz/s	0.003Hz/s
Min overestimation of RoCoF	0.03Hz/s	0Hz/s

The results in Table 4.1 were obtained from 270 samples of system operating points in the ranges $H \in [110, 170]$GWs, $R \in [1.6, 3]$GW, $P_{\text{L}} \in [1.2, 1.8]$GW and $\text{P}_{\text{D}} \in [20, 45]$GW, ranges within GB's 2030 system values. The RoCoF limit in both regions was set to $\text{RoCoF}_{\text{max}} =$

0.5Hz/s and the damping factor to D = 0.5%/Hz, while the transmission corridor considered had a line reactance of $X_{1,2} = 50\Omega$ and voltages of $V_1 = V_2 = 345$kV.

As shown in Table 4.1, the proposed RoCoF constraints are almost perfect for region 2, while they achieve a small degree of conservativeness for region 1 (they overestimate RoCoF by 0.05Hz/s in the worst case). These results are consistent with the analytical deduction of the RoCoF constraint presented in Section 4.4.1: the proposed RoCoF constraint neglects the effect of the attenuation of inter-area oscillations, which entails no approximation for the faulted region but a certain approximation for other regions. This fact is illustrated in Figure 4.1, which shows that the maximum RoCoF in the faulted region occurs at the very instant of the fault, when there is no attenuation of oscillations present; however, the maximum RoCoF in the non-faulted region 1 occurs a few instants afterwards, so neglecting the attenuation entails some conservativeness.

In conclusion, these RoCoF constraints are suitable to be implemented in any frequency-secured optimal scheduling algorithm, which would then guarantee to respect frequency stability in every region of the power system.

4.4.4 Nadir constraint: analytical deduction

In a similar fashion as for the RoCoF constraints discussed in the previous Section 4.4.1, it is not possible to deduce a purely analytical nadir constraint from the solution of Δf_i given by (4.31), as it would involve finding the global minimum of that non-convex function (4.31) (see Figure 4.1 for graphical evidence of the existence of several local minima in the post-fault frequency evolution of a region). Deducing the mathematical expression for this global minimum would be necessary to obtain the expression for t_{nadir}, which is needed to obtain an analytical nadir constraint $|\Delta f_{\text{nadir}}| = |\Delta f(t = t_{\text{nadir}})| \leq \Delta f_{\text{max}}$, as discussed in Chapters 2 and 3.

We then propose to use a mixed analytical-numerical approach for the nadir constraints. The analytical part of this methodology consists on formulating the energy equilibrium at the time of the frequency nadir, as explained in following paragraphs. In Chapters 2 and 3 we have considered a power-equilibrium formulation for the nadir constraints, since the swing equation describes a power balance: at any time instant, the negative power due to a power outage is exactly compensated by the power delivered from inertia, FR, load damping and power transferred (power imported or exported to other areas). In these chapters the nadir constraints were deduced by considering that the power contribution of inertia is zero at the nadir, given that the frequency derivative is zero at that point (see Sections 2.3.1 and 3.2.1 for more details), while here we propose an energy-based formulation that yields linear constraints for multi-region power systems.

Assuming that the generation outage occurs in region 2 as in the example shown in Figure 4.1, the energy-based nadir constraint takes this form for region 1:

$$\underbrace{\mathrm{T}_{1,2}\int_0^{\mathrm{t_{nadir}}}\int_0^{t}\left[\Delta f_1(\tau)-\Delta f_2(\tau)\right]\mathrm{d}\tau\ \mathrm{d}t}_{\text{Energy ``lost''}} \ \leq\ \underbrace{\underbrace{2H_1\Delta f_{\max}}_{\substack{\text{Energy}\\ \text{contribution}\\ \text{from inertia}}}+\underbrace{\frac{R_1}{\mathrm{T_g}}\frac{(\mathrm{t_{nadir}})^2}{2}}_{\substack{\text{Energy}\\ \text{contribution}\\ \text{from FR}}}+\underbrace{\mathrm{D}_1\mathrm{P}_1^{\mathrm{D}}\int_0^{\mathrm{t_{nadir}}}\Delta f_1(t)\ \mathrm{d}t}_{\substack{\text{Energy contribution}\\ \text{from damping}}}}_{\text{Energy ``injected''}} \tag{4.41}$$

This expression has been obtained by integrating the swing equation for region 1, i.e. integrating (4.11.1). In plain words, constraint (4.41) enforces that **the energy "lost" must be lower than the maximum admissible energy "injected"**. This maximum admissible energy "injected" is limited by the maximum kinetic energy that can be extracted from the rotating masses in the system so that frequency does not drop below $\Delta f_{\max}$. It is clear from (4.41) that if the energy related to the inertia term is higher, the frequency deviation would be higher than $\Delta f_{\max}$. The energy "lost" corresponds to the energy sent to the outaged region 2 through the transmissions corridors.

For region 2, where the generation outage happens, the nadir constraint is as follows:

$$\underbrace{P_2^{\mathrm{L}}\cdot \mathrm{t_{nadir}}}_{\substack{\text{Energy}\\ \text{``lost''}}} \ \leq$$

$$\underbrace{\underbrace{2H_2\Delta f_{\max}}_{\substack{\text{Energy}\\ \text{contribution}\\ \text{from inertia}}}+\underbrace{\frac{R_2}{\mathrm{T_g}}\frac{(\mathrm{t_{nadir}})^2}{2}}_{\substack{\text{Energy}\\ \text{contribution}\\ \text{from FR}}}+\underbrace{\mathrm{D}_2\mathrm{P}_2^{\mathrm{D}}\int_0^{\mathrm{t_{nadir}}}\Delta f_2(t)\ \mathrm{d}t}_{\substack{\text{Energy contribution}\\ \text{from damping}}}+\underbrace{\mathrm{T}_{1,2}\int_0^{\mathrm{t_{nadir}}}\int_0^{t}\left[\Delta f_1(\tau)-\Delta f_2(\tau)\right]\mathrm{d}\tau\ \mathrm{d}t}_{\substack{\text{Energy imported}\\ \text{from region 1}}}}_{\text{Energy ``injected''}} \tag{4.42}$$

Which again states that the energy "lost" from the generation outage P_2^{L} cannot be higher than the maximum admissible energy that can be extracted from inertia (while considering the energy contribution from FR, damping and imports).

The integrals including terms Δf_1 and Δf_2 must be estimated in the above constraints, for which we propose to use a numerical methodology similar to the one discussed in Section 4.4.2 for the RoCoF constraints. This numerical methodology, explained in Section 4.4.5, estimates these terms using a linear function of the system parameters (H_1, H_2, P_2^L, etc.) so that the final form of constraints (4.41) and (4.42) is linear.

Finally, since it is not possible to obtain the analytical expression for t_{nadir} as a function of the system parameters (as explained before, it would involve finding the global minimum of a non-convex function), we propose to discretise using several time-intervals and apply conditional nadir constraints, in a similar fashion as in Section 3.2.1. For n segments in the discretisation of time $t \in [t_1, t_2, \ldots, t_{n-1}, \mathrm{T_g}]$, the nadir constraints for a two-region system would take this shape:

if $\frac{R}{\mathrm{T_g}} \cdot t_1 > P_2^{\mathrm{L}} - \mathrm{D} \cdot \mathrm{P_D} \cdot \Delta f_{\max}$ then enforce:

$$\mathrm{T}_{1,2} \int_0^{\mathrm{t}_1} \int_0^t \left[\Delta f_1(\tau) - \Delta f_2(\tau)\right] \mathrm{d}\tau \; \mathrm{d}t \;\leq\; 2H_1 \Delta f_{\max} + \frac{R_1}{\mathrm{T_g}} \frac{(\mathrm{t}_1)^2}{2} + \mathrm{D_1 P_1^D} \int_0^{\mathrm{t}_1} \Delta f_1(t)\; \mathrm{d}t \tag{4.43}$$

$$P_2^{\mathrm{L}} \cdot t_1 \;\leq\; 2H_2 \Delta f_{\max} + \frac{R_2}{\mathrm{T_g}} \frac{(\mathrm{t}_1)^2}{2} + \mathrm{D_2 P_2^D} \int_0^{\mathrm{t}_1} \Delta f_2(t)\; \mathrm{d}t + \mathrm{T}_{1,2} \int_0^{\mathrm{t}_1} \int_0^t \left[\Delta f_1(\tau) - \Delta f_2(\tau)\right] \mathrm{d}\tau \; \mathrm{d}t \tag{4.44}$$

else if $\frac{R}{\mathrm{T_g}} \cdot t_2 > P_2^{\mathrm{L}} - \mathrm{D} \cdot \mathrm{P_D} \cdot \Delta f_{\max}$ then enforce:

$$\mathrm{T}_{1,2} \int_0^{\mathrm{t}_2} \int_0^t \left[\Delta f_1(\tau) - \Delta f_2(\tau)\right] \mathrm{d}\tau \; \mathrm{d}t \;\leq\; 2H_1 \Delta f_{\max} + \frac{R_1}{\mathrm{T_g}} \frac{(\mathrm{t}_2)^2}{2} + \mathrm{D_1 P_1^D} \int_0^{\mathrm{t}_2} \Delta f_1(t)\; \mathrm{d}t \tag{4.45}$$

$$P_2^{\mathrm{L}} \cdot t_2 \;\leq\; 2H_2 \Delta f_{\max} + \frac{R_2}{\mathrm{T_g}} \frac{(\mathrm{t}_2)^2}{2} + \mathrm{D_2 P_2^D} \int_0^{\mathrm{t}_2} \Delta f_2(t)\; \mathrm{d}t + \mathrm{T}_{1,2} \int_0^{\mathrm{t}_2} \int_0^t \left[\Delta f_1(\tau) - \Delta f_2(\tau)\right] \mathrm{d}\tau \; \mathrm{d}t \tag{4.46}$$

$$\ldots$$

While only PFR has been considered for the sake of simplicity, note that any other FR service with different dynamics and activation delay can be directly included in these energy-based nadir constraints. As an example, an EFR service with a certain activation delay could be included in the above constraint by simply adding the following term:

$$\frac{R_{\mathcal{S}}}{\mathrm{T_s}} \cdot \frac{(\mathrm{t_{nadir}} - \mathrm{t_{delay}})^2}{2} \tag{4.47}$$

The analytical part of the methodology proposed in this section to obtain nadir constraints entails no approximation, while the only approximation resides in the linear regressions used to estimate the integrals of Δf_1 and Δf_2. The deduced constraints allow not only to consider the contribution of load damping to support the nadir, neglected in many works due to the mathematical complexity it introduces, but notably also allow to consider the power sharing through transmission corridors between different regions of the power system. While certainly the constraints have some degree of conservativeness due to the approximations, it is nonetheless preferable to somewhat overestimate the need for frequency services in a multi-region system than to neglect the distinct regional post-fault frequencies altogether. Furthermore, the conservativeness introduced by this approximation is assessed in Section 4.4.6, which demonstrates that the overestimation is small for practical purposes in a power system.

4.4.5 Nadir constraint: numerical estimation

This section explains the procedure to perform a numerical estimation for the integrals of post-fault frequency deviation appearing in (4.41) and (4.42). This procedure is described in Algorithm 2, while an implementation of this algorithm using MATLAB and Simulink is freely available in this link: https://github.com/badber/TwoRegion_Frequency.

Algorithm 2 is very similar to Algorithm 1, used for the numerical estimation of inter-area oscillation parameters, with two differences: the condition for the ‘while’ loop in line 11 changes, as well as the the labels used for the regression in line 21. Note that the goal of this regression is now to estimate the value of the integrals of frequency deviation for the energy-based nadir

Algorithm 2 Numerical estimation of frequency integrals for the nadir constraint

Input: range of possible operating conditions for the power system
Output: estimation of frequency integrals for each condition (to be used in eqs. 4.41 and 4.42)

for several feasible values of P_L **do**
  for several splits of D among the regions **do**
    $H_\mathrm{total} = P_\mathrm{L}/(2 \cdot \mathrm{RoCoF_{max}})$
    $R_\mathrm{total} = H_\mathrm{total}/k^*$
    if $R_\mathrm{total} < P_\mathrm{L} - \mathrm{D} \cdot \mathrm{P_D} \cdot \Delta f_\mathrm{max}$ **then**
      $R_\mathrm{total} = P_\mathrm{L} - \mathrm{D} \cdot \mathrm{P_D} \cdot \Delta f_\mathrm{max}$
    end if
    for several splits of R_total among the regions **do**
      for several splits of H_total among the regions **do**
        run dynamic simulation (e.g. Simulink)
        while nadir in the region $> \Delta f_\mathrm{max}$ **do**
          $H_\mathrm{total} = H_\mathrm{total}$ + slight increase
          run dynamic simulation
        end while
        record system operating state (H_1, H_2, P_L, ...) as features for the regression
        record numerical values of integrals in eqs. 4.41 and 4.42, as labels for the regression
      end for
    end for
  end for
end for
run regressions using the recorded features and labels (e.g. using 'Nadir_regression.m')

constraints (4.41) and (4.42), that is, the regressions are performing the following estimations:

$$\int_0^{\mathrm{t_{nadir}}} \int_0^t \left[\Delta f_1(\tau) - \Delta f_2(\tau)\right] \mathrm{d}\tau \ \mathrm{d}t \quad \xrightarrow{\text{approximated by}} \quad f(\text{system operating state}) =$$
$$\mathrm{m}_1' H_1 + \mathrm{m}_2' H_2 + \mathrm{m}_3' P^\mathrm{L} + \mathrm{m}_4' \mathrm{D}_1 \mathrm{P}_1^\mathrm{D} + \mathrm{m}_5' \mathrm{D}_2 \mathrm{P}_2^\mathrm{D} + \mathrm{m}_6' R_1 + \mathrm{m}_7' R_2 + \mathrm{m}_8' \quad (4.48)$$

$$\int_0^{\mathrm{t_{nadir}}} \Delta f_i(t) \ \mathrm{d}t \quad \xrightarrow{\text{approximated by}} \quad f(\text{system operating state}) =$$
$$\mathrm{m}_1'' H_1 + \mathrm{m}_2'' H_2 + \mathrm{m}_3'' P^\mathrm{L} + \mathrm{m}_4'' \mathrm{D}_1 \mathrm{P}_1^\mathrm{D} + \mathrm{m}_5'' \mathrm{D}_2 \mathrm{P}_2^\mathrm{D} + \mathrm{m}_6'' R_1 + \mathrm{m}_7'' R_2 + \mathrm{m}_8'' \quad (4.49)$$

The conservativeness of the resulting nadir constraints is assessed in the following section.

4.4.6 Applicability of the resulting nadir constraint

In this section we demonstrate that the resulting nadir constraints do indeed respect the Δf_max limit in each region, while achieving a small degree of conservativeness.

In order to assess how the resulting nadir constraints for each region perform, a number of system operating states was generated that exactly meet the nadir constraint in each region (i.e. that exactly meet constraints 4.41 and 4.42). Then, each system operating point was fed into a dynamic simulation to compute the actual nadir that would occur for that operating point. The comparison of the computed nadir and the predicted nadir using the proposed constraint in each region is presented in Table 4.2.

Table 4.2: Assessment of conservativeness in regional nadir constraints

	Region 1	Region 2 (faulted)
Mean overestimation of nadir	0.02Hz	0.03Hz
Max overestimation of nadir	0.09Hz	0.09Hz
Min overestimation of nadir	0Hz	0Hz

The results in Table 4.2 were obtained from 300 samples of system operating points in the ranges $H \in [60, 125]$GWs, $R \in [3, 5.2]$GW, $P_{\mathrm{L}} \in [1.2, 1.8]$GW and $\mathrm{P_D} \in [20, 45]$GW, ranges within GB's 2030 system values. The nadir limit in both regions was set to $\Delta f_{\mathrm{max}} = 0.8$Hz and the damping factor to $\mathrm{D} = 0.5\%/\mathrm{Hz}$, while the transmission corridor considered had a line reactance of $\mathrm{X}_{1,2} = 50\Omega$ and voltages of $\mathrm{V}_1 = \mathrm{V}_2 = 345$kV.

The results show that nadir is on average overestimated by around 0.02Hz in either region, while the maximum overestimation is of only 0.09Hz. Therefore, these energy-based nadir constraints are suitable to be implemented in any frequency-secured optimal scheduling algorithm, which would then guarantee to respect frequency stability in every region of the power system.

4.4.7 Quasi-steady-state constraint

Regarding the quasi-steady-state frequency in multi-region systems, this magnitude does not in practice show distinct values across the network, since the inter-area oscillations are attenuated by devices such as Power System Stabilizers [14] or even appropriately controlled wind farms [92]. While the action of these oscillation-damping devices is limited before the frequency nadir (which would happen in a sub-10seconds scale in GB) and therefore can be neglected, the areas are shown to swing back together by the q-s-s in the reported studies. Therefore, the q-s-s constraint aggregates the FR and load damping in all regions to bring frequency back to $\Delta f^{\text{ss}}_{\text{max}}$:

$$\sum_{i}^{2} R_i \geq P_{\text{L}} - \Delta f^{\text{ss}}_{\text{max}} \sum_{i}^{2} \text{D}_i \cdot \text{P}^{\text{D}}_i \tag{4.50}$$

4.5 Conditions for frequency security: N-region case

It has been demonstrated in Section 4.3.2 that the post-fault frequency evolution in an N-region system is that of the COI plus certain inter-area oscillations:

$$\Delta f_i(t) \approx \Delta f_{\text{COI}}(t) + \sum_{j=1}^{N-1} \text{e}^{-\text{a}_j t} \text{A}_j \sin(\omega_j t + \phi_j) + \text{C}_j \tag{4.51}$$

Which is a generalisation of the two-region case described by eq. (4.31). Since the post-fault frequency evolution in any region of an N-region system also behaves as the COI frequency plus some oscillations, the same principles and procedures discussed in Section 4.4 to obtain RoCoF and nadir constraints for a two-region system can be directly applied to the more general N-region case.

4.6 Summary of findings

This chapter has presented the following findings:

- First, the causes of distinct regional frequencies have been identified from simulations of a two-region system. Then, using a mathematical model for post-fault frequency dynamics in multi-region systems, it has been shown that the post-fault frequency evolution in any given region is equal to the frequency of the Centre Of Inertia plus certain inter-area oscillations. This mathematical result is consistent with the results from dynamic simulations presented here and reported in the literature.

- Using this result, conditions for regional frequency security have been deduced for the first time, using a mixed analytical-numerical approach: we have proved that it is not possible to obtain purely analytical constraints, and therefore the proposed methodology uses analytical techniques to go as far as they allow, while the procedure is completed with numerical techniques on simulation samples.

- The deduced constraints are linear, therefore allowing for an efficient subsequent optimisation, and allow to co-optimise every possible frequency service available: inertia, different forms of FR with or without activation delays, a dynamically-reduced largest power infeed and the support from load damping. Although some conservative steps have been taken to deduce these linear constraints (i.e. steps that tighten the feasible region for frequency security, therefore requiring a higher amount of frequency services than absolutely necessary), it has been shown that the conservativeness introduced is not significant for practical purposes in a power system.

As future work, these constraints for multi-region frequency security could be implemented in power system scheduling to run case studies that would allow to analyse the implications of distinct regional frequencies on system costs.

Chapter 5

Concluding Remarks and Further Work

In this thesis we have deduced conditions for respecting frequency security in a low-inertia power system. Several models have been developed to consider novel frequency services such as Frequency Response (FR) with different dynamics or distinct regional frequency caused by non-uniform distributions of inertia. Through extensive case studies, we have shown the advantages that such models could bring to the operation of low-carbon power systems, by extracting the value of the different providers of frequency services available in the system and therefore reducing overall operating costs.

Although some of our models generalise previous models we have deduced, the user should actually consider the characteristics of their power grid when deciding which model to implement. For example, if a grid has a significant load damping contribution, and the providers of FR are mostly slow thermal generators and fast battery storage (or other power-electronics-driven devices), the model presented in Chapter 2 would be the most appropriate one, since it provides and adjustable Mixed-Integer Linear Program (MILP) formulation. The models proposed in Chapters 3 and 4 could be overly-conservative for this system while their advantages would not introduce any value.

On the other hand, for a system in which an heterogeneous fleet of FR providers is available, the efficient Mixed-Integer Second-Order Cone Program (MISOCP) proposed in Chapter 3 should be used, which allows to consider any combination of FR dynamics and activation delays. Furthermore, this model takes into account the inertia contribution from the demand side, while acknowledging that this variable cannot be controlled and only estimated to a certain degree of accuracy, therefore proposing a risk-limiting approach for frequency security. In addition, a marginal pricing scheme for frequency services is proposed based on the MISOCP framework for frequency constraints proposed, which would allow to design a ancillary services market incentivising providers to enhance their performance in delivering frequency services.

Finally, for systems which inherently exhibit a non-uniform inertia distribution driven by significant renewable capacity located in remote regions, the model in Chapter 4 guarantees that frequency regulation will be respected. The mathematical complexity of such multi-region systems makes it necessary to apply a mixed analytical-numerical approach involving some level of conservativeness that tightens the feasible region to guarantee frequency security in all circumstances, and therefore this model should only be used if the system exhibits such multi-region behaviour. Nevertheless, considering constraints deduced from the uniform-frequency model, such as the ones proposed in Chapters 2 and 3 and in all works reported in the literature would be overly optimistic for a system with distinct regions for post-fault frequency purposes: as demonstrated in Chapter 4, such systems always experience higher RoCoF and lower frequency nadirs after a generation outage. The constraints deduced in this Chapter guarantee frequency-security in a linear framework, therefore providing an efficient formulation to be implemented in optimisation problems.

This thesis has built upon the excellent available work on power system scheduling under uncertainty and co-optimisation of frequency services, enhancing some of these models to achieve further cost reductions in low-carbon grids. Nevertheless, there is still room for improvement that could facilitate higher integration of renewables in a cost-effective manner. We have identified the following lines of work as the ones with highest potential impact:

- *Introducing probabilistic metrics in the scheduling of frequency services*

  The frequency-security constraints used in this thesis are deterministic (with the exception of the chance constraint allowing to account for the forecast of inertia from demand proposed in Chapter 3), that is, the largest loss must always be secured against by scheduling enough inertia and FR, and the inertia and FR scheduled are assumed to be fully delivered if needed. These assumptions are well tailored for a system in which frequency services are provided by a few actors (thermal generators also providing energy) and covering the largest loss at all times does not significantly increase system operating costs (due to a high level of inertia available).

However, two characteristics of low-carbon systems imply that the system operation could benefit from taking a probabilistic approach to considering frequency services: 1) since system inertia will be greatly reduced, the costs of covering the largest loss can be very significant, as shown in the different case studies presented in this thesis. Therefore, considering the probability of this largest loss actually taking place could help reduce costs, at the expense of increasing the risk of a blackout if not enough frequency services are eventually available when the fault takes place; and 2) the number of actors in the system will likely greatly increase, with the advent of assets such as Distributed Energy Resources (DER) and Demand Side Response (DSR). While markets for frequency services could greatly benefit from the participation of these actors, due to increased liquidity that would likely drive prices down, the controllability of such a pool of providers is much more complex than that of a few generators. Therefore, considering that these assets can only guarantee the delivery of the agreed amount of FR up to a certain probability would allow to maintain the high reliability standard that society is used to nowadays, while evolving to a less controllable, decentralised system.

Some references have proposed probabilistic approaches for operating power grids [93–95], while the challenge in using such approach for frequency-services scheduling lies in the computational burden: the Stochastic Unit Commitment considered in this thesis accounts for uncertainty in net demand, and therefore schedules reserve in a probabilistic manner; if an additional source of uncertainty, such as the probability of occurrence of the largest loss, was added to the SUC, the size of the optimisation problem would grow exponentially (since every combination of possible realisations for the random variables would have to be considered). Therefore, new methods would have to be developed allowing to considering multiple sources of uncertainty for system scheduling in an efficient manner. A possibility consists on exploring the use of decomposition techniques that allow to better handle stochastic optimization problems [96].

- *Exploring the trade-off between cost and risk*

  Related to the point above, some works have studied how to find the optimal operating point by considering the possibility of risking system instability at the cost of paying a high penalty, but requiring less preventive actions that would increase the cost: reference [34] considered an optimal scheduling of reserve while including load shedding in the objective function, and [97] used a data-driven approach to balance cost and risk from control actions after line outages in a transmission network.

  For the purpose of frequency-services scheduling, the key challenge lies in estimating the volume of load that would be shed if a given shortfall in frequency services is present. The work in [98] started this path by considering Under-Frequency Load Shedding as a decision variable weighted by the Value of Lost Load in the objective function, but the formulation of the MILP proposed would not be applicable to the more general models proposed in this thesis (which allow to consider multiple FR services and the largest loss as a decision variable), as the resulting constraints would be highly non-convex. Furthermore, a shortfall of frequency services could cause a cascading failure leading to a full system blackout, while the cited works assume that the volume of load shed is proportional to the lack of preventive resources.

  In conclusion, while quantifying and optimising the risk due to a shortfall seems to be a challenging task, it is nevertheless one worth exploring, given the high costs associated to this type of ancillary services in a low-carbon scenario, as shown in the case studies included in this thesis.

- *Considering the interactions of other types of power system stability with frequency stability*

  Frequency stability has been the focus of the security constraint developed in this thesis. However, given that power systems are complex networks, cascading failures could be the result of the violation of different types of stability. Therefore, additional layers of security could be added to the frequency-secured scheduling considered in this thesis, notably guaranteeing transient stability and voltage stability.

  Transient stability is closely related to frequency (since frequency is the derivative of phase angle), so including it in optimisation routines along with our frequency formulation would be of interest. Future work can build upon existing studies considering transient stability in Unit Commitment such as [99]. Studying transient stability is particularly important in systems which exhibit distinct regional frequencies, since reference [83] pointed out that the location of FR services is critical in such systems: a fast injection of power from FR in regions which are far from the region where the generation outage took place could cause a further deviation of voltage phase-angle, potentially leading to the system losing synchronism.

Voltage stability can also interact with frequency stability potentially causing blackouts, as recently experienced in Great Britain on August 9$^{\text{th}}$ 2019: the automatic disconnection of an offshore windfarm following an undervoltage caused by a lighting strike resulted in Under-Frequency Load Shedding [100]. Available works have studied the interaction between voltage and frequency stability [101, 102], and therefore combining both layers of security in an optimisation of the system operation would lead to better informed decisions by the system operators.

- *Who should pay for frequency services?*

  In reference [13] a probabilistic approach is used to calculate the amount of reserve needed in a power system to cover against power outages, and it is argued that the cost of reserve should be borne by unreliable generators, who are the drivers for reserve. This cost will eventually be passed on to consumers, but it gives an incentive to these generators to improve their reliability and therefore pay less for reserve provision. One could think that this rule can also apply to frequency services: since the need for frequency services is driven by the power rating of the largest unit (or interconnector), it should be this unit who bears the cost of frequency-services provision. However, it is key to notice that although the $N-1$ reliability requirement is driven by the largest unit, it also secures against the contingency of any other smaller unit in the system. Therefore, a method should be developed to calculate the share of cost that each unit should bear, i.e. a probabilistic way to schedule frequency services by considering the probability of each generator outage, which could then be used to calculate the share of cost of frequency services that each generator must cover. Then, generators would be incentivised to improve their reliability, as the costs they have to bear for frequency services would be reduced.

- *Should reliability standards be re-thought?*

  The Great Britain blackout of August 9$^{\text{th}}$ 2019 [100], which led to 1.1 million customers losing power for around an hour and caused significant disruption to the rail network, was caused by the tripping of 2 generators, therefore an $N-2$ fault. Most system operators in the world, including National Grid, schedule enough reserves for an $N-1$ fault, which was the reason for 5% of the total load having to be shed in Great Britain during the event of 2019. This thesis has considered the $N-1$ reliability requirement, but it is straightforward to consider that the largest power outage P_{L} is actually driven by the sum of any 2 units. Covering the $N-2$ will certainly involve a higher operating cost for the system, since a higher volume of frequency services will need to be scheduled. However, an analysis of the cost increase due to considering the $N-2$ requirement can be made for a particular system using the tools developed in this thesis, and this analysis could be used to start a conversation on the willingness of our society to pay more to increase our reliability, or if on the other hand it would be preferable to have lower average electricity costs but risk having a partial blackout every few years.

- *Analysis of the economic impact of frequency regulation*

  The mathematical models developed in the thesis could be used to analyse the impact in the operating cost of any given system from enforcing frequency regulation constraints, and the benefits that relaxing such regulation would bring. Frequency requirements are historical values established several decades ago, so a cost-benefit analysis is necessary to evaluate the convenience of relaxing them. These requirements, which define the settings of RoCoF and Under-Frequency Load Shedding (UFLS) relays, have the goal of avoiding damage to the different devices. However, the increased need for frequency services if these requirement are too tight might prove to have a counterproductive effect: the high cost from ancillary service provision might overweight the extension of device lifetime from operating within a narrow frequency band.

The mathematical models developed here can be used to quantify the savings from relaxing the RoCoF and nadir requirements. Independently, experts on device operation could quantify the increase in wear-and-tear and associated maintenance costs if generators and motors are more frequently subject to higher RoCoFs and lower frequency nadirs. Finally, the system operator could take this information and also estimate the labour costs for re-tuning the protection relays to relax the frequency requirements, to make an informed decision on the suitability of this proposed change based on this rigorous cost-benefit analysis.

References

[1] L. Badesa, F. Teng, and G. Strbac, "Simultaneous scheduling of multiple frequency services in stochastic unit commitment," *IEEE Transactions on Power Systems*, vol. 34, no. 5, pp. 3858–3868, 2019. [Online]. Available: https://arxiv.org/abs/1809.10391

[2] L. Badesa, F. Teng, and G. Strbac, "Optimal portfolio of distinct frequency-response services in low-inertia systems," *IEEE Transactions on Power Systems*, accepted for publication. [Online]. Available: https://arxiv.org/abs/1908.07856

[3] L. Badesa, F. Teng, and G. Strbac, "Pricing inertia and frequency response with diverse dynamics in a Mixed-Integer Second-Order Cone Programming formulation," *Applied Energy*, vol. 260, p. 114334, 2020. [Online]. Available: https://arxiv.org/abs/1909.06671

[4] J. Guo, L. Badesa, F. Teng, B. Chaudhuri, S. Y. R. Hui, and G. Strbac, "Value of point-of-load voltage control for enhanced frequency response in future Great Britain power system," *IEEE Transactions on Smart Grid*, accepted for publication. [Online]. Available: http://arxiv.org/abs/2006.03559

[5] S. Camal, F. Teng, A. Michiorri, G. Kariniotakis, and L. Badesa, "Scenario generation of aggregated wind, photovoltaics and small hydro production for power systems applications," *Applied Energy*, vol. 242, pp. 1396–1406, 2019. [Online]. Available: https://hal-mines-paristech.archives-ouvertes.fr/hal-02081282

[6] L. Badesa, F. Teng, and G. Strbac, "Conditions for regional frequency stability in power systems—Part I: Theory," *IEEE Transactions on Power Systems*, in preparation.

[7] L. Badesa, F. Teng, and G. Strbac, "Conditions for regional frequency stability in power systems—Part II: Applications," *IEEE Transactions on Power Systems*, in preparation.

[8] L. Badesa, F. Teng, and G. Strbac, "Economic value of inertia in low-carbon power systems," in *2017 IEEE PES Innovative Smart Grid Technologies Conference Europe (ISGT-Europe)*, Torino (Italy), Conference Proceedings. [Online]. Available: https://arxiv.org/abs/2001.03763

[9] L. Badesa, F. Teng, and G. Strbac, "Optimal scheduling of frequency services considering a variable largest-power-infeed-loss," in *2018 IEEE Power & Energy Society General Meeting (PESGM)*, Portland, Oregon (USA), Conference Proceedings. [Online]. Available: https://arxiv.org/abs/2001.03751

[10] "EU low carbon road map 2050," Report, 2011.

[11] "Climate Change Act 2008 (2050 Target Amendment) Order 2019," UK Parliament House of Commons, Report, 2019.

[12] "New nuclear power: support for industry development," UK Department for Business, Energy & Industrial Strategy, Report, 2013.

[13] G. Strbac and D. S. Kirschen, "Who should pay for reserve?" *The Electricity Journal*, vol. 13, no. 8, pp. 32–37, 2000.

[14] P. Kundur, *Power System Stability and Control*, 1st ed. McGraw-Hill Education, 1994.

[15] "Security and quality of supply standards," National Grid, Report, 2017.

[16] "Operation of the grid," Landsnet, Report, 2019.

[17] F. Teng, "Assessment of the value of flexibility by using stochastic scheduling tool," PhD thesis, Imperial College London, United Kingdom, 2015.

[18] F. Teng, M. Aunedi, G. Strbac, V. Trovato, and A. Dallagi, "Provision of ancillary services in future low-carbon UK electricity system," in *2017 IEEE PES Innovative Smart Grid Technologies Conference Europe (ISGT-Europe)*, Torino (Italy), Conference Proceedings.

[19] J. F. Restrepo and F. D. Galiana, "Unit commitment with primary frequency regulation constraints," *IEEE Transactions on Power Systems*, vol. 20, no. 4, pp. 1836–1842, 2005.

[20] E. Ela, V. Gevorgian, A. Tuohy, B. Kirby, M. Milligan, and M. O'Malley, "Market designs for the primary frequency response ancillary service. Part I: Motivation and design," *IEEE Transactions on Power Systems*, vol. 29, no. 1, pp. 421–431, 2014.

[21] W. Li, P. Du, and N. Lu, "Design of a new primary frequency control market for hosting frequency response reserve offers from both generators and loads," *IEEE Transactions on Smart Grid*, vol. 9, no. 5, pp. 4883–4892, 2018.

[22] C. Cardozo, W. van Ackooij, and L. Capely, "Cutting plane approaches for frequency constrained economic dispatch problems," *Electric Power Systems Research*, vol. 156, pp. 54–63, 2018.

[23] H. Chávez, R. Baldick, and S. Sharma, "Governor rate-constrained OPF for primary frequency control adequacy," *IEEE Transactions on Power Systems*, vol. 29, no. 3, pp. 1473–1480, 2014.

[24] G. Zhang, "New ancillary service market design to improve MW-frequency performance: reserve adequacy and resource flexibility," PhD thesis, Iowa State University, United States, 2015.

[25] F. Teng, V. Trovato, and G. Strbac, "Stochastic scheduling with inertia-dependent fast frequency response requirements," *IEEE Transactions on Power Systems*, vol. 31, no. 2, pp. 1557–1566, 2016.

[26] H. Ahmadi and H. Ghasemi, "Security-constrained unit commitment with linearized system frequency limit constraints," *IEEE Transactions on Power Systems*, vol. 29, no. 4,

pp. 1536–1545, 2014.

[27] L. E. Sokoler, P. Vinter, R. Bærentsen, K. Edlund, and J. B. Jørgensen, "Contingency-constrained unit commitment in meshed isolated power systems," *IEEE Transactions on Power Systems*, vol. 31, no. 5, pp. 3516–3526, 2016.

[28] A. Muzhikyan, T. Mezher, and A. M. Farid, "Power system enterprise control with inertial response procurement," *IEEE Transactions on Power Systems*, vol. 33, no. 4, pp. 3735–3744, 2018.

[29] Y. Wen, W. Li, G. Huang, and X. Liu, "Frequency dynamics constrained unit commitment with battery energy storage," *IEEE Transactions on Power Systems*, vol. 31, no. 6, pp. 5115–5125, 2016.

[30] G. Zhang, E. Ela, and Q. Wang, "Market scheduling and pricing for primary and secondary frequency reserve," *IEEE Transactions on Power Systems*, vol. 34, no. 4, pp. 2914–2924, 2019.

[31] "System needs and product strategy," National Grid, Report, 2017. [Online]. Available: https://www.nationalgrid.com/sites/default/files/documents/8589940795-System%20Needs%20and%20Product%20Strategy%20-%20Final.pdf

[32] "Future requirements for balancing services," National Grid, Report, 2016. [Online]. Available: https://www.nationalgrid.com/sites/default/files/documents/Requirements%20Report%202016.pdf

[33] A. J. Wood, B. F. Wollenberg, and G. B. Sheblé, *Power Generation, Operation, and Control*, 3rd ed. Wiley, 2014.

[34] A. Sturt and G. Strbac, "Efficient stochastic scheduling for simulation of wind-integrated power systems," *IEEE Transactions on Power Systems*, vol. 27, no. 1, pp. 323–334, 2012.

[35] A. Sturt and G. Strbac, "Value of stochastic reserve policies in low-carbon power systems," *Proceedings of the Institution of Mechanical Engineers, Part O: Journal of Risk and Reliability*, vol. 226, no. 1, pp. 51–64, 2012.

[36] A. Sturt, "Stochastic scheduling of wind-integrated power systems," PhD thesis, Imperial College London, United Kingdom, 2011.

[37] "System operability framework," National Grid, Report, 2016. [Online]. Available: https://www.nationalgrid.com/sites/default/files/documents/8589937803-SOF%202016%20-%20Full%20Interactive%20Document.pdf

[38] J. Ekanayake and N. Jenkins, "Comparison of the response of doubly fed and fixed-speed induction generator wind turbines to changes in network frequency," *IEEE Transactions on Energy Conversion*, vol. 19, no. 4, pp. 800–802, 2004.

[39] N. R. Ullah, T. Thiringer, and D. Karlsson, "Temporary primary frequency control support by variable speed wind turbines— potential and applications," *IEEE Transactions on Power Systems*, vol. 23, no. 2, pp. 601–612, 2008.

[40] E. Muljadi, V. Gevorgian, M. Singh, and S. Santoso, "Understanding inertial and frequency response of wind power plants," in *2012 IEEE Power Electronics and Machines in Wind Applications*, Denver, Colorado (USA), Conference Proceedings.

[41] T. Xu, W. Jang, and T. Overbye, "An economic evaluation tool of inertia services for systems with integrated wind power and fast-acting storage resources," in *2016 49th Hawaii International Conference on System Sciences (HICSS)*, Koloa, Hawaii (USA), Conference Proceedings, pp. 2456–2465.

[42] "Frequency changes during large disturbances and their impact on the total system," Ofgem, Report, 2014. [Online]. Available: https://www.ofgem.gov.uk/sites/default/files/docs/2014/07/gc0035_authority_decision_0.pdf

[43] "Assessment of risks resulting from the adjustment of RoCoF based loss of mains protection settings," Energy Networks Association, Report, 2015. [Online]. Available: https://www.nationalgrid.com/sites/default/files/documents/Appendix%201%20Strathclyde%20Report%201.pdf

[44] H. P. Williams, *Model Building in Mathematical Programming*, 5th ed. Wiley, 2013.

[45] J. Löfberg, "YALMIP documentation for big-M formulations applied to multiplication of variables." [Online]. Available: https://yalmip.github.io/tutorial/logicprogramming/

[46] "Future energy scenarios," National Grid, Report, 2019. [Online]. Available: http://fes.nationalgrid.com/media/1409/fes-2019.pdf

[47] "Energy trends section 6: renewables," UK Department for Business, Energy & Industrial Strategy, Report, 2016.

[48] R. Doherty, G. Lalor, and M. O'Malley, "Frequency control in competitive electricity market dispatch," *IEEE Transactions on Power Systems*, vol. 20, no. 3, pp. 1588–1596, 2005.

[49] "Enhanced frequency response market information report," National Grid, Report, 2016.

[50] V. Gevorgian, Y. Zhang, and E. Ela, "Investigating the impacts of wind generation participation in interconnection frequency response," *IEEE Transactions on Sustainable Energy*, vol. 6, no. 3, pp. 1004–1012, 2015.

[51] H. Hijazi, P. Bonami, and A. Ouorou, "An outer-inner approximation for separable mixed-integer nonlinear programs," *INFORMS Journal on Computing*, vol. 26, no. 1, pp. 31–44, 2014.

[52] N. A. Temiz, A. Trapp, O. A. Prokopyev, and C. J. Camacho, "Optimization of minimum set of protein-DNA interactions: a quasi exact solution with minimum over-fitting," *Bioinformatics*, vol. 26, no. 3, pp. 319–25, 2010.

[53] S. Chen, T. Zhang, H. B. Gooi, R. D. Masiello, and W. Katzenstein, "Penetration rate and effectiveness studies of aggregated BESS for frequency regulation," *IEEE Transactions on Smart Grid*, vol. 7, no. 1, pp. 167–177, 2016.

[54] F. Teng and G. Strbac, "Assessment of the role and value of frequency response support from wind plants," *IEEE Transactions on Sustainable Energy*, vol. 7, no. 2, pp. 586–595, 2016.

[55] R. Doherty, A. Mullane, G. Nolan, D. J. Burke, A. Bryson, and M. O'Malley, "An assessment of the impact of wind generation on system frequency control," *IEEE Transactions on Power Systems*, vol. 25, no. 1, pp. 452–460, 2010.

[56] S. Boyd and L. Vandenberghe, *Convex Optimization.* Cambridge University Press, 2004.

[57] V. Trovato, A. Bialecki, and A. Dallagi, "Unit commitment with inertia-dependent and multispeed allocation of frequency response services," *IEEE Transactions on Power Systems*, vol. 34, no. 2, pp. 1537–1548, 2019.

[58] Q. Hong, M. Nedd, S. Norris, I. Abdulhadi, M. Karimi, V. Terzija, B. Marshall, K. Bell, and C. Booth, "Fast frequency response for effective frequency control in power systems with low inertia," *The Journal of Engineering*, vol. 2019, no. 16, pp. 1696–1702, 2019.

[59] P. V. Brogan, R. J. Best, D. J. Morrow, K. McKinley, and M. L. Kubik, "Effect of BESS response on frequency and RoCoF during underfrequency transients," *IEEE Transactions on Power Systems*, vol. 34, no. 1, pp. 575–583, 2019.

[60] G. S. Ledva, E. Vrettos, S. Mastellone, G. Andersson, and J. L. Mathieu, "Managing communication delays and model error in demand response for frequency regulation," *IEEE Transactions on Power Systems*, vol. 33, no. 2, pp. 1299–1308, 2018.

[61] S. Majumder, A. P. Agalgaonkar, S. A. Khaparde, S. Perera, S. V. Kulkarni, and P. P. Ciufo, "Allowable delay heuristic in provision of primary frequency reserve in the future power system," *IEEE Transactions on Power Systems*, 2019.

[62] "Product roadmap for frequency response and reserve," National Grid, Report, 2017. [Online]. Available: https://www.nationalgrideso.com/sites/eso/files/documents/Product%20Roadmap%20for%20Frequency%20Response%20and%20Reserve.pdf

[63] D. S. Kirschen and G. Strbac, *Fundamentals of Power System Economics*, 2nd ed. Wiley, 2018.

[64] "DS3 system services agreement," EirGrid, Report, 2017. [Online]. Available: http://www.eirgridgroup.com/site-files/library/EirGrid/Ire-DS3-System-Services-Regulated-Arrangements_final.pdf

[65] E. Ela, V. Gevorgian, A. Tuohy, B. Kirby, M. Milligan, and M. O'Malley, "Market designs for the primary frequency response ancillary service. Part II: Case studies," *IEEE Transactions on Power Systems*, vol. 29, no. 1, pp. 432–440, 2014.

[66] T. Greve, F. Teng, M. G. Pollitt, and G. Strbac, "A system operator's utility function for the frequency response market," *Applied Energy*, vol. 231, pp. 562–569, 2018.

[67] M. Paturet, "Economic valuation and pricing of inertia in inverter-dominated power systems," Master thesis, Swiss Federal Institute of Technology (ETH) Zurich, 2019.

[68] Y. Bian, H. Wyman-Pain, F. Li, R. Bhakar, S. Mishra, and N. P. Padhy, "Demand side contributions for system inertia in the GB power system," *IEEE Transactions on Power Systems*, vol. 33, no. 4, pp. 3521–3530, 2018.

[69] P. M. Ashton, C. S. Saunders, G. A. Taylor, A. M. Carter, and M. E. Bradley, "Inertia estimation of the GB power system using synchrophasor measurements," *IEEE Transactions on Power Systems*, vol. 30, no. 2, pp. 701–709, 2015.

[70] "Dynamic Containment FAQs," National Grid, Report, 2020. [Online]. Available: https://www.nationalgrideso.com/document/164391/download

[71] "Stability Pathfinder for inertia, phase 1 tender results," National Grid, Report, 2020. [Online]. Available: https://www.nationalgrideso.com/document/162091/download

[72] R. Sioshansi and A. Conejo, *Optimization in Engineering*. Springer International Publishing, 2017.

[73] J. Löfberg, "YALMIP documentation for logic constraints." [Online]. Available: https://yalmip.github.io/command/implies/

[74] A. Papoulis and S. U. Pillai, *Probability, Random Variables and Stochastic Processes*, 4th ed. McGraw-Hill Education, 2002.

[75] A. Nemirovski and A. Shapiro, "Convex approximations of chance constrained programs," *SIAM Journal on Optimization*, vol. 17, no. 4, pp. 969–996, 2007.

[76] J. A. Taylor, *Convex Optimization of Power Systems*. Cambridge University Press, 2015.

[77] P. Gribik, W. Hogan, and S. Pope, "Harvard electricity policy group working paper," 2007.

[78] B. Eldridge, R. O'Neill, and B. F. Hobbs, "Near-optimal scheduling in day-ahead markets: Pricing models and payment redistribution bounds," *IEEE Transactions on Power Systems*, 2019.

[79] J. Löfberg, "YALMIP: a toolbox for modeling and optimization in MATLAB," in *2004 IEEE International Conference on Robotics and Automation*, New Orleans, Louisiana (USA), Conference Proceedings, pp. 284–289.

[80] "Enhanced frequency control capability project," National Grid, Report, 2017. [Online]. Available: https://www.nationalgrideso.com/innovation/projects/enhanced-frequency-control-capability-efcc

[81] P. W. Sauer and M. A. Pai, *Power System Dynamics and Stability*, 1st ed. Prentice Hall, 1998.

[82] I. Martínez-Sanz, B. Chaudhuri, A. Junyent-Ferré, V. Trovato, and G. Strbac, "Distributed vs. concentrated rapid frequency response provision in future Great Britain system," in *2016 IEEE Power and Energy Society General Meeting (PESGM)*, Boston, Massachusetts (USA), Conference Proceedings.

[83] P. Wall, N. Shams, V. Terzija, V. Hamidi, C. Grant, D. Wilson, S. Norris, K. Maleka, C. Booth, Q. Hong, and A. Roscoe, “Smart frequency control for the future GB power system,” in *2016 IEEE PES Innovative Smart Grid Technologies Conference Europe (ISGT-Europe)*, Ljubljana (Slovenia), Conference Proceedings.

[84] T. Xu, W. Jang, and T. J. Overbye, “Investigation of inertia’s locational impacts on primary frequency response using large-scale synthetic network models,” in *2017 IEEE Power and Energy Conference at Illinois (PECI)*, Champaign, Illinois (USA), Conference Proceedings.

[85] A. Ulbig, T. S. Borsche, and G. Andersson, “Impact of low rotational inertia on power system stability and operation,” *IFAC Proceedings Volumes*, vol. 47, no. 3, pp. 7290–7297, 2014.

[86] B. K. Poolla, S. Bolognani, and F. Dörfler, “Optimal placement of virtual inertia in power grids,” *IEEE Transactions on Automatic Control*, vol. 62, no. 12, pp. 6209–6220, 2017.

[87] A. Adrees, J. V. Milanović, and P. Mancarella, “Effect of inertia heterogeneity on frequency dynamics of low-inertia power systems,” *IET Generation, Transmission Distribution*, vol. 13, no. 14, pp. 2951–2958, 2019.

[88] F. Milano and A. Ortega, “Frequency divider,” *IEEE Transactions on Power Systems*, vol. 32, no. 2, pp. 1493–1501, 2017.

[89] R. Azizipanah-Abarghooee, M. Malekpour, M. Paolone, and V. Terzija, “A new approach to the online estimation of the loss of generation size in power systems,” *IEEE Transactions on Power Systems*, vol. 34, no. 3, pp. 2103–2113, 2019.

[90] N. Ma and D. Wang, “Extracting spatial-temporal characteristics of frequency dynamic in large-scale power grids,” *IEEE Transactions on Power Systems*, vol. 34, no. 4, pp. 2654–2662, 2019.

[91] A. Gomez-Expósito, A. J. Conejo, and C. Cañizares, *Electric Energy Systems: Analysis and Operation*, 2nd ed. CRC Press, 2018.

[92] Y. Liu, J. R. Gracia, T. J. King, and Y. Liu, “Frequency regulation and oscillation damping contributions of variable-speed wind generators in the U.S. eastern interconnection (EI),” *IEEE Transactions on Sustainable Energy*, vol. 6, no. 3, pp. 951–958, 2015.

[93] C. Qiming and J. D. McCalley, “Identifying high risk N-k contingencies for online security assessment,” *IEEE Transactions on Power Systems*, vol. 20, no. 2, pp. 823–834, 2005.

[94] N. Ming, J. D. McCalley, V. Vittal, and T. Tayyib, “Online risk-based security assessment,” *IEEE Transactions on Power Systems*, vol. 18, no. 1, pp. 258–265, 2003.

[95] E. Heylen, M. Ovaere, S. Proost, G. Deconinck, and D. Van Hertem, “A multi-dimensional analysis of reliability criteria: From deterministic N-1 to a probabilistic approach,” *Electric Power Systems Research*, vol. 167, pp. 290–300, 2019.

[96] A. Conejo, E. Castillo, R. Minguez, and R. Garcia-Bertrand, *Decomposition Techniques in Mathematical Programming*, 1st ed. Springer, 2006.

[97] J. L. Cremer, I. Konstantelos, S. H. Tindemans, and G. Strbac, "Data-driven power system operation: Exploring the balance between cost and risk," *IEEE Transactions on Power Systems*, vol. 34, no. 1, pp. 791–801, 2019.

[98] F. Teng and G. Strbac, "Full stochastic scheduling for low-carbon electricity systems," *IEEE Transactions on Automation Science and Engineering*, vol. 14, no. 2, pp. 461–470, 2017.

[99] S. Naghdalian, T. Amraee, and S. Kamali, "Linear daily UC model to improve the transient stability of power system," *IET Generation, Transmission Distribution*, vol. 13, no. 13, pp. 2877–2888, 2019.

[100] "Technical report on the events of 9 August 2019," National Grid, Report, 2019. [Online]. Available: https://www.nationalgrideso.com/document/152346/download

[101] J. O'Sullivan, A. Rogers, D. Flynn, P. Smith, A. Mullane, and M. O'Malley, "Studying the maximum instantaneous non-synchronous generation in an island system—frequency stability challenges in ireland," *IEEE Transactions on Power Systems*, vol. 29, no. 6, pp. 2943–2951, 2014.

[102] A. Adrees, J. V. Milanovic, P. Papadopoulos, and P. Mancarella, "Increased frequency and voltage interactions affecting frequency and transient stability in networks with large penetration of renewable generation," in *2019 IEEE Power & Energy Society General Meeting (PESGM)*, Atlanta, Georgia (USA), Conference Proceedings.